Quantum repeaters based on atomic ensembles and linear optics

Nicolas Sangouard

Group of Applied Physics, University of Geneva, CH-1211 Geneva 4, Switzerland
Laboratoire Matériaux et Phénomènes Quantiques, UMR CNRS 7162, Université Paris 7, 75013 Paris, France

Christoph Simon

Group of Applied Physics, University of Geneva, CH-1211 Geneva 4, Switzerland
Institute for Quantum Information Science and Department of Physics and Astronomy, University of Calgary, Calgary T2N 1N4, Alberta, Canada

Hugues de Riedmatten

Group of Applied Physics, University of Geneva, CH-1211 Geneva 4, Switzerland
ICFO–Institute of Photonic Sciences, Mediterranean Technology Park, 08860 Castelldefels (Barcelona), Spain
ICREA–Institució Catalana de Recerca i Estudis Avançats, 08015 Barcelona, Spain

Nicolas Gisin

Group of Applied Physics, University of Geneva, CH-1211 Geneva 4, Switzerland

(Received 13 May 2009; published 21 March 2011)

The distribution of quantum states over long distances is limited by photon loss. Straightforward amplification as in classical telecommunications is not an option in quantum communication because of the no-cloning theorem. This problem could be overcome by implementing quantum repeater protocols, which create long-distance entanglement from shorter-distance entanglement via entanglement swapping. Such protocols require the capacity to create entanglement in a heralded fashion, to store it in quantum memories, and to swap it. One attractive general strategy for realizing quantum repeaters is based on the use of atomic ensembles as quantum memories, in combination with linear optical techniques and photon counting to perform all required operations. Here the theoretical and experimental status quo of this very active field are reviewed. The potentials of different approaches are compared quantitatively, with a focus on the most immediate goal of outperforming the direct transmission of photons.

DOI: 10.1103/RevModPhys.83.33 PACS numbers: 03.67.−a

CONTENTS

I. INTRODUCTION

The distribution of quantum states over long distances is essential for potential future applications of quantum technology such as long-distance quantum cryptography (Bennett and Brassard, 1984; Gisin *et al.*, 2002) and quantum networks (Nielsen and Chuang, 2000; Kimble, 2008). In practice, quantum channels such as optical fibers or free-space transmission are affected by loss and decoherence. This limits the distance over which quantum information can be transmitted directly by sending individual quantum systems (typically photons). In practice, the most immediate problem is photon loss. For example, typical telecommunication optical fibers have losses of 0.2 dB/km in the optimal wavelength range around 1.5 μm. In a sense these losses are impressively low. For example, a piece of fiber that is 1 km long has a transmission of 95%. Nevertheless, they become very significant once one envisions distances of hundreds of kilometers or more. Even for very high-repetition rate sources (say 10 GHz, which is a very ambitious value for a source of quantum states), the rate of transmitted photons becomes exponentially low for such distances. For example, for 500 km one would have a rate of 1 Hz. The rate drops to 0.01 Hz for 600 km, and to 10^{-10} Hz for 1000 km. The latter rate corresponds to 1 photon every 300 years.

In classical telecommunications this problem is overcome through the use of amplifiers (''repeaters''). Unfortunately straightforward amplification is not an option in quantum communication because of the no-cloning theorem (Dieks, 1982; Wootters and Zurek, 1982), which shows that noiseless amplification is impossible unless one restricts oneself to sets of orthogonal states, whereas the quantum nature (and thus the advantage) of protocols such as quantum key distribution arises precisely from the existence of nonorthogonal states. However, it turns out that the problem can be overcome using a more sophisticated method based on entanglement, which is known as the ''quantum repeater'' approach (Briegel *et al.*, 1998).

Entanglement is one of the most counterintuitive, nonclassical features of quantum physics. Bell's famous theorem (Bell, 1964; Mermin, 1993) states that entangled states cannot be simulated by local hidden variables, thus showing that entanglement lies at the heart of quantum nonlocality. A very remarkable feature of entanglement is that it can be ''swapped'' (Zukowski *et al.*, 1993). Given an entangled state between two systems A and B and another entangled state between systems C and D, it is possible to create an entangled state between systems A and D by performing a joint measurement of systems B and C in a basis of entangled states, followed by classical communication of the result to the location of system A and/or D. Entanglement between the two latter systems can be created in this way even though they may never have interacted.

Consider a great distance L, such that the overall transmission of the channel is forbiddingly small. As we have just seen, if one has an entangled state of two particles separated by the distance L at one's disposition, one can use this entangled state to teleport quantum states over this distance. One can also use it to perform entanglement-based quantum key distribution (Ekert, 1991) directly. The creation of entanglement over some great distance L can also be seen as a fundamental goal in itself, allowing one to extend tests of quantum nonlocality to a new distance scale.

The key idea of the quantum repeater approach (Briegel *et al.*, 1998) is that entanglement over the distance L can be created by entanglement swapping starting from two entangled pairs, each of which covers only half the distance, $L/2$. Moreover, these entangled states can themselves be created starting from states covering a distance $L/4$ and so on. If one has a way of independently establishing entanglement for $N = 2^n$ adjacent elementary links each covering a distance $L_0 = L/N$, one can then efficiently create entanglement over a distance L with n levels of entanglement swapping operations; see Fig. 1 (n is called the nesting level). For long distances the described protocol scales much better than direct transmission.

One essential requirement for the described approach is thus to be able to establish entanglement for the elementary links in a ''heralded'' way; i.e., one has to know when the

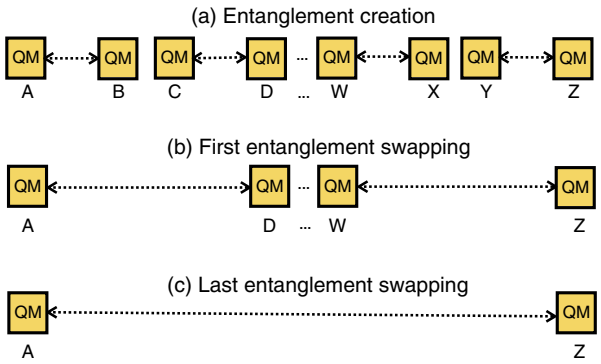

FIG. 1 (color online). Principle of quantum repeaters. In order to distribute entanglement over long distances, say between locations A and Z, one proceeds step by step: (a) Entanglement is first created independently within short elementary links, say between the locations A and B, C and D, …, W and X, Y and Z. (b) Entanglement is then swapped between neighboring links such that the locations A and D, …, W and Z share entanglement. (c) Entanglement swapping operations are performed successively in a hierarchical fashion until entanglement is distributed over the desired distance separating the locations A and Z. Squares represent quantum memories. The dotted arrows connecting two remote memories indicate that they are entangled.

entanglement has been successfully established. At first sight, the most direct approach would be to create entanglement between two systems locally and then send one of the two systems (e.g., a photon) to the distant location. However, the elementary links will still be quite long for realistic protocols, typically of order 100 km, corresponding to a transmission of order 10^{-2}. Implementation of heralding in such an approach would require the ability to measure that the photon has arrived without destroying the entanglement, which is very difficult in practice. A better approach is to create the entanglement "at a distance." For example, entanglement between one atom in A and another atom in B can be created via the detection of a photon that could have been emitted by either atom, provided that the measurement of the photon is performed in such a way that all "which-way" information is erased (Bose *et al.*, 1999; Cabrillo *et al.*, 1999). (This can be seen as another application of the principle of entanglement swapping; see Sec. II.B.1.) The detection of the photon then serves as the heralding event for the creation of the entanglement between the two atoms. If the photon is lost in transmission, there is no detection and one knows that one has to try again.

Another essential requirement for the quantum repeater protocol is that one has to be able to store the created elementary entanglement until entanglement has been established in the neighboring link as well, in order to then be able to perform the required entanglement swapping operation. The resulting higher-level entanglement again needs to be stored until the neighboring higher-level link has been established and so on. Thus quantum repeaters require the existence of "quantum memories" (Lukin, 2003; Tittel *et al.*, 2008; Hammerer *et al.*, 2010). If such memories are not available, the only solution is to create entanglement in all links simultaneously. Such memoryless repeaters, also called "quantum relays," do not help to overcome the problem of photon loss, but can still be useful to alleviate other problems such as detector dark counts (Jacobs *et al.*, 2002; Collins *et al.*, 2005).

Finally, one has to be able to perform the required entanglement swapping operations between the quantum memories, i.e., to perform local joint measurements projecting onto entangled states between two memories. Such measurements are certainly possible if one has a way of performing general quantum gates (e.g., CNOT gates) between neighboring memories. However, this is generally a difficult task, and it is thus of interest to consider dedicated, simpler solutions, e.g., entangling measurements that work only with a certain probability; see below.

The original quantum repeater protocol of Briegel *et al.* (1998) furthermore contains "entanglement purification" (Bennett *et al.*, 1996) steps that allow one in principle to purify the effects of any kind of decoherence. However, the implementation of such general entanglement purification requires the preparation of at least two initial pairs for every purified pair at any given nesting level for which purification is implemented, leading to significant overheads and thus to lower rates. This makes it advantageous to forgo full entanglement purification for simple architectures of just a few links, where it is not necessary for small, but realistic error probabilities per operation. In the present review our focus will be on such simple architectures, because they offer the most realistic chance in the short and medium terms of achieving the most immediate goal of a quantum repeater, namely, to outperform the quantum state distribution rate achievable by direct transmission.

A highly influential proposal for realizing quantum repeaters was made by Duan *et al.* (2001). It is widely known as the DLCZ protocol (for Duan, Lukin, Cirac, and Zoller). The authors showed how to meet all the above requirements using atomic ensembles as quantum memories, and linear optical techniques in combination with photon counting to perform all the required operations. The use of atomic ensembles as opposed to single quantum systems such as individual atoms as memories was motivated by the fact that collective effects related to the large number of atoms in the ensemble make it much easier to achieve a strong and controllable coupling between the memory and the photons that serve as long-distance quantum information carriers.

The basic process at the heart of the DLCZ protocol is the spontaneous Raman emission of a photon, which simultaneously creates a collective spin excitation in the atomic ensemble. This correlation between emitted photons and atomic excitations in each ensemble forms the basis for the generation of entanglement between distant ensembles (for each elementary link), which is done via a single-photon detection that erases all which-way information, following the principle outlined above for the case of individual atoms. The spin excitations can be efficiently reconverted into photons thanks to a collective interference effect. This forms the basis for the entanglement swapping operations, which are again done by detecting single photons while erasing which-way information.

The DLCZ proposal inspired a large number of highly successful experiments [for example, Kuzmich *et al.* (2003), van der Wal *et al.* (2003), Matsukevich and

Kuzmich (2004), Chou *et al.* (2005), Chou *et al.* (2007), and Yuan *et al.* (2008)], showing that the approach of using atomic ensembles, linear optics, and photon counting is indeed very attractive from a practical point of view. Motivated both by the impressive experimental progress and by the growing realization that, while pioneering, the DLCZ protocol does not yet allow one to outperform the direct transmission of photons in practice, several authors have proposed significant improvements to the protocol, while using the same or very similar experimental ingredients. These proposals have in turn spurred new experimental investigations. Here we review this area of research.

We begin with a review of the theoretical proposals, starting with the DLCZ proposal in Sec. II, including a discussion of its practical limitations, followed by a discussion of the most important proposed improvements in Sec. III. In the DLCZ protocol, both entanglement generation and swapping are based on one single-photon detection each. Section III.A describes a protocol where entanglement is swapped based on two-photon detections, leading to an improvement in the overall rate. Section III.B describes protocols where entanglement is generated based on two-photon detections, leading to enhanced robustness with respect to phase fluctuations in the channel. Sections III.C and III.D are devoted to multiplexing. Section III.C reviews the idea of using memories that can store multiple temporal modes. Their use in the present context is made possible by the realization that a DLCZ-type atomic ensemble can be emulated by combining a photon-pair source and an "absorptive" quantum memory (i.e., a memory that can absorb and emit photons). This approach promises a great enhancement in the entanglement generation rate. Section III.D reviews work on spatial multiplexing, which would moreover significantly reduce the requirements on the memory time. Section III.E discusses a protocol based on single-photon sources, which can be effectively implemented with atomic ensembles, and which yields a significantly enhanced rate compared to the DLCZ protocol. Section III.F describes protocols that are based on effectively approximating ideal photon-pair sources with atomic ensembles, leading to both enhanced rates and greatly enhanced robustness.

In Sec. IV we compare the performance of different protocols quantitatively. Section IV.A is devoted to the entanglement distribution rates, whereas Sec. IV.B discusses the robustness of the protocols with respect to storage time limitations, phase errors, and memory and detection inefficiencies. Section IV.C discusses complexity issues.

In Sec. V we review the experimental status quo from the point of view of the different protocols described beforehand. In particular, Sec. V.A is devoted to experiments that realize elements of the DLCZ protocol, and Sec. V.B to experiments that are directed toward the creation and swapping of entanglement via two-photon detections. Section V.C discusses the implementation of quantum light sources compatible with ensemble-based quantum memories, while Sec. V.D discusses the realization of the (absorptive) quantum memories themselves. Section V.E is devoted to photon detectors. Section V.F discusses different realizations of quantum channels. Finally, Sec. V.G discusses the issue of coupling losses.

In Sec. VI we briefly review approaches to quantum repeaters using other ingredients besides or instead of atomic ensembles and linear optics, for example, single trapped ions or nitrogen-vacancy (N-V) centers as quantum memories.

In Sec. VII we give our conclusions and look toward the future.

II. THE DLCZ PROTOCOL

In this section we review the DLCZ protocol for quantum repeaters (Duan *et al.*, 2001). We explain the basic physics underlying the protocol, followed by a description of its individual steps. We then evaluate the required time for long-distance entanglement distribution. Finally, we discuss its limitations.

A. Basic physics

The DLCZ protocol uses atomic ensembles that can emit single photons while creating a single atomic excitation, which is stored in the ensemble. The photons can be used to entangle two distant ensembles. The atomic excitation can be efficiently converted into a photon thanks to collective interference, which is used for entanglement swapping and final use of the entanglement. Here we briefly describe the underlying physics, and the next section explains the protocol.

The basic (idealized) scheme is as follows (see Fig. 2). In an ensemble of three-level systems with two ground states g_1 and g_2 and an excited state e all N_A atoms are initially in the state g_1. An off-resonant laser pulse on the g_1-e transition (the *write* pulse) leads to the spontaneous emission of a Raman photon on the e-g_2 transition. We will denote this photon as the *Stokes* photon, which corresponds to the usual Raman scattering terminology, provided that the energy of g_2 is slightly higher than that of g_1. We will adopt this convention throughout this review. Detection of the Stokes

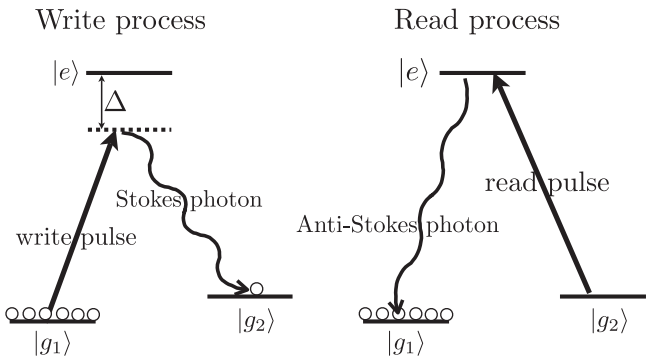

FIG. 2. Basic level scheme for the creation of collective atomic excitations in atomic ensembles via spontaneous Raman emission (write process) and for their readout (read process), as proposed in the DLCZ protocol. Write process: All atoms start out in g_1. A laser pulse off-resonantly excites the g_1-e transition, making it possible for a photon to be emitted on the e-g_2 transition (with small probability). Read process: A resonant laser is applied on the g_2-e transition, promoting the single atomic excitation from g_2 back to e, followed by collective emission on the e-g_1 transition of a Stokes photon in a well-defined direction.

photon in the far field, such that no information is revealed about which atom it came from, creates an atomic state that is a *coherent* superposition of all the possible terms with $N_A - 1$ atoms in g_1 and one atom in g_2, namely,

$$\frac{1}{\sqrt{N_A}} \sum_{k=1}^{N_A} e^{i(\mathbf{k}_w - \mathbf{k}_S)\mathbf{x}_k} |g_1\rangle_1 |g_1\rangle_2 \cdots |g_2\rangle_k \cdots |g_1\rangle_{N_A}, \quad (1)$$

where $\mathbf{k}_w$ is the $\mathbf{k}$ vector of the write laser, $\mathbf{k}_S$ is the $\mathbf{k}$ vector of the detected Stokes photon, and $\mathbf{x}_k$ is the position of the kth atom. In practice, the amplitudes of the different terms may vary, depending on the laser profile and the shape of the atomic ensemble.

A remarkable feature of such collective excitations that are of great interest for practical applications is that they can be *read out* very efficiently by converting them into single photons that propagate in a well-defined direction, thanks to collective interference (Duan *et al.*, 2001; Laurat *et al.*, 2006; J. Simon *et al.*, 2007b). Resonant laser excitation of such a state on the g_2-e transition (the *read* laser pulse) leads to an analogous state with $N_A - 1$ atoms in g_1 and one delocalized excitation in e, but with supplementary phases $e^{i\mathbf{k}_r\mathbf{x}'_k}$, where $\mathbf{k}_r$ is the $\mathbf{k}$ vector of the read laser and $\mathbf{x}'_k$ is the position of the kth atom at the time of the readout (which may be different from its initial position $\mathbf{x}_k$ if the atoms are moving).

All the terms in this state can decay to the initial state $|g_1\rangle^{\otimes N_A}$ while emitting a photon on the e-g_1 transition (the *anti-Stokes* photon). The total amplitude for this process is then proportional to

$$\sum_{k=1}^{N_A} e^{i(\mathbf{k}_w - \mathbf{k}_S)\mathbf{x}_k} e^{i(\mathbf{k}_r - \mathbf{k}_{AS})\mathbf{x}'_k}. \quad (2)$$

The conditions for constructive interference of the N_A terms in this sum depend on whether the atoms are moving during the storage. If they are at rest ($\mathbf{x}_k = \mathbf{x}'_k$ for all k), then there is constructive interference whenever the phase matching condition $\mathbf{k}_S + \mathbf{k}_{AS} = \mathbf{k}_w + \mathbf{k}_r$ is fulfilled, leading to a very large probability amplitude for emission of the anti-Stokes photon in the direction given by $\mathbf{k}_w + \mathbf{k}_r - \mathbf{k}_S$. For atomic ensembles that contain sufficiently many atoms, emission in this one direction can completely dominate all other directions. This allows a very efficient collection of the anti-Stokes photon (Laurat *et al.*, 2006; J. Simon *et al.*, 2007b). If the atoms are moving, there can still be constructive interference, provided that $\mathbf{k}_S = \mathbf{k}_w$ and $\mathbf{k}_{AS} = \mathbf{k}_r$. We will come back to this point in Sec. V.A.

Note that there is no collective interference effect for the emission of the Stokes photon, since its emission by different atoms corresponds to orthogonal final states, e.g., the state $|g_2\rangle_1 |g_1\rangle_2 \cdots |g_1\rangle_{N_A}$ if the Stokes photon was emitted by the first atom, etc. Full which-way information about the origin of the photon is thus stored in the atomic ensemble, making interference impossible (Scully and Zubairy, 2003). As a consequence the total emission probability for the Stokes photon is simply given by the sum of the emission probabilities for each atom, and there is no preferred direction of emission.

We have focused on the emission of a single Stokes photon into the mode of interest. However, since there is an ensemble of atoms, there are also amplitudes for the emission of two or more Stokes photons, accompanied by the creation of the same number of atomic excitations in g_2. This dynamics can be described by the following Hamiltonian:

$$H = \chi(a^\dagger s^\dagger + as), \quad (3)$$

where χ is a coupling constant that depends on the laser intensity, the number of atoms, the detuning, and the transition strengths for the g_1-e and e-g_2 transitions; $a^\dagger$ is the creation operator for a Stokes photon; and $s^\dagger$ is the creation operator for an atomic excitation in g_2. The vacuum state $|0\rangle$ for the mode s corresponds to the atomic state with all atoms in g_1, the state $s^\dagger|0\rangle$ with one excitation in s corresponds to a state as in Eq. (1) with one atom in g_2, etc. Here one focuses on one particular $\mathbf{k}$ vector for both the Stokes photon and the atomic excitation.

This Hamiltonian, whose derivation is discussed in much more detail in Hammerer *et al.* (2010), Sec. II.A, thus describes the creation (and annihilation) of pairs of bosonic excitations. It holds in the single-mode approximation, which can be achieved in cavity QED or in a pulsed scheme with filtering of the produced pair. Note that it is formally equivalent to the Hamiltonian for the nonlinear optical process of parametric down-conversion (Burnham and Weinberg, 1970; Hong and Mandel, 1985; Wu *et al.*, 1986; Hong *et al.*, 1987). Using operator ordering techniques developed by Collett (1988), one can show that, starting from an initial vacuum state for both modes a and s, it creates the following two-mode entangled state:

$$e^{-iHt}|0\rangle|0\rangle = \frac{1}{\cosh(\chi t)} e^{-i\tanh(\chi t)a^\dagger s^\dagger}|0\rangle|0\rangle = \frac{1}{\cosh(\chi t)} \sum_{m=0}^{\infty} (-i)^m \tanh^m(\chi t)|m\rangle|m\rangle. \quad (4)$$

For small values of χt this can be expanded as follows:

$$[1 - \tfrac{1}{2}(\chi t)^2]|0\rangle|0\rangle - i\chi t|1\rangle|1\rangle - (\chi t)^2|2\rangle|2\rangle + O((\chi t)^3). \quad (5)$$

Therefore, if the probability of emitting one photon and creating one atomic excitation is $(\chi t)^2$, then there is a probability $(\chi t)^4$ of emitting two photons and creating two excitations, etc. This possibility of creating multiple pairs of excitations, which becomes more significant as the probability of creating a single excitation is increased, is an important limiting factor in the quantum repeater protocols discussed in this review; see below.

B. Protocol

In this section we review the DLCZ protocol. We discuss the principle for the entanglement creation between two remote ensembles belonging to the same elementary link and the method for entanglement swapping between neighboring links. Finally, we show how the created single-photon entanglement of the form $|1\rangle|0\rangle + |0\rangle|1\rangle$ can be used to postselectively obtain two-photon entanglement that is useful for applications.

1. Entanglement creation for two remote atomic ensembles

The procedure for entanglement creation between two remote locations A and B requires one ensemble at each location; see Fig. 3. The two ensembles are simultaneously excited such that a single Stokes photon can be emitted with a small probability $p/2 = (\chi t)^2$, corresponding to the state

$$\left(1 + \sqrt{\frac{p}{2}}(s_a^\dagger a^\dagger e^{i\phi_a} + s_b^\dagger b^\dagger e^{i\phi_b}) + O(p)\right)|0\rangle. \tag{6}$$

Here we assigned bosonic operators a (b) and s_a (s_b) to the Stokes photon and to the atomic excitation, respectively, associated with the ensemble A (B), ϕ_a (ϕ_b) is the phase of the pump laser at the location A (B), and $|0\rangle$ is the vacuum state for all modes; $O(p)$ represents the multiphoton terms discussed in the previous section.

The Stokes photons are coupled into optical fibers and combined on a beam splitter at a central station between A and B. The modes after the beam splitter are $d = (1/\sqrt{2}) \times (ae^{-i\xi_a} + be^{-i\xi_b})$ and $\tilde{d} = (1/\sqrt{2})(ae^{-i\xi_a} - be^{-i\xi_b})$, where $\xi_{a,b}$ stand for the phases acquired by the photons on their way to the central station. The detection of a single photon in d, for example, projects the state of the two atomic ensembles in

$$|\psi_{ab}\rangle = \frac{1}{\sqrt{2}}(s_a^\dagger e^{i(\phi_a+\xi_a)} + s_b^\dagger e^{i(\phi_b+\xi_b)})|0\rangle. \tag{7}$$

A single atomic excitation is thus delocalized between A and B. This corresponds to an entangled state that can be rewritten as

$$|\psi_{ab}\rangle = \frac{1}{\sqrt{2}}(|1_a\rangle|0_b\rangle + |0_a\rangle|1_b\rangle e^{i\theta_{ab}}), \tag{8}$$

where $|0_{a(b)}\rangle$ denotes an empty ensemble A (B), and $|1_{a(b)}\rangle$ denotes the storage of a single atomic excitation. We have also defined $\theta_{ab} = \phi_b - \phi_a + \xi_b - \xi_a$. Taking into account detections in both d and $\tilde{d}$, the success probability of the entanglement creation is given by $P_0 = p\eta_d\eta_t$ where η_d is the photon detection efficiency and $\eta_t = \exp(-L_0/2L_{\text{att}})$ is the transmission efficiency corresponding to a distance of $L_0/2$, with L_0 the distance between A and B (i.e., the length of the elementary link), and L_{att} the fiber attenuation length. (The losses of 0.2 dB/km mentioned previously, which are achievable in the telecom wavelength range around 1550 nm, correspond to $L_{\text{att}} = 22$ km.)

This way of creating entanglement by a single-photon detection was inspired by similar proposals for entangling two individual quantum systems rather than two ensembles (Bose *et al.*, 1999; Cabrillo *et al.*, 1999). Note that it can be seen as an implementation of entanglement swapping. One starts with entangled states between the modes a and s_a as well as b and s_b as in Eqs. (4) and (5). The single-photon detection at the central station projects onto an entangled state of the photonic modes a and b, creating entanglement between the stored modes s_a and s_b.

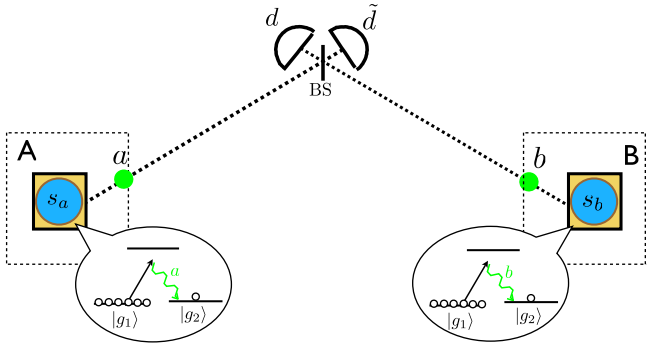

FIG. 3 (color online). Entanglement creation between two remote ensembles located at A and B within the DLCZ protocol. The circles embedded in squares represent DLCZ-type atomic ensembles that probabilistically emit Stokes photons (dots). These photons are sent through long optical fibers (dotted line) to a central station. The detection of a single Stokes photon at the central station in mode d or $\tilde{d}$, which could have come from either location A or B, heralds the storage of a single excitation (s_a or s_b) in one of the two ensembles. Half circles represent photon detectors. The vertical bar represents a beam splitter (BS).

2. Entanglement connection between the elementary links

Once entanglement has been heralded within each elementary link, one wants to connect the links in order to extend the distance of entanglement. This is done by successive entanglement swapping between adjacent links with the procedure shown in Fig. 4.

Consider two links AB and CD in which the ensembles A-B and C-D, respectively, are entangled by sharing a single excitation, as before. They are described by the state $|\psi_{ab}\rangle \otimes |\psi_{cd}\rangle$, where $|\psi_{kl}\rangle$ are defined by Eq. (7). The atomic excitations s_b and s_c that are probabilistically stored in the ensembles B and C are read out with a strong, resonant light pulse to be converted back into "anti-Stokes" photons associated with the mode b' and c'. This readout process is made very efficient thanks to the collective interference described before, which leads to the emission of the anti-Stokes photon in a well-defined mode. The two modes b' and c' are combined on a beam splitter, and the measurement of a single photon, e.g., in the mode $(1/\sqrt{2})(b' + c')$, will project the ensembles A and D into the entangled state

$$|\psi_{ad}\rangle = \frac{1}{\sqrt{2}}(s_a^\dagger + s_d^\dagger e^{i(\theta_{ab}+\theta_{cd})})|0\rangle. \tag{9}$$

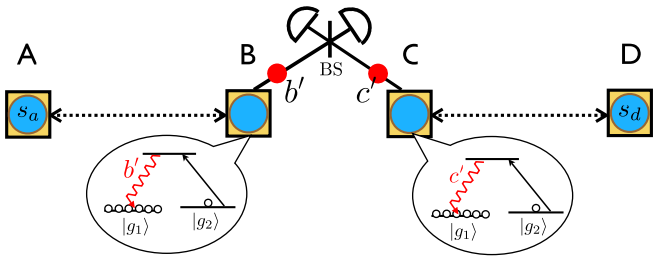

FIG. 4 (color online). Entanglement connection between two links A-B and C-D. The ensemble A (C) is initially entangled with B (D) as described by $|\psi_{ab}\rangle$ ($|\psi_{cd}\rangle$). The memories B and C are read out, and the resulting anti-Stokes photons are combined on a beam splitter. The detection of a single photon after the beam splitter, which could have come from either location B or C, heralds the storage of a single excitation (s_a or s_d) in the ensembles A and D and projects them into an entangled state $|\psi_{ad}\rangle$.

By iterating successive entanglement swapping operations, it is possible to establish entanglement between more and more distant ensembles.

We now analyze the effect of nonunit detector efficiency η_d and memory efficiency η_m on the entanglement swapping procedure. (η_d and η_m are, respectively, the probability of detecting a photon when a single photon enters the detector and the probability of converting a single atomic excitation into an anti-Stokes photon.) The detectors can give the expected click when two photons are stored in the memories B and C, but only one is detected. In this case, the created state contains an additional vacuum component

$$\rho_{ad} = \alpha_1 |\psi_{ad}\rangle\langle\psi_{ad}| + \beta_1 |0\rangle\langle 0|, \tag{10}$$

where $\alpha_1 = 1/(2-\eta)$ and $\beta_1 = (1-\eta)/(2-\eta)$. We have defined η as the product of the detector efficiency by the memory efficiency $\eta = \eta_d \eta_m$. The success probability for the first swapping is given by $P_1 = \eta[1-(\eta/2)]$. Similarly, one can show that the success probability for entanglement swapping at the $(i+1)$th level is given by $P_{i+1} = \alpha_i \eta[1-(\alpha_i \eta/2)]$, where α_i is the weight of the normalized entangled component in the state associated with the level i. It is connected to α_{i-1} by $\alpha_i = [\alpha_{i-1}/(2-\alpha_{i-1}\eta)]$. Using this last formula, one can easily show that after n nesting levels, the ratio $\beta_n/\alpha_n = (1-\eta)(2^n-1)$. The relative weight of the vacuum component thus increases linearly with the number of elementary links $N = 2^n$ composing the quantum repeater. We will see in what follows that in schemes where entanglement swapping is performed via two-photon detections, the vacuum components remain constant.

3. Postselection of two-photon entanglement

Suppose that entanglement has been distributed over the desired distance, say between locations A and Z. The created entanglement, which consists of A and Z sharing a single delocalized excitation, is of limited use on its own, because it is difficult to perform measurements in any basis other than that of the Fock states $|0\rangle$ and $|1\rangle$. This is why in the DLCZ protocol the created single-excitation entanglement is now used as a building block for more directly useful two-photon entanglement; see Fig. 5.

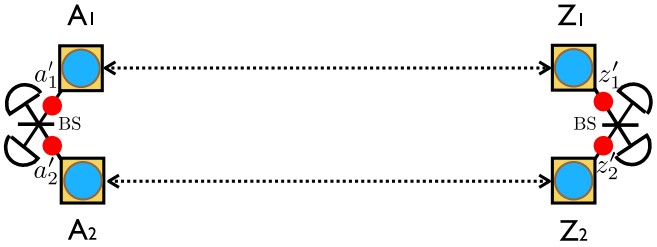

FIG. 5 (color online). Postselection of two-photon entanglement. Entanglement has been distributed independently within two chains (labeled by the subscript 1 or 2) such that the ensembles A_1-Z_1 and A_2-Z_2 share an entanglement. The atomic excitations at the same location are read out and the emitted anti-Stokes photons are combined into a beam splitter and then counted. Measurements in arbitrary basis can be done by changing the beam-splitter transmission coefficients and phases.

One needs two ensembles at each location, labeled A_1 (Z_1) and A_2 (Z_2) for location A (Z). Entanglements between A_1 and Z_1 and between A_2 and Z_2 have been established as presented before, such that we have the state $(1/2)(a_1'^\dagger + e^{i\theta_1} z_1'^\dagger)(a_2'^\dagger + e^{i\theta_2} z_2'^\dagger)|0\rangle$. The projection of this state onto the subspace with one photon in each location is

$$|\Psi_{az}\rangle = \frac{1}{\sqrt{2}}(a_1'^\dagger z_2'^\dagger + e^{i(\theta_2-\theta_1)} a_2'^\dagger z_1'^\dagger)|0\rangle, \tag{11}$$

which is analogous to conventional polarization or time-bin entangled states. The required projection can be performed postselectively by converting the atomic excitations back into anti-Stokes photons and counting the number of photons in each location. Measurements in arbitrary basis are possible by combining modes a_1' and a_2' (and also z_1' and z_2') on beam splitters with appropriate transmission coefficients and phases. The component $|\Psi_{az}\rangle$ of the mixed state ρ_{az} distributed after n swapping operations is postselected with the probability $P_{ps} = \alpha_n^2 \eta^2/2$.

C. Performance

1. Calculation of the entanglement distribution time

The general formula for calculating the time required for a successful distribution of an entangled state $|\Psi_{az}\rangle$ is

$$T_{\text{tot}} = \frac{L_0}{c} \frac{f_0 f_1 \cdots f_n}{P_0 P_1 \cdots P_n P_{ps}}. \tag{12}$$

The first factor is the waiting time at the elementary level, where $L_0 = L/2^n$ is the length of the elementary link, L is the total distance, and n is the "nesting level" of the repeater, as introduced in Sec. I. Entanglement creation attempts for elementary links only succeed with a probability P_0. After every attempt, one has to wait to find out whether the attempt has succeeded (whether there was a photon detection in the central station). If not, the memory has to be emptied, and one tries again. Assuming that the repetition rate is limited neither by the speed of the write and read processes nor by any reinitialization time, this leads to a basic period of L_0/c, and also explains the factor $1/P_0$. Furthermore, the total time is inversely proportional to the success probabilities at each level P_i and to the probability of successful postselection at the end, P_{ps}. The factors f_0 to f_n, which all satisfy $1 \leq f_i \leq 2$, take into account the fact that for every ith level swapping attempt one has to establish two neighboring links at level $i-1$. This takes longer than establishing a single such link by a factor f_{i-1}. The precise values of these factors depend on the ensemble of success probabilities up to the given level. No analytic expression for them is known so far for general i. However, at the lowest order in P_0, f_0 is well approximated by $3/2$ (see Appendix A). Intuitively, if the waiting time for a single link is T, one only has to wait a time $T/2$ for a success in one of two neighboring links. Then one still has to wait a time T for the second link. It is thus rather intuitive to take $f_i = 3/2$ for all i. This agrees well with the empiric estimate found in Jiang *et al.* (2007b). Furthermore, we have limited the maximum number of links used to 16, i.e., $n = 4$, to have link numbers for which it is plausible that entanglement purification might not be necessary. For small

n, numerical calculations show that setting $f_i = 3/2$ for all i is a rather good approximation (Brask and Sorensen, 2008). In what follows, we will use the formula (12) with $f_i = 3/2$ in order to compare the entanglement distribution times for various protocols. In addition, note that since the protocols differ in their performance by orders of magnitude, the approximation in considering $f_i = 3/2$ for all i has no impact on our conclusions. [See Appendix A for a more detailed justification for Eq. (12) and a more detailed discussion of f_i.]

Plugging the expressions for the success probabilities P_0, P_i, and P_{ps} into Eq. (12), one finds

$$T_{\text{tot}} = 3^{n+1}\frac{L_0}{c}\frac{\prod_{k=1}^{n}(2^k-(2^k-1)\eta)}{\eta_d\eta_t p\eta^{n+2}}. \tag{13}$$

This still contains the pair emission probability p. The value of p is constrained by the fact that there is a probability of order p^2 for the emission of two Stokes photons into the desired mode (associated with the creation of two atomic excitations), as discussed in Sec. II.A. This leads to errors that reduce the fidelity F of the distributed state. For the present protocol these errors grow approximately quadratically with the number of links. To first order in p, F is always of the form $1 - A_n p(1-\eta)$, with, for example, $A_0 = 8$, $A_1 = 18$, $A_2 = 56$, $A_3 = 204$, $A_4 = 788$. More details on the multiphoton error calculation are given in Appendix B. In the following we will assume that we can tolerate a fidelity reduction $1 - F = 0.1$ due to multiphoton errors. The maximum allowed value of p for a given n can then be determined directly from the above values for A_n. Note that the choice $F = 0.9$ is arbitrary but the distribution of entangled states with 13% of white noise (the visibility corresponding to a fidelity of $F = 0.9$ is $V \approx 0.87$) is compatible with a long-distance Bell test or with a quantum key distribution based on the BB84 protocol.

2. Comparison to direct transmission

We will now compare the entanglement distribution time for the DLCZ protocol to the time for quantum state distribution using direct transmission. We consider a fiber attenuation of 0.2 dB/km ($\eta_t = e^{-L_0/(2L_{\text{att}})}$, with $L_{\text{att}} = 22$ km) corresponding to typical telecom fibers and telecom wavelength photons. We furthermore take into account the reduced photon velocity within the fiber, $c = 2\times 10^8$ m/s. We assume equal memory and photon-resolving detector efficiencies $\eta_m = \eta_d = 0.9$. This is certainly a demanding choice; however, it is far from the performance levels typically required for fault-tolerant quantum computing based on linear optics, for example. We will describe and discuss the experimental status quo in some detail in Sec. V. We optimize the nesting level n and thus the number of links 2^n for each distance L.

For direct transmission we assume a single-photon source with a repetition rate of 10 GHz, as we did in Sec. I. This will be our reference all through this paper. This is certainly an ambitious value. It might one day be achieved for single-photon sources based on quantum dots in high-finesse semiconductor microcavities (Moreau *et al.*, 2001; Santori *et al.*, 2002), for example, where lifetimes can be of order 100 ps. However, for now these sources are not very efficient. Moreover, the source would have to operate at telecom wavelengths (i.e., about 1.5 μm) (Ward *et al.*, 2005; Hostein *et al.*, 2009). Of course, any such choice is somewhat arbitrary. However, it will become clear later on that our conclusions do not depend very strongly on the exact choice of rate for the reference source, essentially because the scaling with distance is very different for direct transmission and for quantum repeaters. As a consequence, the curve corresponding to direct transmission in our main comparison figure, Fig. 18 in Sec. IV, has a much steeper slope than the curves corresponding to all the considered repeater protocols, so that it intersects them all in the distance range $L = 500$ to 650 km. Changing the reference rate would change the crossover distances only slightly. The most important question in the short and medium terms is what distribution rates a given repeater protocol can achieve in that distance range.

For the DLCZ protocol, we find a crossover point of $L = 630$ km, with an entanglement distribution time $T_{\text{tot}} = 340$ s at that distance, for $n = 2$ (four links). The corresponding value of $p = 0.01$. Note that, thanks to the very different scaling, for longer distances, the repeater is much faster than direct transmission, for example, for 1000 km $T_{\text{tot}} = 4100$ s, compared to 10^{10} s for direct transmission. Nevertheless, this result is somewhat disappointing. On the one hand, a single entangled pair every 340 s is, of course, a very low rate. Even more importantly, for the repeater to work, the memory storage time has to be comparable to the mentioned 340 s. In particular, it has to be long enough for the final postselection to be possible, i.e., long enough to create two independent single-photon entangled states over the whole distance. This is extremely challenging. Briefly anticipating the detailed discussion in Sec. V, the best current results for quantum memory times in DLCZ-type experiments with atomic gases are in the few millisecond range (B. Zhao *et al.*, 2008; R. Zhao *et al.*, 2008). A storage time of order 1 s was achieved in a solid-state system for a memory protocol based on electromagnetically induced transparency (Longdell *et al.*, 2005), though not yet at the quantum level. Decoherence times as long as 30 s have been demonstrated for the same kind of solid-state system (Pr: YSO, where YSO represents Y_2SiO_5) in Fraval *et al.* (2005). Going even further and really implementing the whole protocol at such time scales is likely to be extremely challenging. There is thus strong motivation to try to invent protocols that allow faster generation of long-distance entanglement. Section III is dedicated to various such proposals.

D. Discussion—Limitations

Motivated by the results in the last section, we now describe several limitations of the DLCZ protocol, which have become starting points for further developments that will be described in Sec. V.

(i) There is a trade-off between high fidelity of the distributed state and high distribution rate. We have seen that the errors due to multiple emissions from individual ensembles grow quadratically with the number of elementary links N. In order to suppress these errors, one then has to work with very low emission probability p, which limits the achievable rate. This quadratic growth of the multiphoton errors is related to

the fact that the vacuum component in the created single-photon entangled state grows linearly with N; cf. the discussion at the end of Appendix B. In Secs. III.A, III.B, and III.F, we will see schemes where the vacuum component remains constant, and, as a consequence, the multiphoton errors grow only linearly with N, thanks to the use of entanglement swapping operations based on two-photon detections instead of a single-photon detection. In Sec. III.E we review a scheme where multiphoton errors are greatly reduced through the use of single-photon sources, which can be effectively realized with atomic ensembles.

(ii) The entanglement creation between two remote ensembles requires interferometric stability over long distances. To illustrate the challenge this represents, consider an elementary link with $L_0 = 125$ km. The entanglement in Eq. (11) depends on the phase $\theta_2 - \theta_1$, the contribution to which the given elementary link can be rewritten as $[\theta_{B_2}(t_2) - \theta_{B_1}(t_1)] - [\theta_{A_2}(t_2) - \theta_{A_1}(t_1)]$. We have defined t_1 (t_2) as the moment where the first (second) single-photon entangled state Eq. (8) was created in the elementary link. The phase thus has to remain stable over the time scale given by the mean value of $t_2 - t_1$, which is $L_0/(cP_0)$. For the considered example, this gives $\langle t_2 - t_1 \rangle = 4.5$ s. Over such long time scales, both the phases of the pump lasers and the fiber lengths are expected to fluctuate significantly. This problem has to be addressed in any practical implementation of the protocol, either through active stabilization of the fiber lengths, or possibly through the use of self-compensating Sagnac-type configurations; see Sec. V.F. The described problem stems from the fact that in the DLCZ protocol long-distance entanglement is generated via single-photon detections. In Secs. III.B and III.F we review schemes where entanglement is instead generated via two-photon detections, greatly reducing the stability requirements for the channels.

(iii) We have argued before that in the DLCZ repeater protocol one is *a priori* limited to a single entanglement generation attempt per elementary link per time interval L_0/c. In Secs. III.C and III.D we will describe how this limitation can be overcome using memories that can store a large number of distinguishable modes; see Sec. III.C.

(iv) For long communication distances to be realistic, the wavelength of the Stokes photons has to be in the optimal range for telecom fibers (about 1.5 μm). This either severely restricts the choice of atomic species or forces one to use wavelength conversion techniques (Tanzilli *et al.*, 2005), which for now are not very efficient at the single-photon level, mostly due to coupling losses. In Sec. III.C we describe how this requirement can be overcome by separating entanglement generation and storage.

III. IMPROVEMENTS

In this section we review various improvements to the DLCZ protocol that have been proposed over the past few years. We discuss only architectures that use essentially the same ingredients, i.e., atomic ensembles, linear optics, and photon counting, but that use them in different ways in order to achieve improved performance. We have seen that in the DLCZ protocol both entanglement generation and swapping are based on a single-photon detection. Section III.A describes a protocol where entanglement is swapped based on two-photon detections, which leads to a constant (rather than growing) vacuum component in the created state, resulting in an improvement in the overall entanglement distribution rate. Section III.B describes protocols where entanglement is moreover generated based on two-photon detections, leading to enhanced robustness with respect to phase fluctuations in the channel. Sections III.C and III.D are devoted to multiplexing. Section III.C reviews the idea of using memories that can store multiple temporal modes. Such memories can be realized using inhomogeneously broadened atomic ensembles in certain solid-state systems. Their use in the present context is made possible by the realization that a DLCZ-type atomic ensemble can be emulated by combining a photon-pair source with a memory that can absorb and emit photons. This approach promises a great enhancement in the entanglement generation rate. Section III.D reviews work on spatial multiplexing, which would be even more powerful than the temporal variety. Section III.E discusses a protocol based on single-photon sources, which can be effectively implemented with atomic ensembles, and which yields a significantly enhanced rate compared to the DLCZ protocol. Section III.F describes protocols that are based on effectively approximating ideal photon-pair sources with atomic ensembles, leading to both enhanced rates and greatly enhanced robustness.

A. Entanglement swapping via two-photon detections

In the previous section, it has been pointed out that entanglement swapping based on single-photon detections leads to the growth (linear with the number of links) of vacuum components in the generated state and to the rapid growth (quadratic with the number of links) of errors due to multiple emissions from individual ensembles. The vacuum components are detected at the postselection level and thus reduce the achievable rate. The multiphoton errors reduce the fidelity of the distributed states. In order to suppress these errors, one has to work with very low emission probabilities, further reducing the distribution rate. One possible way of addressing this problem is the use of entanglement swapping operations that are based on two-photon detections instead of a single detection (Z.-B. Chen *et al.*, 2007; Jiang *et al.*, 2007b; Zhao *et al.*, 2007). It turns out that in this case the vacuum component remains stationary under entanglement swapping, and the multiphoton-related errors grow only linearly with the number of links. In the present section we review the proposal of Jiang *et al.* (2007b), where the elementary entanglement is generated by single-photon detections as in the DLCZ protocol, but the entanglement swapping is based on two-photon detections. In the next subsection we discuss the proposals of Z.-B. Chen *et al.* (2007) and Zhao *et al.* (2007) where the entanglement is generated by two-photon detections as well.

1. First-level entanglement swapping

The elementary links in the protocol of Jiang *et al.* (2007b) have the same form as in the DLCZ protocol. Depending on the nesting level, two distinct swapping operations are performed. At the first swapping level, the principle of the entanglement connection is shown in Fig. 6. This requires

two ensembles at each location emitting photons with well-defined polarization: the horizontally (vertically) polarized modes are produced from upper (lower) atomic ensembles A_h and B_h (A_v and B_v). Suppose that the ensembles A_h and B_h (A_v and B_v) are entangled as in the DLCZ protocol, i.e., based on the detection of a single Stokes photon at a central station that could have been emitted by either of the two ensembles. Further suppose that entanglement between C_h and D_h (C_v and D_v) has also been heralded in the same way. The average time for the entanglement creation of these four links is $T_0 = (25/12)(1/P_0)(L_0/c)$, where $P_0 = p\eta_d\eta_t$. The prefactor $25/12$ can be obtained using the same methods as in Appendix A for four variables instead of two. In order to swap the entanglement toward the ensembles A and D, the spin wave stored in the memories B_h-B_v and C_h-C_v are read out and the emitted anti-Stokes modes, labeled b'_h-b'_v and c'_h-c'_v, are combined at a central station where they are detected in modes $d_\pm = b'_h + b'_v \pm c'_h \mp c'_v$ and $\tilde{d}_\pm = \pm b'_h \mp b'_v + c'_h + c'_v$ using the setup shown in Fig. 6. In the ideal case, a twofold coincident detection between d_+ and $\tilde{d}_+$ projects the state of the two remaining spin-wave modes nondestructively into

$$|\Psi_{ad}\rangle = \frac{1}{\sqrt{2}}(s^\dagger_{ah}s^\dagger_{dh} + s^\dagger_{av}s^\dagger_{dv})|0\rangle. \tag{14}$$

This operation thus allows one to exchange single spin-wave entanglement of the form (7) with more standard two-particle entanglement of the form (14). However, only 4 out of the 16 terms in the Schmidt decomposition of $|\psi_{ahbh}\rangle \otimes |\psi_{avbv}\rangle \otimes |\psi_{chdh}\rangle \otimes |\psi_{cvdv}\rangle$ have a contribution to the output state, the remainders being eliminated by projective measurement, reducing the success probability for entanglement swapping to $1/8$. Taking into account nonunit detector efficiency and memory recall, one can get the expected coincident detection when more than two spin waves are stored in the memories B and C but only two are detected. In this case, the created state contains additional terms including single spin-wave modes and a vacuum component

$$\rho^1_{ad} = c^1_2|\Psi_{ad}\rangle\langle\Psi_{ad}| + c^1_1(|s_{ah}\rangle\langle s_{ah}| + |s_{av}\rangle\langle s_{av}| + |s_{dh}\rangle\langle s_{dh}| + |s_{dv}\rangle\langle s_{dv}|) + c^1_0|0\rangle\langle 0|, \tag{15}$$

where $c^1_2 = \eta^2/8P_1$, $c^1_1 = (1-\eta)\eta^2/16P_1$, and $c^1_0 = (1-\eta)^2\eta^2/8P_1$. We have introduced a superscript 1 to label the level of the entanglement swapping. The probability for the successful preparation of this mixed state is $P_1 = (1/8)\eta^2(2-\eta)^2$.

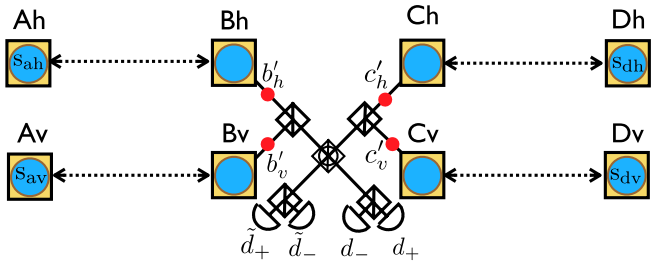

FIG. 6 (color online). First-level entanglement swapping based on a two-photon detection. Long-distance entanglement between the ensembles located at A and B (C and D) is created via single-Stokes-photon detections following the DLCZ protocol; see Fig. 3. The subscript h or v refers to horizontal or vertical polarization. The spin-wave excitation stored in atomic ensembles B_h,B_v,C_h,C_v are read out, and the corresponding anti-Stokes photon in modes b'_h,b'_v,c'_h,c'_v are combined at a central station using the setup shown. Vertical bars within squares label polarizing beam spitters (PBSs) that transmit (reflect) h- (v-) polarized photons. The central PBS with a circle performs the same action in the $\pm 45°$ basis. The coincident detection between modes d_+ and $\tilde{d}_+$ heralds the storage of two excitations (s_{ah}-s_{dh} or s_{av}-s_{dv}), either in the ensembles A_h and D_h or in the ensembles A_v and D_v; cf. Eq. (14).

2. Higher-level entanglement swapping

For further distribution over longer distances of the previous two spin-wave entangled states, one uses the setup shown in Fig. 7. To illustrate the higher-level swapping operations, suppose that two spin-wave entangled states of the form (14) are distributed between ensembles A-D and E-H leading to the state $|\Psi_{ad}\rangle \otimes |\Psi_{eh}\rangle$. This entanglement can be swapped toward the ensembles A-H by combining two anti-Stokes photons at a central station, where one photon is released from the D ensembles and the other from the E ensembles, and performing a projective measurement onto the modes $d'_h \pm e'_v$ and $e'_h \pm d'_v$. The twofold coincident detection between $d'_h + e'_v$ and $e'_h + d'_v$, for example, collapses the two remaining full memories into $|\Psi_{ah}\rangle = (1/\sqrt{2})(s^\dagger_{ah}s^\dagger_{hh} + s^\dagger_{av}s^\dagger_{hv})|0\rangle$.

Using the same set of linear optics and detectors shown in Fig. 7, one can perform successive entanglement swapping operations, such that the state $|\Psi_{az}\rangle$ can be distributed over the full distance after n swapping steps, between the locations A and Z. Because of imperfect detection and memory efficiency, the distributed state ρ^n_{az} includes single spin-wave and vacuum modes. One can show that their weights c^n_2, c^n_1, and c^n_0 are unchanged compared to the weights c^1_2, c^1_1, and c^1_0. Indeed, the condition for having a stationary state is $c_0c_2 = 4(c_1)^2$, which is fulfilled by c^1_2, c^1_1, and c^1_0. This is in contrast to the DLCZ protocol, where the vacuum component is amplified (approximately doubled) through every entanglement swapping operation; see Sec. II. The success probability for the ith entanglement connection is therefore given by $P_i = 2\eta^2(c^1_2/2 + c^1_1)^2 = \eta^2/2(2-\eta)^2$, for $i > 1$. The

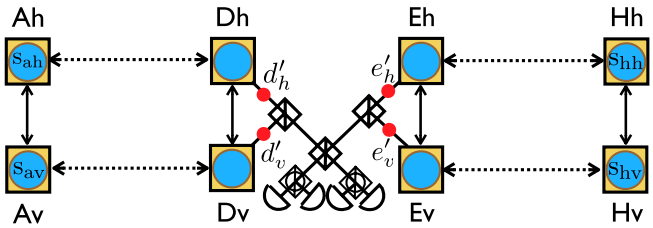

FIG. 7 (color online). Higher-level entanglement swapping based on a two-photon detection. The ensembles located at A and D (E and H) are entangled based on the principle shown in Fig. 6 and are described by the state $|\Psi_{ad}\rangle$ ($|\Psi_{eh}\rangle$) [see Eq. (14)]. The spin waves stored in ensembles D_h, D_v, E_h, and E_v are converted back into anti-Stokes photons, which are combined using the set of linear optics shown. A twofold coincident detection between $d'_h + e'_v$ and $e'_h + d'_v$ nondestructively projects the ensembles A and H into the state $|\Psi_{ah}\rangle$.

entangled component $|\Psi_{az}\rangle$ of the distributed state ρ_{az}^n can be postselected subsequently. The probability for such a successful postselection is $P_{ps} = \eta^2 c_2^n = \eta^2/(2-\eta)^2$.

3. Performance

Using the expressions of T_0, P_1, and P_i for $n \geq i > 1$, and P_{ps}, one can write T_{tot} as

$$T_{\text{tot}} = \frac{50}{3} 3^{n-1} \frac{L_0}{c} \frac{(2-\eta)^{2(n-1)}}{p\eta_t \eta_d \eta^{2n+2}}. \tag{16}$$

As in the DLCZ protocol, one has to take into account the possible errors due to multiple-pair emissions within an elementary link. The fidelity of the distributed state that one wants fixes the value for the success probability p of the Stokes emission that one can use to estimate the distribution rate based on Eq. (16). It is shown by Jiang *et al.* (2007b) that the errors grow linearly only with the number of elementary links, whereas they grow quadratically with the number of links when entanglement connection is based on single-photon detections, as seen before for the DLCZ protocol. This improved scaling is related to the fact that the vacuum component is stationary in the present protocol, since the errors in the final state arise from the interaction of the vacuum and multiphoton components; see Appendix B.

The protocol of Jiang *et al.* (2007b) begins to outperform direct transmission (with a 10 GHz single-photon source as before) for a distance of 610 km, achieving an entanglement distribution time of 190 s; see also Fig. 18 in Sec. IV. Here we assume the same values of $\eta_m = 0.9$ and $\eta_d = 0.9$ as before, and the same desired final fidelity $F = 0.9$. The optimum number of links for this distance is four. This is about a factor of 4 faster than the performance of the DLCZ protocol; however, it is clearly still a very long time for creating a single entangled pair, which moreover is probably still out of reach for realistic quantum memory storage times. The advantage compared to the DLCZ protocol is larger for longer distances, but, of course, the overall entanglement distribution times are even longer.

The main reason why the improvement is so relatively modest is that errors in the elementary link due to multiple excitations still force one to work with low emission probability p. The optimum value for four links is $p = 0.037$ (Jiang *et al.*, 2007b), compared to $p = 0.010$ for the DLCZ protocol. Multiple excitations are hard to detect in the entanglement generation process (which is the same as in the DLCZ protocol), because the corresponding Stokes photons have to propagate far and are lost with high probability. Moreover, the entanglement generation based on a single-photon detection also leads to the phase stability issues discussed at the end of the previous section. It is then natural to consider changing the elementary link. This is the topic of the next section.

B. Entanglement generation via two-photon detections

Simultaneously with the proposal by Jiang *et al.* (2007b), several schemes were proposed where not only the entanglement swapping but also the elementary entanglement generation step is done via a two-photon detection (Z.-B. Chen *et al.*, 2007; Zhao *et al.*, 2007). This approach was inspired by earlier proposals for entanglement creation between distant atoms or ions based on two-photon detections (Duan and Kimble, 2003; Feng *et al.*, 2003; Simon and Irvine, 2003). The main advantage of generating entanglement in this way is that long-distance phase stability is no longer required. In the protocols discussed so far the detection of a single photon that could have come from either of two distant locations creates a single delocalized atomic excitation whose entangled nature depends on the propagation phases of the photon for the two possible paths. In contrast, in the present case entanglement between two distant memories is generated by projecting two photons, one coming from each location, into an entangled state of their internal degrees of freedom. This operation, and thus the created long-distance entanglement, is insensitive to the propagation phases of the two photons, which only contribute an irrelevant global phase to the pair wave function.

In this section we will focus on the protocol presented in Sec. III.B of Z.-B. Chen *et al.* (2007) because it is very similar to the protocol of Jiang *et al.* (2007b) and achieves a better performance than the simpler protocol of Zhao *et al.* (2007), which we will also discuss briefly. The protocol of Sec. III.C of Z.-B. Chen *et al.* (2007), which is based on the local preparation of entangled pairs, followed by two-photon entanglement generation and swapping, and its improved version by Sangouard *et al.* (2008b), which achieves significantly better performance while being equally robust, are discussed separately in Sec. III.F.

1. Principle

Interestingly, even though it was proposed simultaneously and independently, the protocol of Sec. III.B of Z.-B. Chen *et al.* (2007) can be presented as a simple variation of the protocol of Jiang *et al.* (2007b) discussed in the previous section, in which the entanglement generation step of Jiang *et al.* (2007b) is performed locally and the first entanglement swapping step of Jiang *et al.* (2007b) is performed remotely.

At each node, one needs four ensembles, say A_h, A_v, B_h, and B_v at location AB and C_h, C_v, D_h, and D_v at location CD as in Fig. 7, except that the A and B ensembles are close to each other, but far from the ensembles C and D. At each node, the ensembles with identical subscripts are entangled by sharing a single spin-wave excitation, leading to the state $|\psi_{ahbh}\rangle \otimes |\psi_{avbv}\rangle \otimes |\psi_{chdh}\rangle \otimes |\psi_{cvdv}\rangle$.

The average waiting time for the creation of this state is given by $T_{\text{prep}} = (25/12)(1/rP_s)$, with r the repetition rate of the elementary sources and $P_s = p\eta_d$. The prefactor $25/12$ is a very good approximation for $P_s \ll 1$. It can be obtained using the same methods as in Appendix A for four variables instead of two. Note that multiple emissions from the same ensemble are detected with high probability, in contrast to the two previous protocols, since the corresponding Stokes photon does not propagate far and thus does not undergo significant losses.

Entanglement over the distance between AB and CD is now generated using the setup shown in Fig. 8, i.e., by converting the atomic excitation stored in the B and C ensembles into anti-Stokes photons followed by the detection in modes $d_\pm$ and $\tilde{d}_\pm$. Taking into account imperfections of

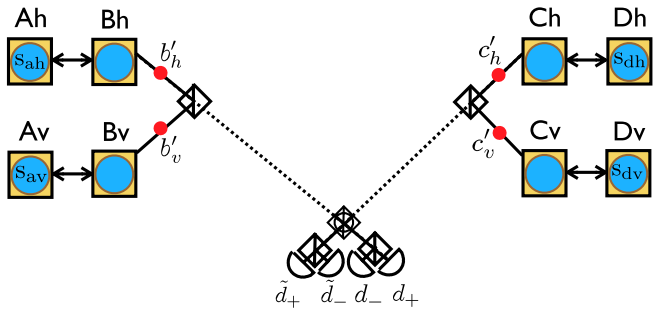

FIG. 8 (color online). Setup for entanglement creation based on two-photon detection as proposed by Z.-B. Chen *et al.* (2007), Sec. III.B. The ensembles A_h and B_h, as well as A_v and B_v, where all four ensembles are located at the same node AB, are entangled two by two as in the DLCZ protocol; see Fig. 3. The ensembles A_h-B_h (A_v-B_v) store a single delocalized photon with horizontal (vertical) polarization. In a similar way, the ensembles C_h and D_h (C_v and D_v), located at a different node CD, have been entangled independently. The excitations stored in the ensembles B_h,B_v,C_h,C_v are read out, and the resulting photonic modes are combined at a central station using the setup shown. Ideally, the coincident detection of two photons in d_+ and $\tilde{d}_+$ projects nondestructively the atomic cells A-D into the entangled state $|\Psi_{\mathrm{ad}}\rangle$ of Eq. (14).

detectors and memories, the twofold coincident detection d_+-$\tilde{d}_+$ projects the state of the ensembles A and D into

$$\rho^0_{ad} = c^0_2|\Psi_{ad}\rangle\langle\Psi_{ad}| + c^0_1(|s_{ah}\rangle\langle s_{ah}| + |s_{av}\rangle\langle s_{av}| + |s_{dh}\rangle\langle s_{dh}| + |s_{dv}\rangle\langle s_{dv}|) + c^0_0|0\rangle\langle 0|, \quad (17)$$

where $c^0_2 = 1/(2-\eta\eta_t)^2$, $c^0_1 = (1-\eta\eta_t)/2(2-\eta\eta_t)^2$, and $c^0_0 = (1-\eta\eta_t)^2/(2-\eta\eta_t)^2$. The probability for the successful preparation of this mixed state is $P_0 = (1/8)\eta^2\eta_t^2(2-\eta\eta_t)^2$.

Figure 7 shows how, using the same combination of linear optical elements as for the previous protocol, one can perform successive entanglement swapping operations in order to distribute the state ρ^n_{az} after n swapping operations. In analogy to the protocol of Jiang *et al.*, the state ρ^n_{az} includes vacuum and single spin-wave components with unchanged weights with respect to the initial ones, i.e., $c^i_2 = c^0_2$, $c^i_1 = c^0_1$, and $c^i_0 = c^0_0$ where the superscript i refers to the ith swapping. The probability for the swapping operation to succeed is given by $P_i = 2\eta^2[(c^0_2/2) + c^0_1]^2 = \eta^2/2(2-\eta\eta_t)^2$. Finally, one can perform a postselection of the entangled component $|\Psi_{az}\rangle$ of the state ρ^n_{az}. The probability for the successful postselection is given by $P_{ps} = \eta^2 c^n_2 = \eta^2/(2-\eta\eta_t)^2$.

2. Performance

Taking into account the expressions of P_0 and P_i with $n \geq i \geq 1$, and P_{ps}, one can write T_{tot} as

$$T_{\mathrm{tot}} = 8 \times 3^n \times \frac{L_0}{c}\frac{(2-\eta\eta_t)^{2n}}{\eta_t^2\eta^{2n+4}}. \quad (18)$$

For this formula to be strictly valid, the time T_{prep} required to prepare entanglement between local ensembles has to be negligible compared to the communication time; i.e., in our case $T_{\mathrm{prep}} = 25/12rp\eta_d \ll L_0/c$, with r the repetition rate with which the ensembles are excited. Otherwise, one has to replace L_0/c by $L_0/c + T_{\mathrm{prep}}$. For a realistic source repetition rate of $r = 10$ MHz, preparation time and communication time become comparable for $p = 10^{-3}$. They did not quantify the multiphoton errors in the protocol in detail, making it difficult to say for what link number this value of p is attained. Unfortunately the results of Jiang *et al.* (2007b) on the multiphoton errors cannot be taken over directly because the strong photon loss corresponding to long-distance propagation intervenes at different stages in the two protocols, even though they are otherwise formally equivalent. For the following estimate we take the simple formula Eq. (18), which gives a lower bound for the entanglement distribution time. Since two photons have to reach the central station, the square of the transmission η_t intervenes in this formula, making the distribution time more sensitive to losses in the elementary link and thus favoring more and shorter links compared to the DLCZ protocol and the protocol of Jiang *et al.* (2007b). We limit the total number of links to 16 in order to stay in a regime where it is reasonably plausible that entanglement purification may not be required. (It is worth noting that increasing the link number improves the rate by less than a factor of 2 in the distance range that we are focusing on.) We choose the same detection and memory efficiencies, $\eta_m = \eta_d = 0.9$, as before. With all the mentioned assumptions, the protocol starts to outperform direct transmission (with a 10 GHz source, as before) for a distance of 640 km, achieving an entanglement distribution time of 610 s; see also Fig. 18 in Sec. IV. The performance in terms of rate is thus comparable to (but slightly worse than) that for the DLCZ protocol.

One important reason for the long time required is that excess photon emissions (three or four photons) in the long-distance entanglement generation step typically remain undetected due to large fiber losses. As a consequence, the generated state has large vacuum and single-photon components, which lead to small success probabilities for the subsequent swapping steps, and thus to a rather low overall entanglement distribution rate. This makes it very difficult to really profit in practice from the main advantage of the protocol, which is its increased robustness with respect to phase fluctuations in the fibers. We will see below that the protocols discussed in Sec. III.F have the same advantage in robustness while achieving much faster entanglement distribution.

3. Another protocol

As mentioned, another protocol based exclusively on two-photon detections was proposed by Zhao *et al.* (2007) simultaneously with the work by Z.-B. Chen *et al.* (2007). In the scheme of Zhao *et al.* (2007), entanglement is directly generated over long distances, without a preceding local DLCZ-type step. Since only a small excitation probability can be used for each entanglement generation attempt in order to avoid multiphoton errors, and since after each attempt one has to communicate its success or failure over a long distance, the required entanglement generation time becomes significantly longer than for the DLCZ protocol. In fact, since the success probability for every entanglement generation attempt is proportional to p^2 (where p is the emission probability as before), the entanglement distribution

time for this protocol is about a factor of $1/p^2$ longer than for the protocol of Sec. III.F. For typical link numbers p has to be smaller than 0.01 in order to avoid multiphoton errors, resulting in a factor of at least 10^4 between these two protocols; see also Fig. 18 in Sec. IV.

So far we have seen that by using improved protocols compared to the original DLCZ proposal it is possible to achieve moderately faster entanglement distribution or to eliminate the need for interferometric stability. However, the achievable rates are still far too low. The next two sections are devoted to multiplexing, an approach that holds great promise for overcoming this key difficulty.

C. Photon-pair sources and multimode memories

In this section we review an approach toward multiplexing (C. Simon *et al.*, 2007b) that starts from the realization that a DLCZ-type atomic ensemble can be emulated by the combination of a photon-pair source and a quantum memory that can absorb and reemit photons. By itself, this has the advantage of allowing greater wavelength flexibility for the memory compared to the DLCZ situation where the Stokes photon has to be emitted at a telecom wavelength. If the memory furthermore has the capacity of storing and reemitting light in a (possibly large) number of different temporal modes, the approach described below promises greatly improved entanglement distribution rates. The implementation of such memories is within reach in certain solid-state atomic ensembles, as will be discussed in more detail in Sec. V.D.

1. Separation of entanglement generation and storage

The basic element of all the protocols discussed so far is an ensemble of three-level atoms that is coherently excited in order to generate a Stokes photon by Raman scattering, heralding the storage of an atomic spin excitation that can later be reconverted into an anti-Stokes photon. Depending on the protocol, either the Stokes photon or the anti-Stokes photon is used to create entanglement between remote memories. One of these photons therefore has to propagate over long distances, and we want its wavelength to match the telecom wavelengths where the fiber attenuation is small (around 1550 nm). This gives a significant constraint on the operating wavelength of the memory. None of the quantum memories that have been demonstrated so far work at this wavelength. Possible technological solutions include the use of wavelength conversion, which, however, so far is not very efficient at the single-photon level (Tanzilli *et al.*, 2005) (primarily due to coupling losses), or the use of erbium-doped crystals as quantum memories, where initial experimental (Staudt *et al.*, 2006, 2007a, 2007b) and theoretical (Ottaviani *et al.*, 2009) investigations have been performed, but implementation of the DLCZ protocol is still a distant and uncertain prospect.

A different approach for long-distance entanglement creation was proposed by C. Simon *et al.* (2007b). It combines pair sources and absorptive memories to emulate the DLCZ protocol; see Fig. 9. The basic procedure for entanglement creation between two remote locations A and B requires one photon-pair source and one memory at each location. The sources are simultaneously and coherently excited such that each of them has a small probability $p/2$ to emit a pair, corresponding to the state

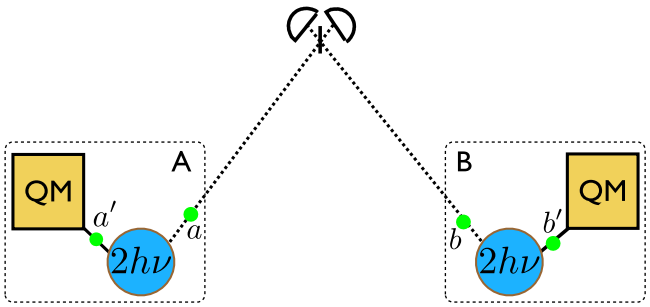

FIG. 9 (color online). Separation between entanglement creation and storage using photon-pair sources and absorptive quantum memories. Circles represent sources emitting photon pairs in modes a-a' for location A and in modes b-b' for location B. The prime modes a' and b' are stored in neighboring quantum memories (squares), whereas the modes a and b are combined on a beam splitter (vertical bar) at a central station such that the detection of a single photon in one of the output modes heralds the entanglement between the quantum memories in A and B.

$$\left[1+\sqrt{\frac{p}{2}}(a^{\dagger}a'^{\dagger}+b^{\dagger}b'^{\dagger})+O(p)\right]|0\rangle. \tag{19}$$

Here a and a' (b and b') are two modes, corresponding, e.g., to two different directions of emission (Fig. 9). The $O(p)$ term describes the possibility of multiple-pair emissions. It introduces errors in the protocol, implying that p has to be kept small, in analogy with the DLCZ protocol. The modes a' and b' are stored in local memories, whereas the modes a and b are combined on a beam splitter at a central station. The modes a and b should thus be at telecom wavelength, but there is no such requirement for the modes a' and b'. Similar to the entanglement creation in the DLCZ protocol, the detection of a single photon after the beam splitter heralds the storage of a single photon in the memories A and B, leading to the state (8). Note that we have set the phases to zero for simplicity. The entanglement can be extended to longer distances by successive entanglement swapping as in the DLCZ protocol. The required photon-pair sources could be realized with atomic ensembles. For example, Chanelière *et al.* (2006) have proposed to use a specific atomic cascade in Rb for which the first photon has a wavelength of 1.53 μm. There are also convenient ways of implementing pair sources not based on atomic ensembles, notably parametric down-conversion (Burnham and Weinberg, 1970; Hong and Mandel, 1985; Wu *et al.*, 1986; Hong *et al.*, 1987) in nonlinear optical crystals, which allows a lot of wavelength flexibility. Pair sources can also be realized based on the DLCZ protocol, by applying the write and read pulses with a small time interval or even simultaneously; see Sec. V.

2. Protocol with temporal multimode memories

In Sec. II.D we pointed out that in the DLCZ protocol one is *a priori* limited to a single entanglement generation attempt per communication time interval L_0/c, because the memories have to be emptied after every unsuccessful attempt. The same is true for the protocols of Secs. III.A and III.B. The

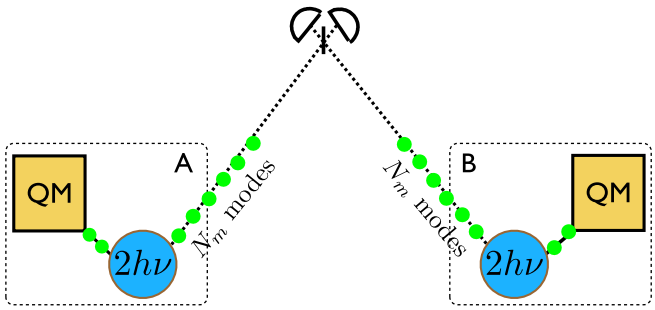

FIG. 10 (color online). Entanglement creation with temporal multimode memories. The source can be triggered a large number of times in every communication time interval $\frac{L_0}{c}$. One mode from each pair is sent to the central station, and the other one is stored in the multimode memory.

architecture described in the present section is particularly well adapted for temporal multiplexing, which overcomes this limitation; see Fig. 10. If the memories can store not only one mode but a train of pulses, one can trigger the sources many times per communication time L_0/c, potentially creating pairs into modes a_i and a_i' (b_i and b_i'), where i ($i = 1, \ldots, N_m$) labels the corresponding "time bin," and N_m is the total number of temporal modes. All the modes a_i' and b_i' are stored in the respective memories at A and B. Any of the modes a_i or b_i can now give rise to a detection after the central beam splitter. This leads to an increase of the entanglement generation probability P_0 by a factor of N_m (for $N_m P_0 \ll 1$), which directly translates into an increase of the entanglement distribution rate by the same factor. The speedup is thus achieved at the most elementary level, that of entanglement generation. As a consequence, the same principle could also be applied to other quantum repeater protocols, although the technological challenges vary depending on the protocol; see below.

In order to do entanglement swapping using multimode memories, one has to be able to recombine exactly those modes, whose partners have given rise to a detection, and thus a successful entanglement generation, in the respective links; see Fig. 11. If this is ensured, entanglement swapping can again proceed in analogy with the DLCZ protocol. Temporal multimode memories with the required characteristics can be realized, for example, based on the photon-echo principle in inhomogeneously broadened solid-state atomic ensembles (notably in rare-earth-ion-doped crystals). A particularly promising approach toward the efficient realization of such memories is based on "atomic frequency combs" (Afzelius *et al.*, 2009). This is discussed in more detail in

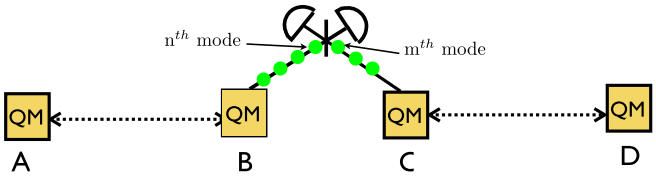

FIG. 11 (color online). Entanglement swapping with temporal multimode memories. One has to be capable of recombining at the beam splitter exactly those modes whose partners have participated in a successful entanglement generation at the lower level.

Sec. V.D. In addition to the requirements on memory efficiency and storage time discussed previously, an important characteristic for such a multimode memory is its bandwidth, since this may limit the number of modes that can be stored in a given time interval L_0/c, even if the memory is in principle capable of storing more modes. This is not a major limitation for the present protocol. Afzelius *et al.* (2009) argue, for example, that a memory based on an Eu-doped crystal with a bandwidth of 12 MHz (limited by hyperfine transition spacings in Eu) would be capable of storing a train of $N_m = 100$ pulses with a total length of 50 μs, which is still much shorter than the communication time for a typical link length $L_0 = 100$ km, which is of order 500 μs, taking the reduced speed of light in the fiber into account. Note that a first experimental demonstration of an interface with $N_m = 32$ was recently performed in a Nd-doped crystal (Usmani *et al.*, 2010). Assuming $N_m = 100$, and $\eta_m = \eta_d = F = 0.9$ as before, the protocol of C. Simon *et al.* (2007b) starts to outperform direct transmission (assuming the usual 10 GHz single-photon source) for a distance of 510 km, achieving an entanglement distribution time of 1.4 s, using a repeater architecture with four elementary links; see also Fig. 18 in Sec. IV. This is a significantly improved rate compared to the previous sections. Moreover, this time scale is also much more compatible with realistically achievable quantum memory times (Fraval *et al.*, 2005; Longdell *et al.*, 2005), as mentioned and discussed in more detail in Sec. V.

The present protocol closely follows the original DLCZ protocol, in particular, relying on entanglement generation via a single-photon detection, leading to similar phase stability issues, even though they are somewhat reduced by the shorter time scale of entanglement distribution. It is natural to ask whether it is possible to implement multimode versions of more robust protocols, such as those of Sec. III.B or that (still to be discussed) of Sec. III.F. This may well be possible. It is, however, more challenging than for the present protocol, mainly because the fastest robust protocols rely on the local preparation of stored single-photon (Sec. III.B) or two-photon (Sec. III.F) entanglement. Such preparation requires a lot of repetitions, which reduces the time available for temporal multiplexing per time interval L_0/c.

D. Spatially multiplexed memories

For temporal multimode memories as described in the previous section, the gain in entanglement distribution time is due to the lowest level of the repeater protocol, as P_0 is enhanced by a factor of N_m. All higher levels of the protocol are unchanged with respect to the protocols without multiplexing. Collins *et al.* (2007), which was published before C. Simon *et al.* (2007b), studied a more far-reaching form of multiplexing, which might be possible, in particular, in the spatial domain. They envisioned a situation where several different subensembles of the DLCZ type can be addressed completely independently. In particular, photons can be retrieved independently from each subensemble and combined at will. Most importantly, even when some of the subensembles have been "filled," i.e., entangled atomic excitations that involve these subensembles have been created, one can use others that are still empty to make new attempts at

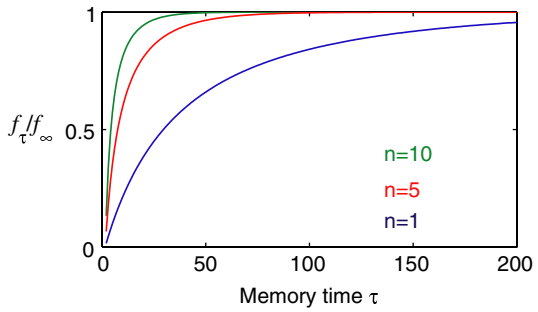

FIG. 12 (color online). Reduced memory time requirements due to spatial multiplexing. The horizontal axis corresponds to the memory storage time τ, which is measured in units of L_0/c. The vertical axis shows the ratio of the repeater rate for storage time τ, labeled f_τ, over the ideal rate for infinite storage time, labeled f_∞. n is the number of multiplexed memories per site. Memory time requirements for strictly parallel operation always correspond to $n = 1$. From Collins *et al.*, 2007.

entanglement creation. There is no known way of implementing such a step-by-step "accumulation" of stored entanglement in the temporal multimode case. The temporal multimode memories discussed in the previous section can be charged only once (although with a large number of modes), and then they have to be read out before being useful again; see Sec. V.

Collins *et al.* (2007) compared such strongly multiplexed repeaters to the case where N_r completely independent repeater architectures are used in parallel (for which the rate enhancement is exactly equal to N_r, of course). They found a moderate advantage in terms of rate for the strongly multiplexed case, without explicitly quantifying the advantage. Note that Jiang *et al.* (2007b) addressed the same question in Sec. V of their paper and find a scaling of the entanglement distribution rate with $N_r^{1.12}$ instead of N_r, which is consistent with the modest improvement found by Collins *et al.* (2007). However, Collins *et al.* (2007) also showed that there is a very significant advantage for the multiplexed approach in terms of the necessary memory time. Whereas for strictly parallel repeaters the necessary memory times are determined by the waiting times for each repeater individually (and thus are extremely long), the multiplexed architecture leads to greatly reduced requirements on the storage times; see Fig. 12. Initial experimental efforts toward spatial multiplexing are described in Sec. V.B.2. Further theoretical work includes Surmacz *et al.* (2007) and Vasilyev *et al.* (2008). The ideal in the long run would clearly be to combine temporal and spatial multiplexing in the same system, in order to maximize potential quantum repeater rates. Multiplexing of different completely independent frequency channels is another attractive possibility, in particular, for the inhomogeneously broadened solid-state ensembles that are being investigated in the context of temporal multimode storage.

E. Protocol based on a single photon source

In Sec. II and Appendix B it was shown that multiphoton emission events impose significant limitations on the performance of the DLCZ protocol. Motivated by this fact, Sangouard *et al.* (2007b) suggested a protocol based on single-photon sources, which makes it possible to eliminate such errors. The protocol was conceived for ideal single-photon sources. However, a good approximation of such a source can be implemented with atomic ensembles. The resulting scheme leads to a significantly improved entanglement distribution rate compared to the DLCZ protocol. In the following we first describe the ideal protocol and its performance; then we discuss how to implement a single-photon source to good approximation with atomic ensembles.

1. Principle

The architecture of the scheme proposed by Sangouard *et al.* (2007b) is shown in Fig. 13. The locations A and B each contain one single-photon source and one memory. When they are excited, each of the two sources ideally creates one photon that is sent through a beam splitter with reflection and transmission coefficients α and β satisfying $|\alpha|^2 + |\beta|^2 = 1$, such that after the beam splitters, the state of the two photons is $(\alpha a'^\dagger + \beta a^\dagger)(\alpha b'^\dagger + \beta b^\dagger)|0\rangle$, which can be developed as

$$(\alpha^2 a'^\dagger b'^\dagger + \alpha\beta(a^\dagger b'^\dagger + a'^\dagger b^\dagger) + \beta^2 a^\dagger b^\dagger)|0\rangle. \quad (20)$$

The modes a', b' are stored in local memories. The modes a, b are coupled into optical fibers and combined on a beam splitter at a central station, with the modes after the beam splitter denoted by $d = (1/\sqrt{2})(a + b)$ and $\tilde{d} = (1/\sqrt{2})(a - b)$, as before. We are interested in the detection of one photon, for example, in mode d. We detail separately the contributions from the three terms in Eq. (20). The term $a'^\dagger b'^\dagger|0\rangle$, which corresponds to two full memories, cannot generate the expected detection and thus does not contribute to the entanglement creation. The term $(a^\dagger b'^\dagger + a'^\dagger b^\dagger)|0\rangle$ may induce the detection of a single photon in mode d with probability $\alpha^2\beta^2\eta_t\eta_d$. Such detection creates the desired

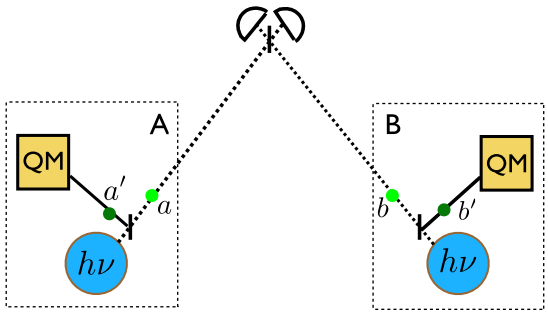

FIG. 13 (color online). Entanglement creation between two remote ensembles located at A and B based on single-photon sources. Circles represent single-photon sources. A single photon is generated at each location and sent through an asymmetric beam splitter with small transmission and high reflectivity, leading to a superposition of modes a and a' (b and b') at location A (B). The modes a' and b' are stored in local memories, whereas a and b are sent to a central station where they are combined on a 50:50 beam splitter. The detection of a single photon at the central station heralds the storage of the second one within the memories with high probability, due to the asymmetry of the local beam splitters. This creates the entanglement of the two remote memories that share a single excitation.

state $(1/\sqrt{2})(a'^{\dagger}+b'^{\dagger})|0\rangle$ associated with entangled memories. Finally the term $a^{\dagger}b^{\dagger}|0\rangle$ may also produce a single photon in mode d if one of the two photons is lost. The probability that this term produces the expected detection is approximately $\beta^4\eta_t\eta_d$, since for long distances $\eta_t \ll 1$. This detection heralds the vacuum state $|0\rangle$ for the remaining modes a' and b'. Taking into account all these contributions, the state created by the detection of a single photon in mode d is thus given by

$$\alpha^2|\psi_{ab}\rangle\langle\psi_{ab}| + \beta^2|0\rangle\langle 0|, \tag{21}$$

where $|\psi_{ab}\rangle = (1/\sqrt{2})(a'^{\dagger}+b'^{\dagger})|0\rangle$. The state $|\psi_{ab}\rangle$ describes the entanglement of the two memories located at A and B, while the vacuum state $|0\rangle$ corresponds to empty memories. We emphasize that none of the three terms in Eq. (20) leads to an error of the form $a'^{\dagger}b'^{\dagger}|0\rangle$. This is a crucial difference compared to the DLCZ protocol; see Appendix B. By considering both detections in modes d and $\tilde{d}$, one can show that the success probability for entanglement creation in an elementary link is $P_0 = 2p_1\beta^2\eta_t\eta_d$, with p_1 the probability that the source emits one photon ($p_1 = 1$ in the ideal case).

The further steps are as for the DLCZ protocol: Neighboring links are connected via entanglement swapping, creating the entanglement between two distant locations A and Z. One shows that the success probability for entanglement swapping at the ith level is given by

$$P_i = \frac{p_1\alpha^2\eta}{2}\frac{[2^i-(2^i-1)p_1\alpha^2\eta]}{[2^{i-1}-(2^{i-1}-1)p_1\alpha^2\eta]^2}$$

(with $i \geq 1$). Moreover, each location contains two memories, denoted A_1 and A_2 for location A, etc. Entangled states of the given type are established between A_1 and Z_1 and between A_2 and Z_2. By postselecting the case where there is one excitation in each location, one generates an effective state of the form

$$\frac{1}{\sqrt{2}}(|1_{A_1}1_{Z_2}\rangle + |1_{A_2}1_{Z_1}\rangle). \tag{22}$$

The probability for a successful projection onto the state Eq. (22) is given by

$$P_{ps} = \frac{\eta^2}{2}\frac{(p_1\alpha^2)^2}{[2^i-(2^i-1)p_1\alpha^2\eta]^2}.$$

The vacuum component in Eq. (21) does not contribute to this final state, since if one of the two pairs of memories contains no excitation, it is impossible to detect one excitation in each location. The vacuum components thus have no impact on the fidelity of the final state. This is not the case for components involving two full memories as in Duan *et al.* (2001) and C. Simon *et al.* (2007b), which may induce one excitation in each location and thus decrease the fidelity. Note that vacuum components, which exist for the single-photon source protocol already at the level of the elementary links, occur for the DLCZ protocols as well, starting after the first entanglement swapping procedure.

2. Performance

As previously indicated before, the absence of fundamental errors proportional to the entanglement creation probability leads to significantly improved entanglement distribution rates for the single-photon source protocol with respect to the DLCZ protocol. We now discuss this improvement quantitatively. The weight of the vacuum component at each nesting level is larger in the single-photon source protocol, and thus the success probabilities P_i (with $i \geq 1$) for entanglement swapping are somewhat lower. However, the probability P_0 can be made much larger than in the photon-pair source protocols. Overall, this leads to higher entanglement distribution rates, as we detail now. Taking into account the expression of P_0, P_i, and P_{ps}, one can show that the total time required for entanglement distribution with the single-photon protocol is

$$T_{\text{tot}} = \frac{3^{n+1}}{2}\frac{L_0}{c}\frac{\prod_{k=1}^{n}(2^k-(2^k-1)p_1\alpha^2\eta)}{\eta_d\eta_t p_1^{n+3}\beta^2\alpha^{2n+4}\eta^{n+2}}. \tag{23}$$

Assuming $\eta_m = \eta_d = p_1 = 0.9$ as before, the present protocol starts to outperform direct transmission (with a 10 GHz single-photon source) for a distance of 580 km, achieving an entanglement distribution time of 44 s, with a repeater composed of four links and a beam-splitter transmission $\beta^2 = 0.16$; see also Fig. 18 in Sec. IV. This is about an order of magnitude faster than the DLCZ protocol. The significant improvement compared to the DLCZ protocol can be understood as due to a higher value of P_0 (9.2×10^{-3} as opposed to 3.4×10^{-4} for DLCZ). On the other hand, the vacuum component is larger in the present protocol, reducing the success probability for the swapping operations, which is why the improvement is not as large as the difference in P_0.

3. Implementation of the single-photon-source protocol with atomic ensembles

In Sec. II we explained how the emission of a Stokes photon in a DLCZ-type atomic ensemble creates a single stored atomic excitation and how this atomic excitation can subsequently be reconverted into a photon. This implies that an ensemble charged with a single excitation can serve as a single-photon source. The efficiency of this source reduces to the memory readout $p_1 = \eta_m$. The possibility of multiphoton emissions, which can go undetected even for photon-number-resolving detectors since they do not have perfect efficiency in practice, means that this source is not ideal, but that there is a two-photon contribution with an amplitude given by $p_2 = 2p(1-\eta_d)\eta_m$, where p is the emission probability for the Stokes photon, η_m is the memory efficiency, and η_d is the efficiency of the detector that detects the Stokes photon and thus announces that the ensemble is charged. If one chooses p sufficiently small, one can therefore realize a very good approximation to an ideal single-photon source. However, this means that the excitation triggering the potential Stokes-photon emission has to be repeated many times before the ensemble is successfully charged. In an implementation one has to check whether this imposes significant limits on the distribution rate. Fortunately, this is not the case for realistic repetition rates for the Stokes emission, say 10 MHz. For a repeater with four links one can show that the maximum

value of p_2 compatible with $F = 0.9$ is $p_2 = 0.0011$, giving $p = 0.006$ for the emission probability. With a repetition rate of $r = 10$ MHz, the ensemble will thus be charged on average every $T_s = 1/rp = 18$ μs. Comparing to a typical communication time L_0/c of order 750 μs for a 150 km link, this even leaves considerable scope for temporal multiplexing, provided one has appropriate multimode memories. It should be emphasized, in particular, that in the present protocol both the source and the memory have to be at telecom wavelength. Note that a single-photon source can also be realized by combining a photon-pair source (which can be ensemble based, but also, e.g., based on parametric down-conversion) and an absorptive memory in analogy with the approach described in Sec. III.C; see also Sec. V.

4. Alternative implementation via partial readout

We presented the protocol as consisting of the creation of single photons, followed by their *partial storage*, i.e., the storage of one of the two output modes of a beam splitter. Alternatively, once the ensemble that serves as the single-photon source has been charged by the emission of a Stokes photon as previously described, it can be *partially read out*, i.e., the atomic spin waves can be partially converted back into propagating photons; see Fig. 14. In principle, this could be done using read pulses whose area is smaller than the standard π, chosen to give the same values of α and β as above. There is a subtlety concerning this idea in the usual DLCZ-type experiments because the anti-Stokes photon is typically emitted during the duration of the read pulse, so that it seems difficult to assign a fixed pulse area to the read. However, a Rabi oscillation regime was nevertheless observed by Balic *et al.* (2005) and theoretically described by Kolchin (2007) even for ensembles with large optical depth. (The optical depth of an atomic ensemble is a measure of transparency, and is defined as the negative logarithm of the fraction of light that is not absorbed by the atoms.) It may thus be possible nevertheless to pick a pulse area that corresponds to the desired values of α and β. The described idea certainly works for other kinds of memories, where readout pulse and emission are separated in time, such as the memories based on the photon-echo principle discussed in Sec. V.D.2, which is particularly relevant if the single-photon source is realized by combining a photon-pair source and an absorptive memory as discussed above. The partial readout approach discussed here is important for the protocol described in the following Sec. III.F as well.

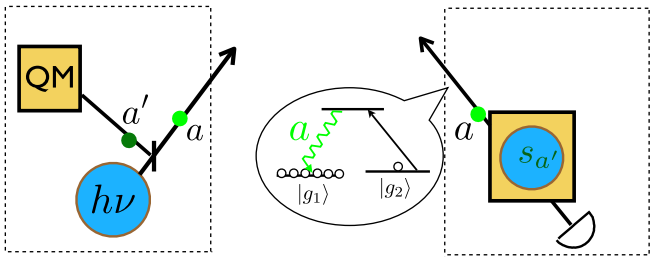

FIG. 14 (color online). Partial readout of a single collective excitation. A single-photon source whose output is partially stored in a memory, as required in the protocol of Sangouard *et al.* (2007b) described in Sec. III.E, can be emulated with a DLCZ-type atomic ensemble, in which an atomic excitation is first created, accompanied by a Stokes-photon emission, and then partially read out through the application of a read pulse with an area that is smaller than π. The same principle is also used in the protocol of Sangouard *et al.* (2008b) described in Sec. III.F.

F. Protocols based on local generation of entangled pairs and two-photon entanglement swapping

In the previous section we saw that, for quantum repeaters where the entanglement creation is based on a single-photon detection, it is advantageous to have an ideal single-photon source, or even a good approximation of such a source realized with atomic ensembles. Analogously, it is fairly natural to ask whether it might be possible to achieve an efficient repeater protocol with entanglement creation based on two-photon detections if one had an ideal photon-pair source or a good approximation of such a source implemented with atomic ensembles. This is indeed a fruitful approach.

The first such protocol was proposed in Sec. III.C of Z.-B. Chen *et al.* (2007), without an evaluation of its performance. Sangouard *et al.* (2008b) proposed an improved version of the same approach and showed that this leads to a powerful quantum repeater protocol, which both is robust under phase fluctuations and achieves the best entanglement creation time of all known nonmultiplexed protocols with ensembles and linear optics; see below.

In order to effectively realize a single-pair source, Z.-B. Chen *et al.* (2007) proposed to generate entangled pairs of atomic excitations locally by using four single-photon sources (which, as we saw in the previous section, can be realized with DLCZ-type ensembles), linear optical elements, and two quantum memories based on electromagnetically induced transparency (EIT); see Fig. 11 of Z.-B. Chen *et al.* (2007). Four photons are emitted by the ensembles serving as sources; two of them are detected, and two are absorbed again by the EIT memories. This double use of ensembles (emission followed by storage) leads to relatively large errors (vacuum and single-photon contributions) in the created state if the memory efficiencies are smaller than 1. These errors then have a negative impact on the success probabilities of the entanglement generation and swapping operations, and thus on the overall time needed for long-distance entanglement distribution.

The proposal of Sangouard *et al.* (2008b), which is based on partial readout of the memories, allows one to produce entangled pairs of atomic excitations with higher fidelity. Indeed, this scheme does not use any emission followed by storage. For the same memory and detection efficiency, it thus leads to higher-quality entangled pairs compared to the method of Z.-B. Chen *et al.* (2007), and as a consequence to a significantly improved rate for the overall quantum repeater protocol. In the following we describe the proposal of Sangouard *et al.* (2008b) in more detail and evaluate its performance.

1. Local generation of entangled pairs of atomic excitations

The proposed setup for the generation of high-fidelity entangled pairs requires four atomic ensembles. As before,

the four ensembles are repeatedly excited independently with a repetition rate r until four Stokes photons are detected, heralding the storage of an atomic spin wave in each ensemble. The Stokes photons have a well-defined polarization: The horizontally (vertically) polarized modes are labeled by $a_h^\dagger$ and $b_h^\dagger$ ($a_v^\dagger$ and $b_v^\dagger$), and are produced from upper (lower) atomic ensembles A_h and B_h (A_v and B_v) as represented in Fig. 15. The associated single atomic spin excitations are labeled by $s_{ah}^\dagger$, $s_{av}^\dagger$, $s_{bh}^\dagger$, or $s_{bv}^\dagger$ depending on the location. The average waiting time for successful charging of all four ensembles is given by $T = 25/12rp$, as can be shown by the same methods that are used in Appendix A. Thanks to the independent creation and storage, it scales only as $1/p$, with p the probability for a Stokes photon to be emitted.

Once all ensembles are charged, the four stored spin-wave modes are then partially converted back into photonic excitations, leading to the state $(\alpha a_h'^\dagger + \beta s_{ah}^\dagger) \otimes (\alpha a_v'^\dagger + \beta s_{av}^\dagger) \otimes (\alpha b_h'^\dagger + \beta s_{bh}^\dagger) \otimes (\alpha b_v'^\dagger + \beta s_{bv}^\dagger)|0\rangle$ with $|\alpha|^2 + |\beta|^2 = 1$. The primed modes $a_h'^\dagger$,$a_v'^\dagger$ ($b_h'^\dagger$,$b_v'^\dagger$) refer to the emitted anti-Stokes photons from memories located at A_h and A_v (B_h and B_v), respectively. The discussion concerning the implementation of partial readout at the end of the preceding section also applies in the present case. The released anti-Stokes photons are combined at a central station where they are detected in modes $d_\pm = a_h' + a_v' \pm b_h' \mp b_v'$ and $\tilde{d}_\pm = \pm a_h' \mp a_v' + b_h' + b_v'$, using the setup shown in Fig. 15. In the ideal case, a twofold coincident detection between d_+ and $\tilde{d}_+$ projects the state of the two remaining spin-wave modes nondestructively onto

$$|\Psi_{ab}\rangle = (1/\sqrt{2})(s_{ah}^\dagger s_{bh}^\dagger + s_{av}^\dagger s_{bv}^\dagger)|0\rangle. \tag{24}$$

The stored atomic excitations can be reconverted into photons as desired. In the proposed quantum repeater protocol, one excitation (e.g., the one in the B ensembles) is reconverted into a photon right away and used for entanglement generation. The other excitation is reconverted later for entanglement swapping or for the final use of the entanglement. Note that the setup can also be used as a source of single-photon pairs, if both excitations are converted into photons simultaneously.

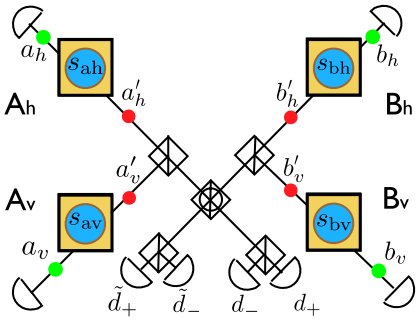

FIG. 15 (color online). Setup for generating high-fidelity entangled pairs of atomic excitations. Squares containing a circle represent atomic ensembles that probabilistically emit Stokes photons (dots). The conditional detection of a single Stokes photon heralds the storage of one atomic spin-wave excitation. In this way an atomic excitation is created and stored independently in each ensemble. Then all four ensembles are simultaneously read out partially, creating a probability amplitude to emit an anti-Stokes photon (dots). The coincident detection of two anti-Stokes photons in d_+ and $\tilde{d}_+$ projects nondestructively the atomic cells into the entangled state $|\Psi_{ab}\rangle$ of Eq. (24).

Given an initial state where all four memories are charged, the probability for a coincidence between d_+ and $\tilde{d}_+$ is given by $(1/2)\alpha^4\beta^4$. Since the twofold coincidences d_+-$\tilde{d}_-$, d_--$\tilde{d}_+$, d_--$\tilde{d}_-$ combined with the appropriate one-qubit transformation also collapse the state of the atomic ensembles into $|\Psi_{ab}\rangle$, the overall success probability for the entangled pair preparation is given by $P_s = 2\alpha^4\beta^4$.

We now analyze the effect of nonunit detector efficiency and memory recall efficiency. The waiting time for the memories to be charged is now $T^\eta = T/\eta_d = 25/12rp\eta_d$. Furthermore, the detectors can now give the expected coincidences when three or four anti-Stokes photons are released by the memories, but only two are detected. In this case, the created state contains additional terms including single spin-wave modes and a vacuum component,

$$\rho_{ab}^s = c_2^s|\Psi_{ab}\rangle\langle\Psi_{ab}| + c_1^s(|s_{ah}\rangle\langle s_{ah}| + |s_{av}\rangle\langle s_{av}| + |s_{bh}\rangle\langle s_{bh}| + |s_{bv}\rangle\langle s_{bv}|) + c_0^s|0\rangle\langle 0|, \tag{25}$$

where $c_2^s = 2\alpha^4\beta^4\eta^2/P_s^\eta$, $c_1^s = \alpha^6\beta^2\eta^2(1-\eta)/P_s^\eta$, and $c_0^s = 2\alpha^8(1-\eta)^2\eta^2/P_s^\eta$. We have introduced a superscript s for "source." The probability for the successful preparation of this mixed state is $P_s^\eta = 2\eta^2\alpha^4(1-\alpha^2\eta)^2$. The fidelity of the conditionally prepared state is equal to the two-photon component $c_2^s = \beta^4/(1-\alpha^2\eta)^2$. As can be seen from the two previous equations, there is a trade-off on the readout coefficients α, β. The creation of an entangled state with a high fidelity favors $\alpha \approx 0$, whereas a high success probability favors $\alpha \approx \beta \approx 1/\sqrt{2}$.

2. Repeater protocol using two-photon detections

We now describe how this source of heralded pairs can be inserted within a quantum repeater protocol. The setup for entanglement creation between two remote sources involving the ensembles AB and CD is shown in Fig. 16. The central station is identical to the one used for the higher-level entanglement swapping operations in the protocol of

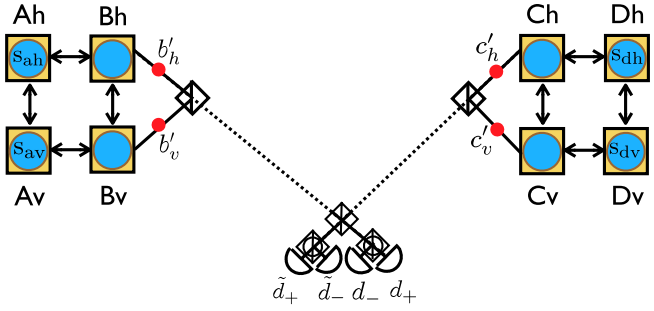

FIG. 16 (color online). Entanglement creation based on two-photon detections using two locally prepared entangled pairs. The excitations stored in the ensembles B_h,B_v,C_h,C_v are read out, and the resulting photonic modes are combined at a central station using the setup shown. Ideally, the coincident detection of two photons in d_+ and $\tilde{d}_+$ projects nondestructively the atomic cells A-D into the entangled state $|\Psi_{ad}\rangle$.

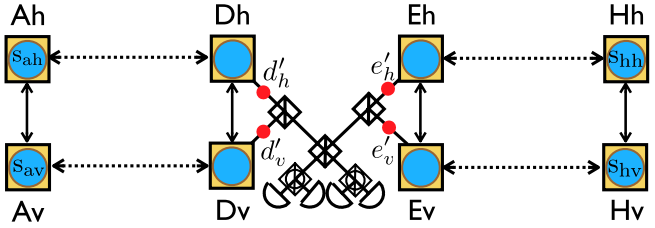

FIG. 17 (color online). Entanglement swapping based on two-photon detections. The spin waves stored in ensembles D_h,D_v,E_h, and E_v are converted back into anti-Stokes photons, which are combined using the set of linear optics shown. A twofold coincident detection between $d'_h + e'_v$ and $e'_h + d'_v$ nondestructively projects the ensembles A and H into the state $|\Psi_{ah}\rangle$.

Jiang *et al.* (2007b) (see also Sec. III.A, Fig. 7), and for all swapping operations in the protocol of Sec. III.B of Z.-B. Chen *et al.* (2007), see also Sec. III.B of the present review. Two anti-Stokes photons are combined at a central station, where one photon is released from the B ensembles and the other from the C ensembles and a projective measurement is performed into the modes $D^{bc}_{\pm} = b'_h \pm c'_v$ and $D^{cb}_{\pm} = c'_h \pm b'_v$. The twofold coincident detection D^{bc}_{+}-D^{cb}_{+} (D^{bc}_{+}-D^{cb}_{-}, D^{bc}_{-}-D^{cb}_{+}, or D^{bc}_{-}-D^{cb}_{-} combined with the appropriate one-qubit operations) collapses the two remaining full memories into $|\Psi_{ad}\rangle$. Because of imperfections, the distributed state ρ^0_{ad} includes vacuum and single spin-wave modes. The weights c^s_2, c^s_1, and c^s_0 of the source state ρ^s_{ab} satisfy $c^s_0 c^s_2 = 4(c^s_1)^2$ such that they are unchanged after the entanglement creation, as before. We thus have $c^0_2 = c^s_2$, $c^0_1 = c^s_1$, and $c^0_1 = c^s_0$. The success probability for the entanglement creation is given by $P_0 = 2\eta^2\eta_t^2(c^s_2/2 + c^s_1)^2$.

Using the same set of linear optical elements and detectors (see Fig. 17), one can perform n successive entanglement swappings such that the state ρ^n_{az} is distributed between the distant locations A and Z. In analogy to above, the distributed state ρ^n_{az} includes vacuum and single-spin-wave components with unchanged weights with respect to the initial ones, i.e., $c^n_2 = c^s_2$, $c^n_1 = c^s_1$, and $c^n_0 = c^s_0$. From the expression of P_0 and keeping in mind that the entanglement swapping operations are performed locally such that there are no transmission losses, one deduces the success probability for the ith swapping, $P_i = 2\eta^2(c^s_2/2 + c^s_1)^2$. The two-spin-wave component of the distributed mixed state $|\Psi_{az}\rangle$ is finally postselected with the probability $P_{ps} = c^s_2\eta^2$.

3. Performance

From the expressions of P_0, P_i (with $i \geq 1$), and P_{ps}, one can rewrite T_{tot} as

$$T_{\text{tot}} = 2 \times 3^n \times \left(T_s + \frac{L_0}{c}\right)\frac{(1-\alpha^2\eta)^{2(n+2)}}{\eta_t^2\eta^{2(n+2)}\beta^{4(n+2)}}. \quad (26)$$

For realistic values of the repetition rate (say $r = 10$ MHz) the source preparation time $T_s = 3T^\eta/2P^\eta_s$ will be comparable to the communication time L_0/c. With the usual assumptions $\eta_m = \eta_d = F = 0.9$, the protocol starts to outperform direct transmission with a 10 GHz single-photon source for a distance of 560 km, with an entanglement distribution time of 15 s, for a repeater with eight links, $p = 0.013$, and $\alpha^2 = 0.26$; see also Fig. 18 in Sec. IV. Note that for these values $T_s = 380$ μs and $L_0/c = 350$ μs, with $c = 2 \times 10^8$ m/s in the fiber as usual. Since the repetition rate is already limited by the source preparation time, multiplexing is difficult in the present case. However, the protocol achieves the best performance of all known nonmultiplexed protocols using only atomic ensembles and linear optics, and is moreover robust with respect to channel phase fluctuations owing to the use of two-photon detections for entanglement generation. Multiplexing would become possible if the source preparation could be accelerated, in particular, if an ideal photon-pair source (such as a single-atom cascade) in combination with an appropriate memory was available.

IV. COMPARISON AND DISCUSSION

We now compare the performance of the various proposed protocols in more detail. The first section is devoted to the time needed for entanglement distribution. Then we review the robustness of the protocols with respect to several important technological imperfections. Finally we briefly discuss the complexity of implementing the proposed protocols.

A. Entanglement distribution time

Figure 18 shows the time required for distributing a single entangled pair as a function of distance for the protocols discussed in detail in the previous sections. We have again chosen a final target fidelity $F = 0.9$. It should be noted that this takes into account only errors due to multiphoton emission, which occur in all the discussed protocols. In practice there are other sources of errors in addition, such as imperfect mode overlap and phase fluctuations, that affect different protocols differently, as previously discussed, requiring, e.g., different degrees of fiber length stabilization depending on whether entanglement is generated via single-photon or two-photon detections.

Schemes that use two-photon detections for long-distance entanglement generation are more sensitive to photon losses than schemes that use single-photon detections for the same purpose. As a consequence, two-photon protocols favor larger numbers of elementary links for the same distance compared to the single-photon schemes. In Fig. 18 we have limited the maximum number of links to 16 to make the protocols more comparable and to have link numbers for which it is plausible that entanglement purification may not be necessary. In the shown distance range, this has no effect on the performance of protocols based on single-photon entanglement generation (curves B, C, E, and F), which favor fewer links, nor on the protocol of Sangouard *et al.* (2008b) (curve G), based on two-photon detection. It has a slight effect (of order a factor of 2) for the protocol of Z.-B. Chen *et al.* (2007) (curve D).

Figure 18 shows that all protocols start to outperform direct transmission somewhere in the range 500 to 650 km. It also shows the significant differences in the required entanglement distribution time that we have already seen in Sec. III. Focusing first on protocols that create entanglement by single-photon detection, one can see the improvement in going from the original DLCZ protocol (curve B) to the

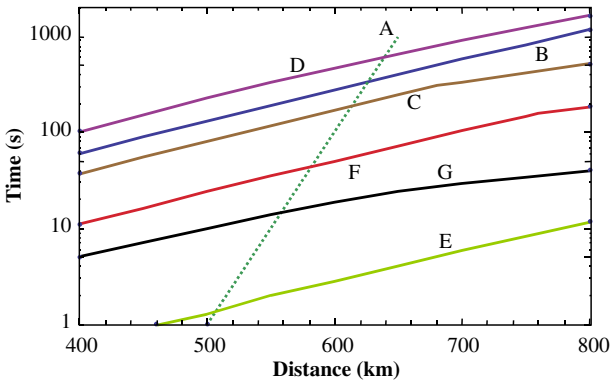

FIG. 18 (color online). Comparison of quantum repeater protocols based on atomic ensembles and linear optics. The quantity shown is the average time needed to distribute a single entangled pair with a final fidelity $F = 0.9$ for the given distance. We assume losses of 0.2 dB/km, corresponding to telecom fibers at a wavelength of 1.5 μm. *A*: as a reference, the time required using direct transmission of photons through optical fibers with a single-photon generation rate of 10 GHz. *B*: original DLCZ protocol that uses single-photon detections for both entanglement generation and swapping (Duan *et al.*, 2001). *C*: protocol of Jiang *et al.* (2007b), which uses entanglement swapping based on two-photon detections. *D*: the protocol of Sec. III.B of Z.-B. Chen *et al.* (2007), which first creates single-photon entanglement locally using single-photon detections, and then generates long-distance entanglement using two-photon detections. *E*: protocol of C. Simon *et al.* (2007b) that uses photon-pair sources (which can be realized with ensembles) and multimode memories to implement a temporally multiplexed version of the DLCZ protocol. The corresponding entanglement distribution time is that of the DLCZ protocol divided by the number of temporal modes N that can be stored. Based on the analysis of Afzelius *et al.* (2009), we have assumed a memory that can store $N = 100$ modes. *F*: protocol of Sangouard *et al.* (2007b) that uses quasi-ideal single-photon sources (which can be implemented with atomic ensembles) plus single-photon detections for generation and swapping. *G*: protocol of Sangouard *et al.* (2008b), which creates high-fidelity entangled pairs locally and uses two-photon detections for entanglement generation and swapping, thus following the approach of Sec. III.C of Z.-B. Chen *et al.* (2007), but using an improved method of generating the local entanglement. We have assumed a basic source repetition rate of 10 MHz, which is a limiting factor for this protocol. For all the curves we have assumed memory and detector efficiencies of 90%. We imposed a maximum number of 16 links, which is larger than or equal to the optimal link number for all protocols apart from curve *D*, for which the effect is also less than a factor of 2.

protocol of Jiang *et al.* (2007b) (curve *C*) and then to the protocol of Sangouard *et al.* (2007b) (curve *F*). On the other hand, for protocols where entanglement is created by two-photon detection, one sees that the protocol of Z.-B. Chen *et al.* (2007), Sec. III.B (curve *D*), already achieves a performance that is fairly similar to that of the DLCZ protocol (while significantly improving its robustness), whereas the protocol of Sangouard *et al.* (2008b) is significantly faster (curve *G*). However, even the fastest protocol (curve *G*) still requires very long times for entanglement distribution, which not only leads to very low rates of quantum communication but also is extremely taxing in terms of quantum memory requirements. Note that the two-photon-detection-based protocol of Zhao *et al.* (2007) is slower than the protocols shown; see Sec. III.B.

Curve *E*, which corresponds to the multimode memory-based protocol of C. Simon *et al.* (2007b), emphasizes the advantage of multiplexing. In this protocol, which is essentially a multiplexed version of the DLCZ protocol, entanglement is created by single-photon detections, requiring long-distance phase stability. Multiplexing the other protocols is more challenging in terms of source repetition rate and memory bandwidth, as we discussed in the previous section, but certainly worth investigating in detail. We have focused on temporal multiplexing because this seems particularly promising in practice; however, other forms of multiplexing (spatial, frequency) may be possible as well, and promise additional benefits in addition to improved rate, such as greater robustness with respect to storage time limitations (Collins *et al.*, 2007); see Sec. III.D.

B. Robustness

We have mentioned the importance of long memory times and of long-distance phase stability (for most of the discussed protocols) repeatedly in the previous sections. Here we will briefly review what is known about the effects of imperfections in these respects on the performance of the various quantum repeater protocols. We will also discuss imperfections of other important parameters, in particular, memory and detection efficiencies. We note that multiphoton emission errors are not an imperfection in the same sense, but inherent to the ensemble-based protocols. For many protocols they directly determine the achievable rates by forcing one to work with a certain value of the emission probability p, which is why we studied them already in the previous sections. Their elimination would be possible with different resources, such as ideal single-photon sources or single-pair sources.

1. Storage time

We emphasized that it is essential for the storage time to be long enough to allow the highest-level entanglement swapping (or the final postselection in most protocols) to be performed. This means that the memory time has to be comparable to the total entanglement creation time. Razavi *et al.* (2008) have recently studied quantitatively how the performance of quantum repeaters declines if this is not the case. They found, for example, that the repeater rate declines as a power of $\exp(-\sqrt{L/c\tau})$, where L is the total distance, c the speed of light, and τ the memory time, in the regime where $\tau \ll L/c$. As discussed in Sec. III.D, Collins *et al.* (2007) pointed out that certain kinds of multiplexing can greatly reduce memory time requirements, whereas simply running several repeaters in parallel does not. Developing quantum memories with long storage times is thus essential for the implementation of quantum repeaters. The storage time of a collective spin excitation (1) is mainly limited by the coherence time of the ground state transition $|g_1\rangle$-$|g_2\rangle$. Note that decoherence processes limit the storage time but leave the fidelity of the quantum storage unaffected in the absence of background (Staudt *et al.*, 2007a). In certain solid-state atomic ensembles storage times over 1 s (Longdell *et al.*, 2005) and coherence times up to 30 s (Fraval *et al.*, 2005)

have already been demonstrated. This, as well as the experimental status quo for atomic gases, will be discussed in more detail in Sec. V.

2. Phase stability and entanglement purification

As already discussed, phase stability is particularly important for protocols based on single-photon detections. Not only do the fiber links have to be interferometrically stable over long time scales, but also the laser phases. The relevant time scale is given by the creation of entanglement in an elementary link, not over the whole distance, but this will typically also be at least in the millisecond range. This requires stabilization of the channel, e.g., through active feedback or through the implementation of self-compensating Sagnac-type setups, and distribution of a phase reference. This is an active field of investigation, which will be reviewed in more detail in Sec. V.F. Any phase error not eliminated by stabilization will typically be amplified by a factor of 2 in every entanglement swapping operation, similarly to the vacuum and multiphoton components discussed in previous sections.

The difficulty is less severe for two-photon-detection-based protocols, where propagation and laser phases only contribute to an irrelevant global phase. However, if fiber length fluctuations become too large, they reduce the overlap between the two photons, which also leads to phase errors. Active stabilization is thus likely to still be required, but less precision is sufficient. The level of stabilization required depends on the coherence length of photons used in a given implementation, which will typically be on the scale of meters. Again any remaining errors are amplified in every entanglement swapping step. This is why we have limited the number of links in our comparison above. The experimental status of single-photon and two-photon visibilities is discussed in more detail in Sec. V, in particular, Secs. V.B.1 and V.F.

There is, of course, the possibility of using entanglement purification, as originally discussed by Briegel *et al.* (1998). This introduces a supplementary layer of complexity, causing a further slowdown, which is why we have not included it explicitly in our discussions and comparisons. We believe that for the most immediate goal of beating direct transmission it will probably be a better strategy to minimize all errors and do without purification. However, purification procedures have now been developed that can be used in all the discussed protocols. On the one hand, a protocol for the entanglement purification of photon pairs with linear optics was proposed by Pan *et al.* (2001). The protocol was adapted to parametric down-conversion sources by Simon and Pan (2002), leading to an experimental realization (Pan *et al.*, 2003). This topic is well reviewed by Pan *et al.* (2008). On the other hand, single-photon entanglement plays an essential role in several of the protocols discussed in this review: Duan *et al.* (2001), Jiang *et al.* (2007b), Sangouard *et al.* (2007b), and C. Simon *et al.* (2007b). A protocol for the purification of single-photon entanglement with linear optics has also recently been proposed (Sangouard *et al.*, 2008a). The effects of phase errors and the inclusion of entanglement purification in repeater protocols were studied by Z.-B. Chen *et al.* (2007), Jiang *et al.* (2007b), and Zhao *et al.* (2007) with some quantitative results.

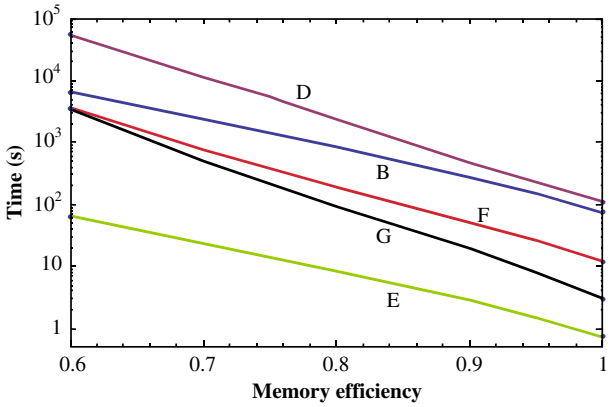

FIG. 19 (color online). Robustness of various protocols with respect to nonunit memory efficiency. The quantity exhibited is the average time for the distribution of an entangled pair for a distance $L = 600$ km as a function of the memory efficiency. The letters refer to the same protocols as in Fig. 18.

3. Memory efficiency

Up to now, we have characterized the performance of protocols by considering a memory efficiency of $\eta_m = 0.9$. It is important to know how the entanglement distribution rates vary with the memory efficiency. In Fig. 19, the average time for the distribution of an entangled state over 600 km is plotted as a function of the memory efficiency, with all other parameters as before, in particular, $\eta_d = 0.9$. It clearly appears that because single-photon-detection-based protocols require fewer memories, they are less sensitive to nonunit memory efficiency than protocols based on two-photon detections. The main conclusion from Fig. 19, however, is the enormous importance of highly efficient memories in order to achieve reasonable entanglement distribution rates. For example, a reduction in the memory efficiency from 90% to 89% leads to an increase in the entanglement distribution time by 10%–14%, depending on the protocol. This is understandable because the memory efficiency intervenes in every entanglement swapping operation. Intrinsic memory efficiencies above 80% have already been achieved (J. Simon *et al.*, 2007b); however, overall efficiencies are typically much lower due to coupling losses. The experimental status quo will be reviewed in more detail in Sec. V, in particular, Secs. V.A.1, V.D, and V.G.

4. Photon detection efficiency

It is also interesting to know the influence of the photon detector efficiency on the protocol performance. Hitherto, we have considered photon detectors capable of resolving the photon number, and with an efficiency of $\eta_d = 0.9$. Figure 20 shows the average time for the distribution of one entangled pair for various photon detector efficiencies, with all other parameters as before, in particular $\eta_m = 0.9$. Since they require fewer detectors, the protocols based on single-photon detections are more robust with respect to photon detector inefficiency than protocols based on two-photon detections. Again the main conclusion is that the detection efficiency is clearly very important, as it too intervenes in every swapping operation. For example, a reduction in detection efficiency from 0.90 to 0.89 leads to an increase in the entanglement

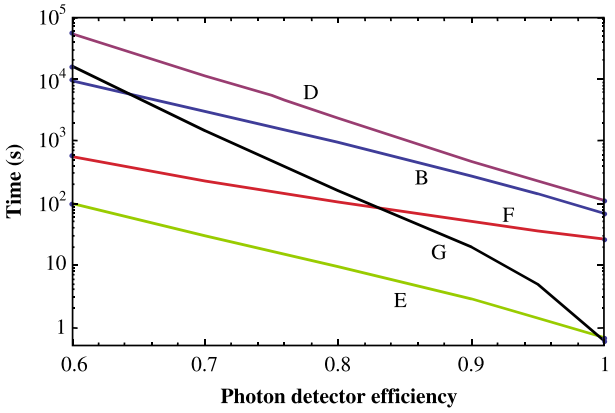

FIG. 20 (color online). Robustness of various protocols with respect to imperfect photon detector efficiency. The quantity shown is the average time for the distribution of an entangled pair for a distance $L = 600$ km as a function of the photon detector efficiency. The letters refer to the same protocols as in Fig. 18.

distribution time that ranges from 7% for the single-photon source based protocol of Sangouard *et al.* (2007b) (curve *F*) to 19% for the local entangled pair based protocol of Sangouard *et al.* (2008b). Note that the effect of noncounting detectors has been studied by Brask and Sorensen (2008) for the DLCZ protocol. During an entanglement swapping operation, the use of detectors that do not resolve the photon number leads to a vacuum component each time one photon is released by each of the neighboring memories. A faster growing of vacuum components leads to a longer entanglement distribution time.

Photon-number resolving detectors with efficiencies as high as 95% have been demonstrated (Lita *et al.*, 2008). We review the experimental status quo concerning photon detectors in more detail in Sec. V.

5. Dark counts

Realistic detectors not only have imperfect efficiency, but also a certain level of dark counts, which, however, depends strongly on the type of detector used. The effect of dark counts on quantum repeater protocols has been analyzed for specific protocols, in particular, for the single-photon-source-based protocol by Sangouard *et al.* (2007b) and for the DLCZ protocol by Brask and Sorensen (2008), who studied the impact of a number of imperfections. However, considerable efforts are being made currently to increase the efficiency of single-photon detectors and to decrease the noise from dark counts. For example, superconducting transition edge sensors already resolved photon number with 95% efficiency and with negligible noise; see Sec. V.E. It is also interesting to note, as already remarked in Sec. I, that "memoryless" repeaters, also known as quantum relays, can help alleviate the effects of dark counts on the transmission of quantum states (Jacobs *et al.*, 2002; Collins *et al.*, 2005).

C. Complexity

Quantifying and comparing the complexity of different quantum repeater protocols is not a straightforward task. One simple way of assessing complexity is by counting elements. For example, outperforming direct transmission with the protocol of C. Simon *et al.* (2007b) will require at least two links, each of which has four sources and four multimode memories. The crossover occurs for a distance of 510 km, for an entanglement distribution time of 2.8 s; a repeater with four links is slightly faster, achieving a time of 1.4 s. Similar resource counts for the protocols discussed in the present review are given in Sangouard *et al.* (2008b).

However, in practice the number of elements is not the only (nor necessarily the most important) consideration. We already emphasized the importance of phase stabilization, for example, where the required level of precision is different for protocols based on single-photon or two-photon detection. There are other distinctions where it is less clear which side is favored. For example, temporal multimode memories would typically be realized in solid-state atomic ensembles at cryogenic temperatures. On the other hand, DLCZ-type experiments so far were performed with atomic gases, requiring optical cooling and trapping.

Our overall conclusion is that outperforming direct transmission appears possible with repeater architectures of quite moderate complexity. However, the individual components have to be excellent. For example, successful quantum repeaters will probably require storage times of several seconds, memory and detection efficiencies of 90% or more, length-stabilized long-distance fiber links, and minimal coupling losses between the various local components; see Sec. V.

V. IMPLEMENTATIONS

We will now review experiments that are relevant to the different quantum repeater architectures described above. We first review in Sec. V.A experiments that are directly relevant to the DLCZ protocol itself. Section V.B is devoted to the experiments relevant to the protocols based on two-photon entanglement generation and swapping. In Sec. V.C, we review the various quantum light sources at the single-photon level that are compatible with ensembles based on quantum memories, before describing in Sec. V.D light storage experiments in atomic ensembles, in particular, the storage of single photons. Section V.E is devoted to the various single-photon detectors that may be used in a quantum repeater architecture. Section V.F briefly describes the quantum channels that may be used in a quantum repeater, in particular, optical fibers (including phase stabilization) but also free-space links. Finally, we mention in Sec. V.G an important practical and technological aspect, the coupling losses. In all of Sec. V, we are mainly concerned with experiments performed with photon counting in the single-excitation regime. In particular, the various experiments demonstrating the storage and teleportation of quantum continuous variables of light in atomic ensembles performed with homodyne detection, e.g., Julsgaard *et al.* (2001), (2004), Sherson *et al.* (2006), Appel *et al.* (2008), Cviklinski *et al.* (2008), and Honda *et al.* (2008) will not be discussed here. This area of research has been reviewed recently by Hammerer *et al.* (2010).

A. DLCZ protocol

The publication of the article of DLCZ in 2001 triggered an intense experimental effort to realize the basic elements of this protocol. Over the past few years there have been a large number of DLCZ-type experiments in atomic gases. In this section, we review these experiments. We start in Sec. V.A.1 with the experimental realization of the fundamental building block: the generation of strong quantum correlations between emitted Stokes photons and stored collective spin excitations, followed by the efficient mapping of the stored excitation into an anti-Stokes photon. We then describe in Sec. V.A.2 experiments demonstrating heralded entanglement between remote atomic ensembles. Section V.A.3 describes the experimental realization of an elementary segment of DLCZ quantum repeater. Finally, Sec. V.A.4 is devoted to an experiment attempting to demonstrate entanglement swapping between DLCZ ensembles.

1. Creation of correlated photon pairs with a programmable delay

a. Quantifying quantum correlations

As we have seen in Sec. II.A, the number of Stokes photons $|n_S\rangle$ emitted during the spontaneous Raman process is in the ideal case strongly correlated with the number of collective spin excitations $|n_a\rangle$ stored in the level $|g_2\rangle$. The joint atom-photon state can be written as [cf. Eq. (5)]

$$\left(1-\frac{p}{2}\right)|0_S\rangle|0_a\rangle+\sqrt{p}|1_S\rangle|1_a\rangle+p|2_S\rangle|2_a\rangle+O(p^{3/2}). \tag{27}$$

This state is sometimes referred as a two-mode squeezed state. The probability p of creating a pair Stokes photon–collective excitation is directly proportional to the write laser intensity. In practice, various sources of noise can degrade the quantum correlations, and it is important to experimentally quantify these correlations. The first step is to convert the atomic collective excitations into anti-Stokes photons, with a read laser. The correlations between Stokes photons and stored excitations will now be mapped into correlations between Stokes and anti-Stokes fields, which can be measured by photon counting techniques. In particular, the various probabilities p_S and p_{AS} of detecting a Stokes and an anti-Stokes photon, respectively, and the joint probabilities $p_{S,AS}$, $p_{S,S}$, and $p_{AS,AS}$ of detecting a pair Stokes–anti-Stokes, two Stokes, and two anti-Stokes photons in a given trial can easily be accessed.

With these measured probabilities, it has been shown that there exists a well-defined border between classical and quantum fields (Clauser, 1974; Kuzmich *et al.*, 2003). Specifically, for classical fields, we have the following Cauchy-Schwartz inequality:

$$R=\frac{g^2(S,AS)}{g(S,S)g(AS,AS)}\leq 1, \tag{28}$$

where

$$g(S,AS)=\frac{p_{S,AS}}{p_S p_{AS}} \tag{29}$$

is the normalized intensity cross-correlation function between Stokes and anti-Stokes fields, and $g(S,S)=p_{S,S}/p_S^2$ and $g(AS,AS)=p_{AS,AS}/p_{AS}^2$ are the normalized intensity autocorrelation functions for the Stokes and anti-Stokes fields, respectively.

For a perfect two-mode squeezed state as in Eq. (27), the nonconditional Stokes and anti-Stokes fields exhibit thermal statistics and hence bunching, with $g_{S,S}=g_{AS,AS}=2$. In that case, a measured value of $g_{S,AS}>2$ is a signature of nonclassical correlations between Stokes and anti-Stokes fields.

The correlations between the Stokes and anti-Stokes fields, as defined by $g_{S,AS}$, describe the correlations in photon number between the two fields. If the Stokes and anti-Stokes fields can be in different modes (e.g., polarization modes), then they can also be entangled in these degrees of freedom. It can then be shown that the quality of this entanglement is directly related to the value of the cross-correlation function $g_{S,AS}$ (de Riedmatten *et al.*, 2006). For example, a value of $g_{S,AS}\approx 6$ is required to violate a Bell inequality with the Stokes and anti-Stokes photons (S. Chen *et al.*, 2007; de Riedmatten *et al.*, 2006).

While a formal proof of nonclassical correlations requires the measurement of the Cauchy-Schwartz inequality, the measurement of a cross-correlation function $g_{S,AS}>2$ already gives strong evidence of nonclassical behavior. This is because in practice the presence of background noise such as leakage of excitation lasers and dark counts decreases the bunching of the nonconditional fields, such as $g_{S,S}=g_{AS,AS}<2$. In addition, the cross-correlation function is very important, since many parameters crucial for applications, such as the autocorrelation function of the heralded anti-Stokes photon (Chou *et al.*, 2004; Chen *et al.*, 2006; Laurat *et al.*, 2006; Matsukevich *et al.*, 2006a), the visibility of two-photon interference (de Riedmatten *et al.*, 2006; S. Chen *et al.*, 2007), the visibility of the Hong-Ou-Mandel interference (Felinto *et al.*, 2006; Yuan *et al.*, 2007), and the visibility in measurement-induced entanglement experiments (Laurat, Choi *et al.*, 2007) are directly related to $g_{S,AS}$. For a perfect two-mode squeezed state, the normalized cross-correlation function is linked to the probability p of creating a Stokes–anti-Stokes pair as

$$g_{S,AS}=1+\frac{1}{p} \tag{30}$$

for $p\ll 1$. In that case the finite value of $g_{S,AS}$ is due to multiple-pair creation. As mentioned in Sec. II.B, multiple-pair creation is a major source of errors in the DLCZ architecture that should be minimized by working in the regime of high quantum correlations. For an ideal state, this regime can in principle be accessed by using very low pump power. This is true, of course, as long as the background noise is negligible. A major experimental challenge of this type of experiment is to preserve the quantum character of the emitted single photons, which requires excellent filtering of the various sources of noise, such as leakage of the excitation lasers, fluorescence, and stray light.

The strong correlations between Stokes and anti-Stokes photons enable the generation of heralded single-photon states. For example, the detection of a Stokes photon by detector D_S projects the anti-Stokes field on a single-photon

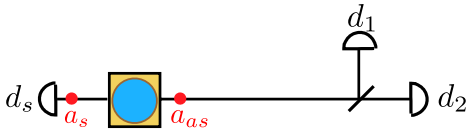

FIG. 21 (color online). Typical experimental configuration used to measure the single-photon character of the conditional anti-Stokes fields. A detection of the Stokes field in detector D_s is used as a trigger, and the anti-Stokes field is split at a beam splitter and detected by detectors D_1 and D_2.

state. The quality of this single-photon state can be measured with a Hanbury-Brown–Twiss setup, i.e., by splitting the anti-Stokes field at a beam splitter and recording the detection events in the two output modes with detectors D_1 and D_2 (see Fig. 21). As shown by Grangier *et al.* (1986), the single-photon character of the conditional anti-Stokes field can be characterized with the autocorrelation function:

$$\alpha = \frac{p_{(1,2)|S}}{p_{(1|S)}p_{(2|S)}} = \frac{p_{(S)}p_{(S,1,2)}}{p_{(S,1)}p_{(S,2)}}, \tag{31}$$

where the various p's correspond to the probability of a joint detection event in the corresponding combination of detectors D_S, D_1, and D_2. For classical fields, a Cauchy-Schwartz inequality leads to $\alpha \geq 1$. For coherent fields, we have $\alpha = 1$ while $\alpha = 2$ for thermal fields. In contrast, for a perfect conditional single-photon field $\alpha = 0$. The measurement of the "anticorrelation parameter" α thus provides a way to quantify the two-photon suppression of the conditional field with respect to a coherent field.

b. Initial experiments

The first enabling step toward a practical realization of the DLCZ quantum repeater is the observation of nonclassical correlations between the Stokes and anti-Stokes fields emitted with a controllable delay by one atomic ensemble. The first experiments were performed simultaneously in 2003 at Caltech (Kuzmich *et al.*, 2003) and Harvard (van der Wal *et al.*, 2003). The Caltech experiment used ensembles of cold cesium atoms in a magneto-optical trap (MOT) and observed quantum correlations in the single-excitation regime. The write and read pulses were separated by 400 ns and sent in a collinear copropagating configuration through the ensemble. A challenging aspect of the experiment was to separate the classical pulses from the weak nonclassical fields, since they were temporally and spatially overlapped, and their frequencies were only 9 GHz apart. In the first experiment the filtering had three stages. First, the Stokes (anti-Stokes) fields was separated from the write (read) pulse in a polarizing beam splitter (PBS) right after the MOT chamber. Later, the leakage of the excitation pulses that still escapes the PBS in the wrong direction was spectrally filtered by optically pumped vapor cells. Finally, the Stokes (anti-Stokes) field was distinguished from the read (write) pulse by temporal gating of the detection.

The nonclassical character of the fields was demonstrated using the Cauchy-Schwartz inequality of Eq. (28). A value of $R = 1.84 \pm 0.06 > 1$ was measured, thereby demonstrating that the Stokes and anti-Stokes fields in the single-photon regime were nonclassically correlated. The size of the violation of the inequality was limited mostly by uncorrelated fluorescence from individual atoms in the atomic sample and by the residual leakage of excitation pulses.

The Harvard experiment used a hot vapor of rubidium atoms. The first experiment was carried out in the regime of high excitation number (10^3–10^4) (van der Wal *et al.*, 2003). Strong intensity correlation between the Stokes and anti-Stokes fields were observed, and their quantum nature was demonstrated by an analysis of the fluctuation spectral density with respect to the shot-noise (or vacuum-state) limit. In more recent experiments, nonclassical correlations were also observed in the single-excitation regime with hot vapors (Eisaman *et al.*, 2004, 2005).

Since the initial experiments, tremendous progress has been made on several fronts in various experiments. We now review relevant experiments, based on three important properties of the DLCZ source: the quality of nonclassical correlations between Stokes and anti-Stokes photons, the efficiency of atomic to photonic conversion for the anti-Stokes field (called retrieval efficiency), and the storage time of the stored excitation.

c. Quantum correlations

In the initial experiment (Kuzmich *et al.*, 2003) the measured $g_{S,AS}$ was only slightly above 2. Various improvements in the experiments have allowed the observation of substantially higher quantum correlations between Stokes and anti-Stokes fields. A first important step was to set the write laser slightly off resonance to avoid uncorrelated fluorescence. A further improvement was to use a four-level scheme of excitation, in which write and read pulses are 42 nm apart. This allows a fourth filtering stage by narrow-bandwidth optical filters, and the study of correlations with temporally overlapped write and read pulses. Experiments in that regime yielded values of $g_{S,AS}$ of order 10 (Chou *et al.*, 2004; Polyakov *et al.*, 2004; Felinto *et al.*, 2005). More recently, Chen *et al.* (2006) achieved a value of $g_{S,AS} = 100$ with an improved version of the setup of Kuzmich *et al.* (2003). Another important step was achieved by using an off-axis geometry in which the Stokes (anti-Stokes) photon is collected at a small angle with respect to the write (read) beam direction. This configuration was first used in the classical regime by Braje *et al.* (2004) and in the quantum regime by Matsukevich *et al.* (2005). This geometry allows for a very efficient spatial filtering of the write and read lasers, which decreases the background light by a substantial amount. Much higher values of cross-correlation function have been obtained in this case, e.g., $g_{S,AS} \simeq 300$ in Matsukevich *et al.* (2006a) and $g_{S,AS} \simeq 600$ in Laurat *et al.* (2006).

Note that the detection of Stokes and anti-Stokes photons at an angle cannot be used with hot atomic vapors, due to the motion of atoms (see below). In addition, the detuning of the write pulse in order to be off resonance must be much larger than in cold gases, because of the Doppler inhomogeneous broadening (which is approximately 500 MHz). Consequently, the write pulse intensity is also much larger than in cold gases. For these reasons, the filtering of the write and read pulses is more challenging in hot vapors than in cold gases. Strong nonclassical correlations have nevertheless been observed by using a counterpropagating configuration

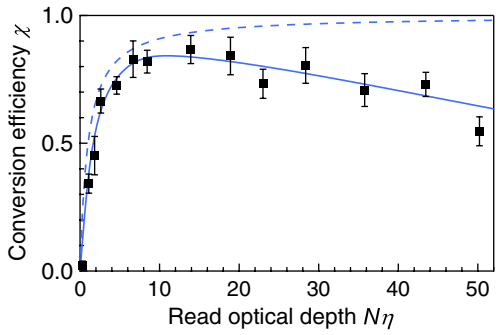

FIG. 22 (color online). Retrieval efficiency vs read optical depth d (denoted here as $N\eta$) at a write-read delay of 120 ns with the atomic ensemble inserted into an optical cavity. The dashed line shows the predicted retrieval efficiency for a three-level system; the solid line is the prediction from a model including dephasing from additional excited states. From J. Simon *et al.*, 2007b.

for the write and read beams (Eisaman *et al.*, 2005; Walther *et al.*, 2007).

d. Retrieval efficiency

The single spin excitation stored in the ensemble can in principle be retrieved with unit efficiency in a well-defined spatiotemporal mode, due to the collective enhancement effect, as discussed in Sec. II.A. The retrieval efficiency is defined as the probability to have an anti-Stokes photon in a well-defined spatiotemporal mode at the output of the atomic ensemble conditioned on the successful detection of a Stokes field. In practice, however, several factors can limit the retrieval efficiency. For example, it depends on the available optical depth and read beam power. The collective interference can also be decreased by various dephasing effects due, e.g., to spatial intensity profile mismatch between read beam and stored excitation, inhomogeneous broadening (Ottaviani *et al.*, 2009) or atomic motion (for atomic motion, see below and Sec. II.A). While early experiments suffered from low retrieval efficiencies, progress has been made on several fronts, leading to retrieval efficiencies of 50% in free space (Laurat *et al.*, 2006) and of more than 80% in cavities (J. Simon *et al.*, 2007b). Figure 22 shows the measured retrieval efficiency as a function of the optical depth with the atomic ensemble inserted inside an optical cavity (J. Simon *et al.*, 2007b). Note that the conditional probability to *detect* an anti-Stokes photon is usually much lower than these values, due to the various passive losses and to detection inefficiency (see Sec. V.G).

e. Storage time

A crucial parameter for using DLCZ quantum memories in a repeater scheme is the storage time of the collective spin excitation, which is limited by the coherence time of the ground state transition $|g_1\rangle$-$|g_2\rangle$. There are several factors that affect the storage time at different time scales. The main factors can be divided into two classes: the inhomogeneous broadening of the spin transition and the atomic motion. We now describe these effects in more detail.

i. Inhomogeneous broadening of the spin transition. In most experiments to date, the spin excitation was stored in a hyperfine state containing a Zeeman state manifold. In the absence of external magnetic fields, all the Zeeman states with different m_F are degenerate. In practice, however, it is difficult to suppress external magnetic fields completely. For experiments with cold atoms, for example, a strong magnetic field gradient is needed in order to trap the atoms. This leads to an inhomogeneous broadening of the spin transition. In that case, the collective spin excitation undergoes a strong inhomogeneous dephasing, which effectively suppresses the collective enhancement necessary for efficient retrieval of the photons. This decoherence mechanism was studied in detail by Felinto *et al.* (2005). The inhomogeneous broadening due to the trapping magnetic field gradient leads to storage times of the order of a few hundreds of nanoseconds (Kuzmich *et al.*, 2003; Matsukevich and Kuzmich, 2004; Polyakov *et al.*, 2004). A direct solution to this problem is to switch off the magnetic field gradient during the write-read sequence. This solution was tested experimentally and led to an increase of storage time by 2 orders of magnitude (of order of 10 μs) (Black *et al.*, 2005; Felinto *et al.*, 2005; Matsukevich *et al.*, 2005; Chen *et al.*, 2006; Matsukevich *et al.*, 2006a). The storage time was in that case mostly limited by the residual magnetic field. It is experimentally difficult to further decrease residual magnetic fields. Another solution to avoid the inhomogeneous broadening of the spin transition is to use first-order magnetically insensitive hyperfine transitions, known as "clock transitions," connecting two specific Zeeman states. Such transitions exist in Cs and Rb atoms. This requires one to prepare all the atoms in a specific Zeeman state (typically with $m_F = 0$). This preparation can be implemented with optical pumping techniques. A storage time of 1 ms has recently been demonstrated using this technique in a collinear configuration (B. Zhao *et al.*, 2008).

While turning off the trapping magnetic field allows a strong reduction in the inhomogeneous broadening of the spin transition, it has a major drawback: In that case, the atoms are no longer trapped and are free to fly away, which severely decreases the available optical depth in the time scale of a few milliseconds. To overcome this problem, use of an optical dipole trap was suggested to maintain a sufficient atom density. This solution was tested experimentally by Chuu *et al.* (2008). The storage time was, however, limited to a few tens of microseconds by atomic motion since the experiment was performed in the configuration with an angle between the write (read) and the Stokes (anti-Stokes) fields (see below).

ii. Atomic motion. Another important cause of decoherence is the motion of atoms. This is obviously a bigger problem for experiments with hot gases, but is also a strong limitation for cold ensembles, as we shall see. The motion of atoms can cause two different problems. The first one is the diffusion of the atoms out of the excitation region during the storage of the spin excitation. This is the prime cause of decoherence for the experiments with hot gases realized to date. For hot gases, this leads to a coherence time of a few microseconds (Eisaman *et al.*, 2004, 2005), while for cold ensembles the diffusion time is of the order of 1 ms (Felinto *et al.*, 2005). This diffusion can be mitigated by using bigger beams and/or colder atoms. There is, however, a much more severe effect of the atomic motion: the disturbance of the

phase of the collective spin excitation. In Sec. II.A we have seen that the motion of the atoms is not a problem for the phases of the collective state, as long as a collinear configuration with $\mathbf{k}_w = \mathbf{k}_s$ and $\mathbf{k}_r = \mathbf{k}_{as}$ is used. For all other configurations, the motion of the atoms will induce a dephasing that depends on the angle between $\mathbf{k}_w$ and $\mathbf{k}_s$, as was demonstrated experimentally by B. Zhao *et al.* (2008). The wavelength of the stored spin wave can be written as

$$\Lambda = \frac{2\pi}{\Delta k_{SW}} = \frac{2\pi}{|\mathbf{k}_w - \mathbf{k}_s|} \approx \frac{2\pi}{k_w \sin\theta}, \tag{32}$$

where θ is the angle between the write beam and the Stokes field. The time scale of the dephasing can be estimated by calculating the average time to cross $1/2\pi$ of the wavelength of the spin wave, leading to a storage lifetime of $\tau \sim (\Lambda/2\pi v)$ with $v = \sqrt{k_B T/m}$ the one-dimensional speed of the atoms, where k_B is the Boltzmann constant, T the temperature, and m the mass of the atoms. The reduced wavelength of the spin wave due to the angle θ severely limits the achievable storage time. For example, for a typical $\theta = 3°$ and for $T = 100$ μK, we find $\Lambda = 15$ μm and $\tau = 25$ μs. B. Zhao *et al.* (2008) confirmed this prediction experimentally by measuring the storage time as a function of θ using a clock transition in a cold Rb ensemble, as shown in Fig. 23. For $\theta = 0°$ (collinear configuration) they achieved a storage lifetime of order 1 ms.

In practice, however, there is a great advantage of using a noncollinear configuration since it enables a very efficient spatial filtering to suppress the excitation beams in the quantum channel. In that case, the only way to avoid motion-induced dephasing is to suppress the atomic motion. With atomic gases, one possibility is to load the atoms into an optical lattice. R. Zhao *et al.* (2008) demonstrated a DLCZ quantum memory using a clock transition in rubidium atoms confined in a one-dimensional optical lattice. They achieved a storage lifetime exceeding 6 ms, which is currently the longest storage lifetime observed in the single-photon regime (see Fig. 24). A light storage experiment with bright coherent pulses based on EIT has also been recently demonstrated with Rb atoms confined in a three-dimensional optical lattice, leading to a storage lifetime of 240 ms (Schnorrberger *et al.*, 2009). Another possibility might be to use colder atoms, for example, a Bose-Einstein condensate, where collective coherences in the high-excitation-number ($>10^4$) regime have been created and stored recently (Yoshikawa *et al.*, 2007, 2009). These two techniques are, however, complex and technically demanding. Another potential solution, which may be more practical, is the use of atomic ensembles in the solid state, implemented with rare-earth-ion-doped solids. In such a medium, the atoms behave as a "frozen gas," and a storage lifetime exceeding 1 s has been

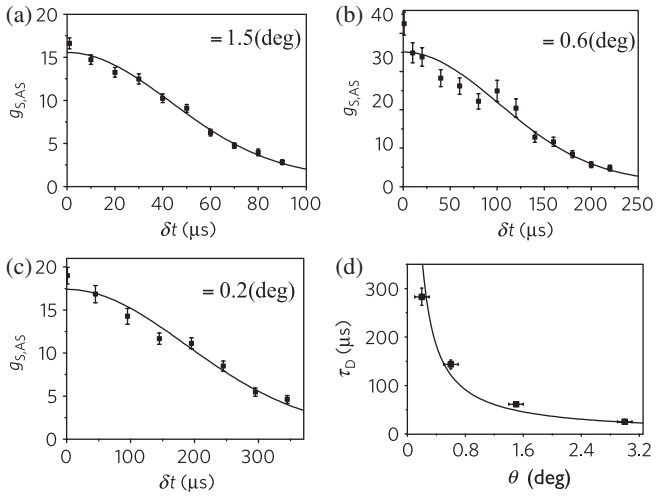

FIG. 23. (a)–(c) The cross-correlation $g_{A,AS}$ vs the storage time δt for different angles θ between the write beam and the Stokes field. By reducing the angle, the lifetime is increased from 25 to 283 μs, which implies that the decoherence is mainly caused by the dephasing induced by atomic random motion. (d) The measured lifetime τ_D as a function of detection angle θ, where the horizontal error bars indicate measurement errors in the angles. The solid line is the theoretical curve with $T = 100$ μK. The experimental results are in good agreement with the theoretical predictions. From B. Zhao *et al.*, 2008.

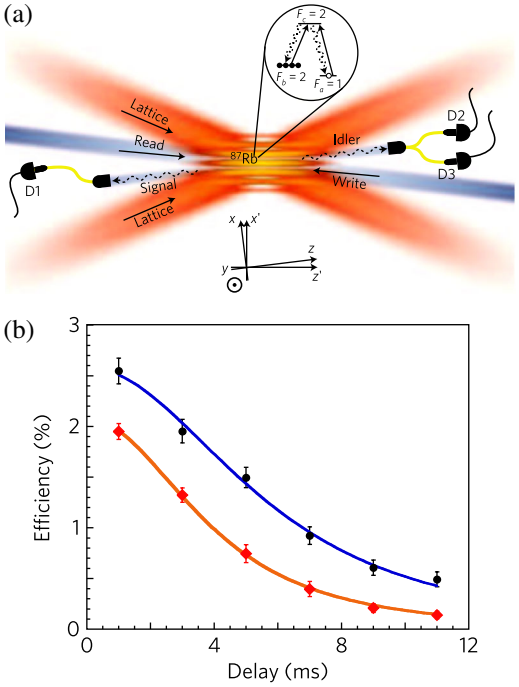

FIG. 24 (color online). (a) Experiment demonstrating a DLCZ quantum memory with an atomic ensemble loaded into a one-dimensional optical lattice. (a) Schematic of the experiment. Between 10^5 and 10^6 sub-Doppler-cooled ^{87}Rb atoms are loaded into an optical lattice, and detection of the signal field, generated by Raman scattering of the write laser pulse (red detuned by 20 MHz), heralds the presence of a write spin-wave excitation. A resonant read-control field converts the surviving atomic excitation into an idler field after a storage period Ts. The inset shows the atomic level scheme of ^{87}Rb with levels a and b being the hyperfine components of the ground $^5S_{1/2}$ level, and level c being a hyperfine component of the excited $^5P_{1/2}$ level. (b) Retrieval efficiency (including detection) as a function of storage time for atoms optically pumped in clock states in the optical lattice for two different lattice depths U_0 (diamonds, U_0 80 μK; circles U_0 40 μK). The intrinsic retrieval efficiency at the output of the ensemble is roughly 4 times larger. From R. Zhao *et al.*, 2008.

demonstrated, though not yet in the quantum regime (Longdell *et al.*, 2005).

2. Heralded entanglement between two atomic ensembles

A crucial step toward the implementation of a quantum repeater is the demonstration of heralded entanglement between two spatially separated atomic ensembles in the single-excitation regime. This was first demonstrated by Chou *et al.* (2005) with two cold Cs atomic ensembles in two vacuum chambers separated by 3 m; see Fig. 25. Entanglement for excitation stored in remote ensembles was created by a quantum interference in the detection of light emitted by the quantum memories. Following the DLCZ protocol described in Sec. II.B, the two ensembles are simultaneously and coherently excited by a weak write beam, and the two Stokes fields created by spontaneous Raman scattering are collected into single-mode optical fibers and mixed at a beam splitter, forming a long Mach-Zehnder interferometer. If the two Stokes fields are indistinguishable, the information about the origin of the photon is erased and a detection after the beam splitter projects the ensembles in the ideal case onto an entangled state with one delocalized excitation, of the form

$$|\Psi_{ab}\rangle = \frac{1}{\sqrt{2}}(|1_a\rangle|0_b\rangle + e^{i\theta_{ab}}|0_a\rangle|1_b\rangle), \tag{33}$$

where the phase $\theta_{AB} = \phi_B - \phi_A + \xi_B - \xi_A$, with $\phi_{A,B}$ the phase of the laser at ensembles A and B, respectively, and $\xi_{A,B}$ the phase acquired by the Stokes photons from the ensembles to the beam splitter. In order to generate a measurable entangled state, it is important that the phase θ_{AB} is stable during the duration of the experiment. Chou *et al.* (2005) used an auxiliary laser for active stabilization. The state of Eq. (33) is an idealized state. In practice, various sources of noise can turn the heralded state into a mixed state.

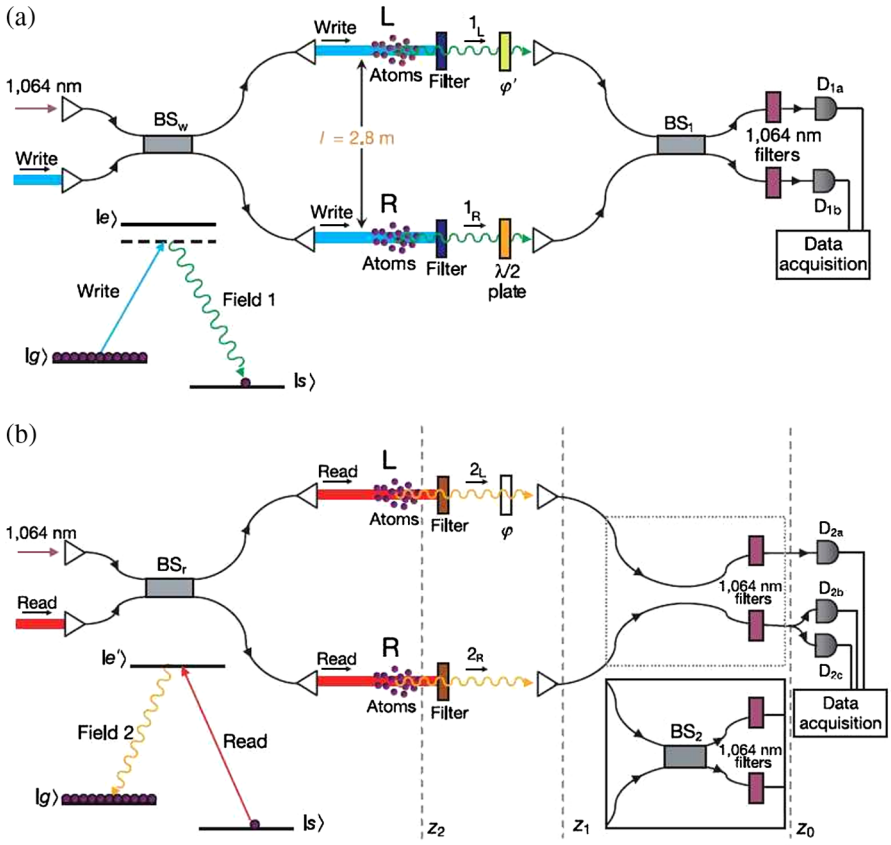

FIG. 25 (color online). An overview of the experiment to entangle two atomic ensembles . (a) Setup for generating entanglement between two pencil-shaped ensembles L and R located within spherical clouds of cold cesium atoms. The atomic level structure for the writing process consists of the initial ground state $|g\rangle$ ($^6S_{1/2}$, $F = 4$ level of atomic cesium), the ground state $|s\rangle$ for storing a collective spin flip ($^6S_{1/2}$, $F = 3$ level), and the excited level $|e\rangle$ ($^6P_{3/2}$, $F = 4$). The transition $|g\rangle \rightarrow |e\rangle$ in each ensemble is initially coupled by a write pulse detuned from resonance to generate the forward-scattered anti-Stokes field 1 from the transition $|e\rangle \rightarrow |s\rangle$. The L and R ensembles are excited by synchronized writing pulses obtained from beam splitter BS$_w$. After filtering, the anti-Stokes fields $1L$ and $1R$ are collected, coupled to fiber-optic channels, and interfere at beam splitter BS$_1$, with outputs directed toward two single-photon detectors D_{1a} and D_{1b}. (b) Schematic for verification of entanglement between the L and R ensembles by conversion of atomic to field excitation by way of simultaneous read pulses obtained from BS$_r$. The read pulses reach the samples after a programmable delay from the write pulses and couple the transition $|s\rangle \rightarrow |e\rangle$ ($|e\rangle$ being the $^6P_{1/2}$, $F = 4$ level), leading to the emission of the forward-scattered Stokes fields 2_L and 2_R from the transition $|e\rangle \rightarrow |g\rangle$. The upper inset shows the configuration used to measure the diagonal elements of the density matrix from the photodetection events at D_{2a}, D_{2b}, and D_{2c}. The off-diagonal elements are measured by interfering the fields 2_L and 2_R at the beam splitter BS$_2$ (see lower inset). The 12 m arms of both write and read interferometers are actively stabilized using an auxiliary Nd:YAG laser at 1.06 mm. From Chou *et al.*, 2005.

For example, because of the probabilistic nature of the spontaneous Raman process, there is an unavoidable finite probability to create higher-order terms with two or more excitations (see Sec. II.A). Nonperfect filtering of the excitation light will also alter the heralded state. To prove entanglement experimentally, it is therefore crucial to demonstrate the single-excitation character of the atomic state as well as the coherent superposition of the delocalized excitation (van Enk *et al.*, 2007). Chou *et al.* (2005) devised a way to prove unambiguously the entanglement of the heralded atomic state, based on quantum tomography. They reconstructed the density matrix of the stored state in a Hilbert space spanned by the state $|0_A 0_B\rangle, |1_A 0_B\rangle, |0_A 1_B\rangle, |1_A 1_B\rangle$, where $|n_A n_B\rangle$ is the state with n excitations in ensemble A and n excitations in ensemble B. In order to measure the density matrix, the atomic state is first transferred into a photonic state and the state of the atoms is inferred from the state of the electromagnetic fields. The diagonal terms of the density matrix are measured by direct photon counting, while the coherences are inferred from an interference measurement with the conditional anti-Stokes photons (see Fig. 26). The density matrix can then be used to calculate the amount of entanglement using an entanglement measure, for example,

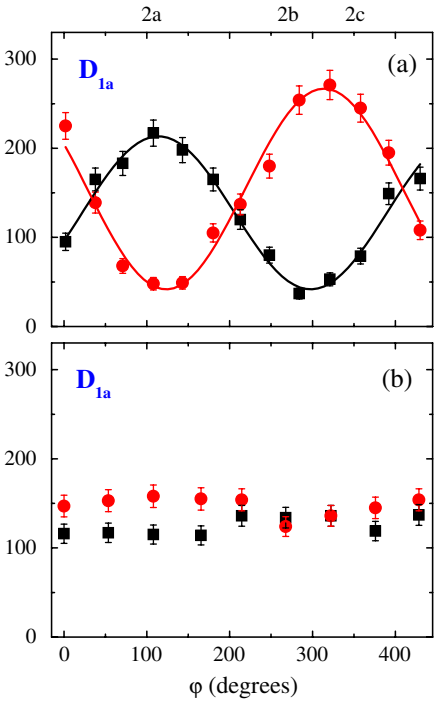

FIG. 26 (color online). Signature of the coherent superposition of a single excitation delocalized between two atomic ensembles located 3 m away. After the detection heralding entanglement, the stored excitations are converted into anti-Stokes photons and combined at a beam splitter, forming a Mach-Zehnder interferometer. (a) The detection of the anti-Stokes fields after the beam splitter as a function of the phase of the interferometer conditioned on the detection of a Stokes photon (heralding event), when the Stokes fields are combined with the same polarization. (b) The same measurement when the Stokes fields are combined with orthogonal polarizations. This highlights the importance of the indistinguishability of the Stokes photons in order to generate an entangled state. From Chou *et al.*, 2005.

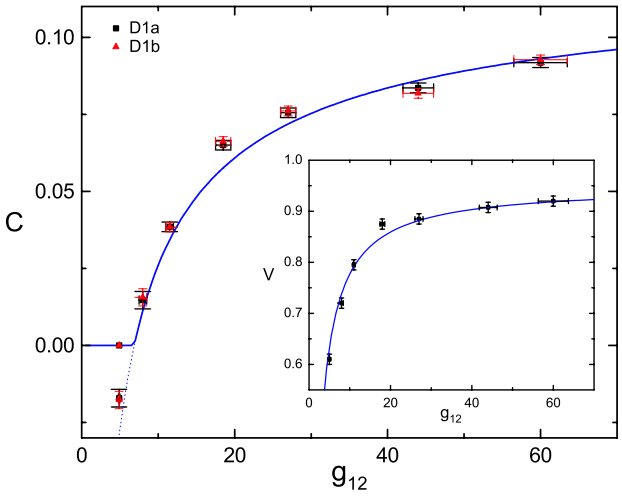

FIG. 27 (color online). Heralded entanglement between two atomic ensembles. Concurrence C (without correcting for propagation and detection losses) as a function of the normalized cross-correlation function $g_{S,AS}$ (denoted here g_{12}), for the two possible heralding events (detection at D_{1a} or D_{1b} after the beam splitter). Inset: Average visibility of the interference fringe between the two field-2 modes. From Laurat, Choi *et al.*, 2007.

the concurrence C, where $C = 0$ for unentangled states, and $C = 1$ for maximally entangled states (Wootters, 1998). Using this technique, Chou *et al.* (2005) were able to demonstrate measurement-induced entanglement between the two spatially separated atomic ensembles, albeit with a low concurrence (of order $C = 2 \times 10^{-2}$ at the output of the ensembles).

The main reason for the low concurrence in the first experiment was the limited retrieval efficiency (10%). This was considerably improved in a more recent experiment with two ensembles in the same MOT (Laurat, Choi *et al.*, 2007). The concurrence was measured as a function of the cross-correlation function (see Fig. 27), with a maximum value of $g_{S,AS} = 60$. At this value, a concurrence of $C = 0.35 \pm 0.1$ has been measured at the output of the ensemble, leading to an inferred $C = 0.9 \pm 0.3$ for the atomic state. The decoherence of the stored entangled state was also analyzed in this experiment, with entanglement persisting for at least 20 μs.

3. Elementary segment of DLCZ quantum repeater

Number state entanglement of the form of Eq. (33) is not practical for performing quantum communication tasks, such as quantum key distribution. It is indeed difficult to implement single-qubit rotations in the excitation number basis. The solution proposed by DLCZ to this problem is the implementation of two chains of entangled number state ensembles in parallel (see Sec. II.B). In this way, it is possible to create an effective two-excitation entangled state by post-selection when the two chains are combined at the remote locations. This architecture also considerably relaxes the constraints for phase stability. If the light fields for the two chains are combined and multiplexed in the same quantum channel, the phase of the quantum channel must be constant only during the time interval Δt between the successful entanglement generation in the two chains. An advantage of

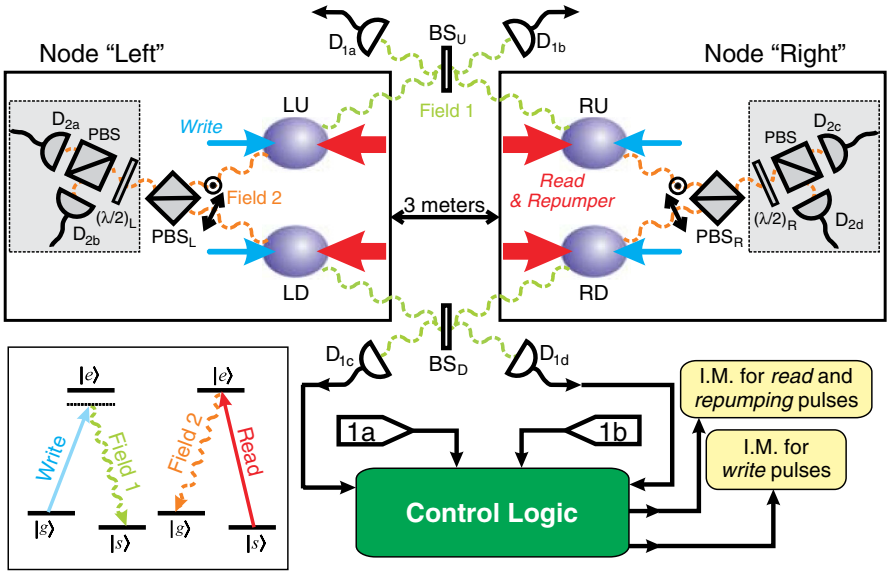

FIG. 28 (color online). Setup for the elementary link of a DLCZ quantum repeater between two quantum nodes (L, R) separated by 3 m. The inset at the bottom left shows the relevant atomic levels for the ${}^6S_{1/2} \rightarrow {}^6P_{3/2}$ transition in atomic cesium, as well as the associated light fields. With this setup, a photodetection event at either detector D_{1a} or D_{1b} indicates entanglement between the collective excitation in LU and RU, and a photodetection event at either detector D_{1c} or D_{1d} indicates entanglement between the collective excitation in LD and RD (20). Two orthogonal polarizations in one fiber beam-splitter implement BS_U and BS_D, yielding excellent relative path stability. A heralding detection event triggers the control logic to gate off the light pulses going to the corresponding ensemble pair (U or D) by controlling the intensity modulators (I.M.). The atomic state is thus stored while waiting for the second ensemble pair to be prepared. After both pairs of ensembles U and D are entangled, the control logic releases strong read pulses to map the states of the atoms to photons that are combined with orthogonal polarizations on the polarizing beam splitters PBS_L and PBS_R. If only coincidences between the fields at both nodes are registered, the state is effectively equivalent to a polarization maximally entangled state. From Chou *et al.*, 2007.

this scheme compared to two-photon schemes (see below) is that the entanglement by single-photon detection can be generated independently in the two chains, which leads to higher generation rates for the elementary link. The realization of this scheme (Chou *et al.*, 2007) was the first experimental demonstration of an elementary segment of a quantum repeater. The experiment was realized with four cold atomic ensembles, as shown in Fig. 28. The two quantum nodes were in different apparatuses, about 3 m apart. Each node was composed of two ensembles about 1 mm apart, implemented by addressing two different parts of a cold atomic cloud with orthogonal polarizations. The Stokes light emitted by the ensembles was recombined and coupled in the same single-mode fiber, with two orthogonal polarizations (polarization multiplexing). The light from the two nodes was then mixed at a beam splitter, followed by polarization optics to separate the two polarizations corresponding to the two chains of ensembles. The entanglement was generated in a heralded fashion, using a conditional control (Felinto *et al.*, 2006) that stopped sending excitation pulses once a successful detection was obtained for the corresponding chain. In this way, the entanglement could be obtained independently in the two chains (up to the limited memory time of about 10 μs in the present experiment).

Once the two chains of ensembles have been successfully entangled, the stored excitations are retrieved simultaneously in all ensembles, and the retrieved light is combined at each node. The desired effective two-photon entangled state is finally postselected by conserving only the events where one detection is present at each node. The effective entanglement was verified by violating a Bell inequality with the two fields.

Note that the optical phases were not actively stabilized in this experiment. The passive phase stability of the quantum channels during the time interval corresponding to the memory time (10 μs) was good enough to ensure a proper phase compensation.

4. Entanglement connection

Entanglement connection is obviously a crucial step in order to extend the entanglement distance in quantum repeater architectures. While many experimental demonstrations of entanglement swapping have been realized with entangled photons (Pan *et al.*, 1998; de Riedmatten *et al.*, 2005; Halder *et al.*, 2007; Kaltenbaek *et al.*, 2009), only one attempt has been made so far to demonstrate the swapping of entanglement with ensemble quantum memories (Laurat, Chou *et al.*, 2007). The experiment was realized in a setup similar to that of Chou *et al.* (2007). Heralded number state entanglement was again generated independently in two chains of ensembles. One ensemble of each chain is then read out simultaneously, and the retrieved light is combined at a beam splitter. A detection after the beam splitter transfers the entanglement to the remaining ensembles, which have never interacted. While the authors have been able to demonstrate the transfer of a substantial amount of quantum coherence, the demonstration of entanglement was not

possible using the method developed by Chou *et al.* (2005). Actually, this experiment highlights one of the main limitations of the DLCZ protocol: the quadratic propagation of two-photon errors with the number of links. In order to keep the two-photon error low enough to demonstrate entanglement, the excitation probability has to be kept to a very low level. The resulting count rate was not high enough to be able to determine the two-excitation probability, as required for the quantum tomography, in a reasonable time.

B. Entanglement creation and swapping based on two-photon detections

We will now review experiments that are particularly relevant to the schemes where the entanglement creation and/or connection are based on two-photon detections.

1. Two-photon quantum interference from separate ensembles

Two-photon quantum interference plays an essential role in all of the protocols discussed in this review. Depending on the protocols, it is used for entanglement swapping (see Secs. III.A, III.B, and III.F) and for entanglement generation in the elementary links (see Secs. III.B and III.F). It also intervenes in the protocols that are primarily based on single-photon detections (see Secs. II, III.C, and III.E) in the final step, where two-photon entanglement is postselected. At the heart of two-photon interference lies the Hong-Ou-Mandel effect (Hong *et al.*, 1987). Because of the bosonic nature of photons, two indistinguishable photons mixed at a beam splitter stick together (photon bunching) and always exit in the same spatial mode. This is due to a destructive interference between the probability amplitudes of both photons being reflected and both transmitted. This effect manifests itself by the absence of coincidence detection between the two output modes of the beam splitter when the two photons are made indistinguishable, a property known as the Hong-Ou-Mandel (HOM) dip. The observation of a HOM dip is an efficient way to quantify the degree of indistinguishability of photons generated by spatially separated atomic ensembles.

In 2006, Felinto and co-workers reported the first observation of a two-photon quantum interference with photons emitted by separate atomic memories. They used heralded single photons generated independently in two cold Cs ensembles. Write pulses were sent in the two ensembles simultaneously, and Stokes light was collected in an optical fiber and sent to a single-photon detector. In order to be able to address independently the two clouds, they used a conditional control that stopped sending write pulses in the corresponding ensemble when a Stokes photon was detected. In this way, they could generate single spin excitations independently in the two ensembles. After a time corresponding to the memory time of the device, the two spin excitations were converted into single photons, coupled in a single-mode optical fiber and combined at a beam splitter in order to measure the two-photon quantum interference. A visibility of 70% was measured for the Hong-Ou-Mandel dip. From this value, taking into account the loss of visibility due to the remaining two-photon contribution, they inferred an indistinguishability of 90% between the two photons.

Beyond the two-photon interference, this experiment was also the first one to show that the use of a quantum memory could increase the generation rate of the quantum state of light in separated sources. The conditional control resulted in a 28-fold increase in the probability of obtaining a pair of single photons, relative to the case without memory.

A similar setup with Rb atoms was used in a more recent experiment by Yuan *et al.* (2007). The Hong-Ou-Mandel dip was measured by varying the relative delay between the two read pulses. In this way, they could infer the coherence time of the photons, 25 ns. A HOM visibility of 80% was obtained, also limited by two-photon contributions. They also measured the HOM dip in the frequency domain by changing the relative detuning between the two read beams. They found a similar visibility and a dip width of 35 MHz, in accordance with the time measurement.

In the two experiments mentioned above, the quantum interference is realized with conditional anti-Stokes single photons retrieved from the stored excitations. However, if the creation of entanglement is realized with a two-photon detection [as in the protocol of Zhao *et al.* (2007)], the interference will take place between the Stokes photons. This configuration was tested experimentally by Chanelière and co-workers (2007) with two cold Rb ensembles separated by 5.5 m. The two-photon interference was measured by recording the coincidence rate after the beam splitter for photons combined with the same and with orthogonal polarization. When the two unconditional Stokes photons are combined at the beam splitter, a HOM visibility of 33% is observed. This low visibility reflects the fact that the non-conditional Stokes fields are thermal fields. The probability of creating two Stokes photons in the same ensemble is equal to the probability of creating one Stokes photon in each ensemble. This is similar to what has been observed with two separate parametric down-conversion sources (de Riedmatten *et al.*, 2003). However, if only those cases are taken into account where the stored excitations are converted into anti-Stokes photons and detected (using a four-photon delayed coincidence procedure), then the conditional Stokes fields are single-photon fields, and a high-visibility HOM dip can be achieved, provided that the two fields are indistinguishable. They observed a visibility of $86\% \pm 3\%$.

In order to keep a high fidelity in a quantum repeater architecture, it is essential that the visibility of the Hong-Ou-Mandel interference is very high. The dip visibility indeed determines the fidelity of the swapping operations. The errors acquired during each swapping will then grow linearly with the number of links. The visibility of the Hong-Ou-Mandel interference for the experiments described here is still too low in that context. However, it is mainly limited by the two-photon components, which is already taken into account in the theoretical description of the protocols in Sec. III. By working in a lower-excitation regime, it should thus be possible to significantly improve the visibility. Besides the two-photon components, other factors can also decrease the visibility, such as waveform or polarization distinguishability. In that context, it is informative to look at the experiments demonstrating Hong-Ou-Mandel interferences with independent parametric down-conversion sources. The visibility has steadily improved over the past few years with the

best result so far being 0.96 (Kaltenbaek *et al.*, 2009). Note that the two-photon error is suppressed only in the very-low-excitation regime. That regime can be experimentally accessed if the measurement is done with two photons from the same source. In that case, visibilities approaching unity (0.994) have been measured (Pittman and Franson, 2003).

2. Entanglement between a photon and a stored excitation

Entanglement between photons and atomic excitations plays an important role in a number of repeater protocols; see Secs. III.B and III.F. Note that we consider here entangled states involving two excitations, one photonic and one atomic spin excitation. This entanglement can be realized in different ways: by encoding one logical qubit in two ensembles and by using internal spin states. We now describe these techniques in more detail.

a. Collective excitations in different spatial modes

This first technique uses two collective excitations in different ensembles or spatial modes to encode one logical atomic qubit. It was first proposed and experimentally realized by Matsukevich and Kuzmich (2004). In this experiment two nearby ensembles A and B within the same atomic cloud are simultaneously excited with orthogonally polarized write beams. Similarly to Eq. (6), the joint state of the atom-photon system after the Raman excitation can be written as follows:

$$\left(1+\sqrt{\frac{p}{2}}(\alpha s_a^\dagger a_H^\dagger e^{i\phi_a}+\beta s_b^\dagger b_V^\dagger e^{i\phi_b})+O(p)\right)|0\rangle. \quad (34)$$

The resulting orthogonally polarized Stokes fields in different spatial modes are then combined into a single spatial mode at a polarizing beam splitter. Neglecting vacuum and higher-order terms, the state can then be written as follows:

$$|\Psi\rangle=\alpha|1_a,V\rangle+\beta e^{i\Phi}|1_b,H\rangle, \quad (35)$$

where $1_{a,b}$ represents the terms with one collective spin excitation in ensemble A and B, respectively, and $|H\rangle$ ($|V\rangle$) is a photon with horizontal (vertical) polarization. By measuring the Stokes photon in the polarization basis, Matsukevich and Kuzmich were able to project the atomic ensembles into a superposition state. Then they showed that the atomic qubit could be mapped into a photonic qubit with a fidelity exceeding classical thresholds, by simultaneously reading out the two ensembles. In 2007, this technique was used to demonstrate the quantum teleportation of a polarization qubit carried by a weak photonic coherent state onto a matter qubit implemented with two cold Rb ensembles (Chen *et al.*, 2008).

An interesting development has been proposed in 2007 (S. Chen *et al.*, 2007). Instead of using two separate ensembles, they used a single ensemble, but collected the Stokes photon in two different spatial modes separated by a small angle, as shown in Fig. 29. After rotating the polarization of one of the modes by 90°, the two modes are combined at a PBS. The read beam is then sent in a counterpropagating way. Thanks to the phase matching, the anti-Stokes photons are emitted in the opposite direction of their respective Stokes photons. The entanglement between the two photons was verified by a violation of a Bell inequality, persisting for a storage time of 20 μs.

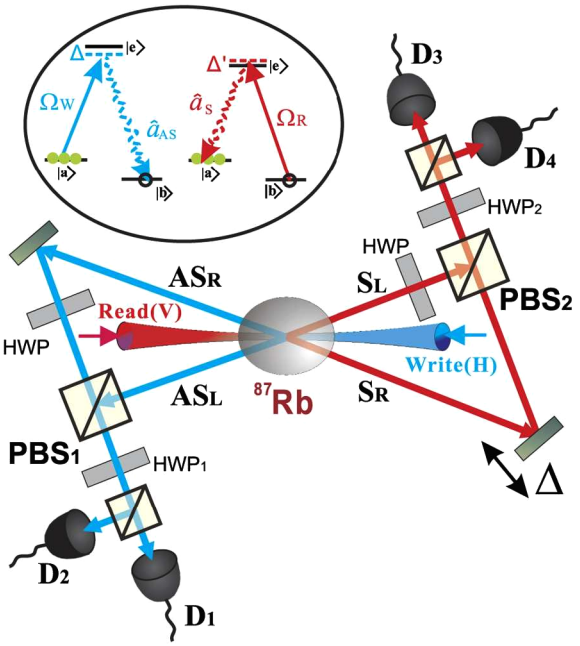

FIG. 29 (color online). The scheme of the experimental setup to generate entanglement between a photon and a stored atomic excitation using the two-modes approach. A weak horizontal polarized write pulse illuminates the cold Rb atom cloud. The spontaneous Raman scattered anti-Stokes fields AS_L and AS_R with vertical polarization are collected at $\pm 3°$ to the propagating direction of the write beam, defining the spatial mode of the atomic ensembles L and R, respectively. (Note that in this experiment the storage state has a lower energy than the initial state. Hence, the field generated by the write beam is called the anti-Stokes field and the collective field generated by the read beam is called the Stokes field, contrary to the convention used in this review.) The AS_R mode is rotated to be horizontally polarized, combined with AS_L mode on a polarizing beam splitter PBS1, and sent to the polarization analyzer. This creates the entanglement between the polarization of the anti-Stokes field and the spatial modes of spin excitation in the atomic ensemble. From S. Chen *et al.*, 2007.

The advantage of the entanglement with collective excitation in different spatial modes is that the relative probability of excitation of the two modes can be tuned, in contrast to the entanglement with internal spin states (see below). The drawback is that it requires interferometric stability between the two spatial modes.

The experiments mentioned here can also be seen as an elementary realization of spatial multiplexing, as described in Sec. III.D. Note that, recently, such a multiplexing has been successfully extended to 12 spatial modes (Lan *et al.*, 2009) and spatial multimode memories are being used to store images (Shuker *et al.*, 2008; Vudyasetu *et al.*, 2008; Heinze *et al.*, 2010).

b. Internal spin states

The second possibility to generate entanglement between light and stored excitation uses entanglement between the polarization of the Stokes photon and the internal spin state of the ensemble (Matsukevich *et al.*, 2005;

de Riedmatten *et al.*, 2006). This technique is similar to the one used to entangle single atoms or ions and emitted photons (Duan and Kimble, 2003; Feng *et al.*, 2003; Simon and Irvine, 2003). Suppose an ensemble of three-level atoms with two ground states $|g_1\rangle$ and $|g_2\rangle$, and one excited state $|e\rangle$. The atoms are initially in $|g_1\rangle$. A weak write pulse induces spontaneous Raman scattering via the excited state, and the excitation is transferred to $|g_2\rangle$ while emitting a Stokes photon. The emission of this photon can follow two different decay paths, leaving the atoms in different spin states. For example, for a circularly polarized write beam and for atoms initially in $|g_1, m_F\rangle$, the spontaneous Raman scattering can lead to spin excitation in $|g_2, m_F\rangle$ with emission of a Stokes photon with polarization σ^-, and to a spin excitation in $|g_2, m_F + 2\rangle$ with a σ^+-polarized Stokes photon. As long as the final states are indistinguishable in all other degrees of freedom, the nonvacuum part of the joint state of the light is given by

$$|\psi\rangle = \sqrt{p}(\cos\eta_{m_F}|\sigma^+, 1_a^+\rangle + \sin\eta_{m_F}|\sigma^-, 1_a^-\rangle) + O(p). \tag{36}$$

The coefficient η_{m_F} is given by the Clebsch-Gordan coefficient for the relevant transition. In the more general case where the initial state is an incoherent mixture of that various $|g, m_F\rangle$, the collective atomic states are mixed states. This scheme was first demonstrated by Matsukevich *et al.* (2005), with a cold Rb ensemble. The entanglement was verified by the violation of a Bell-Clauser-Horne-Shimony-Holt inequality between the Stokes and anti-Stokes photons, after a storage time of 200 ns. More recent results with cold Cs atoms (de Riedmatten *et al.*, 2006) led to a violation of Bell inequality close to the quantum limit and to the measurement of decoherence of entanglement, with violation of Bell inequality for up to 20 μs.

Besides these two techniques, two other experiments have demonstrated entanglement between collective matter qubits and photonic qubits. The first one is based on frequency encoded photonic qubits and dual species atomic ensembles (Lan *et al.*, 2007). The matter qubit basis consists in single collective excitations in each of the cotrapped atomic species (Rb^{85} and Rb^{87}). The second experiment demonstrated entanglement between the orbital angular momentum of the Stokes photon and the stored excitation (Inoue *et al.*, 2006).

3. Elementary segment of quantum repeater

Yuan *et al.* (2008) reported the experimental realization of an elementary segment of a quantum repeater, following the protocol of Zhao *et al.* (2007). In that protocol, the entanglement creation is based on two-photon detection. This requires the combination of light-matter entanglement and two-photon quantum interference. Probabilistic entanglement between stored excitations and emitted photons is first generated simultaneously in remote atomic ensembles. The two Stokes photons are then combined at a beam splitter (or a polarizing beam splitter) in the middle station for the Bell state measurement (BSM). A successful BSM projects the atomic ensembles in an entangled state. This stored atomic entangled state can be retrieved on demand by simultaneously reading out the memories. Yuan *et al.* (2008) used two cold Rb ensembles connected by 6 m or by 300 m of optical fibers. In each ensemble, they created entanglement between the polarization of the Stokes photon and the spatial mode of the stored excitations, as in Eq. (35), using the technique introduced by Z.-B. Chen *et al.* (2007). The two Stokes photons were then combined at a polarizing beam splitter, thus analyzing the projection on the Bell state:

$$|\Phi^+\rangle = \frac{1}{\sqrt{2}}(|H, H\rangle + |V, V\rangle). \tag{37}$$

A successful BSM projects the atomic ensembles in the state:

$$|\Phi^+\rangle_{1,2} = \frac{1}{\sqrt{2}}(|L_1, L_2\rangle + |R_1, R_2\rangle), \tag{38}$$

where $|L_i\rangle$ and $|R_i\rangle$ correspond to an excitation in spatial modes L and R with $i = 1, 2$ denoting the remote quantum nodes. In order to verify the entanglement, atomic qubits are converted into photonic qubits. In this scheme, the double excitations in each ensemble induce spurious events in the BSM that do not result in successful entanglement swapping. Hence, the probability to successfully project the ensembles in the state of Eq. (38) conditioned on a BSM is $1/2$ (Yuan *et al.*, 2008). The events that lead to a state with two excitations in one ensemble and none in the other can be eliminated by postselection during the entanglement verification stage. More important, they can be in principle discarded after the first entanglement connection, with a properly designed BSM (Zhao *et al.*, 2007).

In the experiment of Yuan *et al.* (2008), the quality of the postselected atomic state was good enough to violate a Bell inequality with the retrieved photons when the two ensembles were connected by 6 m of fiber for a storage time of up to ~ 4 μs. When the ensembles were connected by 300 m of fiber, a postselected fidelity $F = \mathrm{Tr}(\rho_{\mathrm{expt}}|\Phi^+\rangle_{1,2}\langle\Phi^+|) = 0.83 \pm 0.02$ was measured.

4. Deterministic local generation of entanglement

As mentioned in Sec. III.B, the local generation of high-fidelity pairs of entangled ensembles is an important capability for the implementation of robust quantum repeater architectures, in particular, for the realization of the protocol of Z.-B. Chen *et al.* (2007), Sec. III.B. We briefly mention here two deterministic schemes to create number state entanglement between two ensembles that may be useful in this context. The first experiment is based on the adiabatic transfer of one excitation between two ensembles using a quantum bus in an optical cavity (J. Simon *et al.*, 2007a). The second experiment is based on the absorption of a delocalized one photon state by two atomic ensembles using EIT (Choi *et al.*, 2008).

Note that these techniques, while very effective for deterministically entangling nearby ensembles, cannot be used to directly generate a large amount of entanglement between remote ensembles. The reason is that the resulting state would contain a large vacuum component, due to the transmission loss. A direct use of such an entangled state over a long distance would be very inefficient for quantum repeaters applications.

C. Quantum light sources compatible with ensemble-based quantum memories

An alternative to DLCZ-like quantum memories, where the photon source and the memory are implemented within the same atomic ensembles, is to use different systems for the generation and for the storage of quantum light; see Sec. III.C. This configuration has the distinct advantage that the photon to be stored and the photon to be transmitted over long distances can have different wavelengths. The separation of entanglement creation and storage also allows the use of a class of quantum memories that are well adapted to the storage of multiple temporal modes (see Sec. V.D.2).

In order to be compatible with ensemble-based quantum memories, the single photons must be at the resonance frequency of the atoms and have a narrow spectrum that matches the quantum memory bandwidth (typically between 10 and 100 MHz). Several ways have been proposed to create quantum light with such specific properties. The first technique, described in Sec. V.C.1, is based on the generation of photon pairs and heralded single photons with atomic ensembles. We also briefly mention two other promising approaches based on parametric down-conversion (Sec. V.C.2) and on single quantum emitters (Sec. V.C.3).

1. Photon-pair and single-photon sources based on atomic ensembles

A natural way to create single photons or photon pairs compatible with ensemble-based quantum memories is to use the same atomic ensembles as the photon source.

a. Photon-pair sources

In principle, any DLCZ-like memory, such as those described in Sec. V.A.1, can be used as a source of nonclassical photon pairs, since the Stokes and anti-Stokes fields are strongly correlated. While the previously described experiments were performed in the pulsed regime with write and read beams separated in time, photon-pair creation has also been demonstrated in the continuous regime. In 2005, Balic *et al.* reported a four-wave mixing experiment that generated counterpropagating paired photons with coherence time of about 50 ns and linewidth of about 9 MHz using cw write and read lasers in a cold Rb ensemble. They used a four-level system with two hyperfine ground states. The wavelengths of the Stokes and anti-Stokes photons were 780 and 795 nm, respectively. The waveforms of the photon pairs were shown to be controllable at a rudimentary level by changing the read beam Rabi frequency. The photons were coupled into opposing single-mode fibers at a rate of 12 000 pairs/s and violated the Cauchy-Schwartz inequality by $R = 400$. Using a similar setup, Kolchin *et al.* (2006) generated photon pairs with 5 ns coherence time with the use of a single driving laser. This is possible by using a far-off-resonance (6.8 GHz) Raman transition for the Stokes-photon generation. Simultaneously, Thompson *et al.* (2006) reported the generation of nearly identical photon pairs of 1.1 MHz bandwidth at a rate of 5×10^4 pairs/s from a cold Cs atomic ensemble inside a low-finesse ($F = 250$) optical cavity. In order to generate degenerate photons, they also used a single driving laser, but two Zeeman ground state levels, instead of two hyperfine ground state levels. The two photons were shown to be nonclassically correlated ($R = 760$). They were also shown to be indistinguishable to a large degree by performing a Hong-Ou-Mandel–type experiment. The results of Balic *et al.* (2005) were recently improved by the use of a two-dimensional magneto-optical trap with optical depth as high as 62 (Du *et al.*, 2008). Photon pairs with coherence time up to 900 ns with a subnatural linewidth of 0.75 MHz were generated. They observed that 74% of the Stokes photons were paired, and there was a strong violation of the Cauchy-Schwartz inequality ($R = 11\,600$).

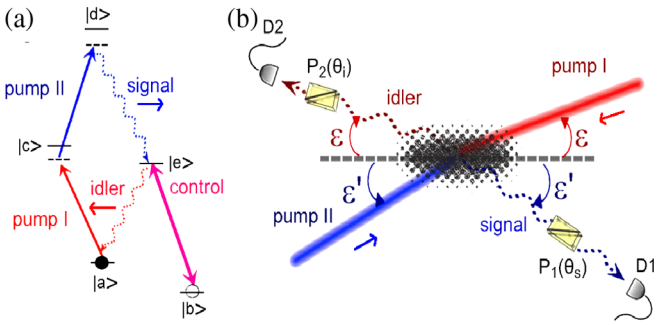

FIG. 30 (color online). Source of nondegenerate photon pairs using atomic cascade transitions. (a) The atomic structure for the proposed cascade emission scheme involving excitation by pumps I and II. Pump II and the signal photons lie in the telecommunication wavelength range when a suitable level of orbital angular momentum $L = 0$ or $L = 2$ is used as level $|d\rangle$. (b) Schematic of experimental setup based on ultracold ^{85}Rb atomic gas. From Chanelière *et al.*, 2006.

The previously described DLCZ-type photon sources do not offer much flexibility with the photon wavelength (see Sec. II.A). In particular, it is not possible to directly create a photon at 1.5 μm, as required for quantum repeater applications. As mentioned in Sec. III.C, one possibility is to use wavelength conversion techniques. Another interesting possibility for creating nondegenerate photon pairs in ensembles is based on atomic cascade transitions. Chanelière *et al.* (2006) demonstrated an entangled pair of 1530 and 780 nm photons generated from an atomic cascade transition in a cold Rb ensemble (see Fig. 30). While the 1530 nm photon can be transmitted with low loss in optical fibers, the 780 nm is naturally suited for mapping to an ensemble-based Rb memory. They observed polarization entanglement between the two photons and superradiant temporal profiles for the photon at 780 nm.

b. Single-photon sources

The strong correlation between Stokes and anti-Stokes fields enables the generation of heralded single-photon fields with programmable delay. The detection of the Stokes field heralds the presence of a stored excitation that can be converted into a single-photon field at a programmable time, as described previously. This was first reported by Chou *et al.* (2004). The single-photon character of the emitted anti-Stokes field, conditioned on the detection of a Stokes photon, was demonstrated with a Hanbury-Brown–Twiss setup, leading to an anticorrelation parameter (Grangier *et al.*, 1986) [see Eq. (31)] $\alpha = 0.24 \pm 0.05$. Improvements in the filtering

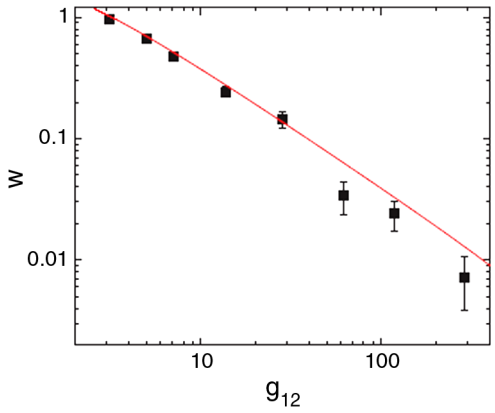

FIG. 31 (color online). Suppression of the two-photon component of the anti-Stokes field conditioned on the detection events in the Stokes field, measured by the autocorrelation parameter α (denoted here w) as a function of $g_{S,AS}$ (denoted here g_{12}). The lowest value obtained is 0.007 ± 0.003. From Laurat *et al.*, 2006.

of the Stokes and anti-Stokes photons with cold ensembles (see Sec. V.A.1) led to improved suppression of the two-photon component (Chanelière *et al.*, 2005; Chen *et al.*, 2006), with the best values of α close to (Matsukevich *et al.*, 2006a) or below 0.01 (Laurat *et al.*, 2006) (see Fig. 31). Another interesting possibility is to use the heralded source of photons combined with a measurement feedback protocol for implementing a deterministic single-photon source, as was first proposed and demonstrated in Matsukevich *et al.* (2006a) and later in Chen *et al.* (2006) and R. Zhao *et al.* (2008).

For hot gases, the filtering is more challenging, and the two-photon components of the heralded anti-Stokes field reported so far are sensibly higher than with cold ensembles, with the lowest value being $\alpha = 0.1 \pm 0.1$ (Eisaman *et al.*, 2005; Walther *et al.*, 2007).

2. Narrow band photon-pair sources based on parametric down-conversion

A well-known technique to generate correlated or entangled photon pairs is based on spontaneous down-conversion in nonlinear crystals (Burnham and Weinberg, 1970; Hong and Mandel, 1985; Wu *et al.*, 1986; Hong *et al.*, 1987). The bandwidth of the photon generated with this method is, however, usually of the order of 10 THz, very far from atomic memory bandwidth, of order 10 to 100 MHz. Two techniques have been proposed to achieve the extreme reduction in photon bandwidth required to efficiently map the light produced by spontaneous down-conversion in atomic memories. The first one is based on cavity enhanced down-conversion (Ou and Lu, 1999). In that case, the nonlinear crystal is placed inside an optical cavity and the light is emitted only in the cavity modes. The system is operated as an optical parametric oscillator far below threshold. The reduction in spectral bandwidth is compensated by the enhancement in the efficiency of the photon-pair generation due to the cavity resonance. Without further filtering, the output of the cavity is spectrally multimode (Wang *et al.* 2004; Kuklewicz *et al.*, 2006; Wolfgramm *et al.*, 2008; Scholz *et al.*, 2009a). Ideally, a single cavity mode should be selected, such that the bandwidth of the parametric light is given by the width of the cavity mode. This can be done by using etalons or filter cavities with different free spectral range. Neergaard-Nielsen *et al.* (2007) generated single high-purity heralded single photons of 8 MHz bandwidth at 860 nm using such a system. More recently, Scholz *et al.* (2009b) also demonstrated a single-mode operation of a cavity enhanced parametric down-conversion narrow band single-photon source, with a spectral width of 2.7 MHz and a spectral brightness of 330 photon pairs/[s mW MHz]. Finally, single-mode polarization entangled photons have been generated at 780 nm with 10 MHz bandwidth (Bao *et al.*, 2008). In order to profit from the enhanced generation efficiency, the cavity must be resonant with the two down-conversion modes. Hence, all the experiments demonstrated so far have worked in the regime of degenerate or near-degenerate photon pairs.

The second technique is based on passive filtering. In that case, the massive reduction of bandwidth is accompanied by a corresponding reduction in conversion efficiency. It is thus extremely challenging to implement such a filtering with traditional nonlinear crystals. A possible solution is the use of highly efficient waveguide sources (Tanzilli *et al.*, 2001) based on periodically poled (PP) crystals, such as lithium niobate (LN) or $KTiOPO_4$ (KTP). These sources feature a conversion efficiency about 4 orders of magnitude larger than conventional bulk crystals. Using a PPLN waveguide together with fiber Bragg grating filters, Halder *et al.* (2008) generated photon pairs at telecommunication wavelength with a bandwidth of 1.2 GHz. With 7 mW of pump power, the source achieved a spectral radiance of 0.08 photon pairs per coherence time. A photon-pair source adapted for a rubidium atomic memory was also recently realized with a PPLN waveguide. The 10 THz bandwidth of the parametric fluorescence was first reduced to 23 GHz using a holographic grating, and further decreased to 600 MHz using an etalon before detection (Akiba *et al.*, 2007). In a more recent experiment (Akiba *et al.*, 2009), a third filtering stage was introduced with a moderate-finesse optical cavity, and the bandwidth of the photon pairs was reduced to 9 MHz.

3. Single-photon sources based on single quantum emitters

We now briefly mention some single quantum systems that generate single photons with the required spectral properties to be compatible with atomic memories. The advantage of using single quantum emitters is that the photons can be emitted on demand. The first example is single trapped atoms. Single photons have been emitted deterministically from single atoms trapped in high-finesse optical cavities (McKeever *et al.*, 2004; Hijlkema *et al.*, 2007) and in free space (Darquie *et al.*, 2005). More recently, entangled photons have been generated from a single atom trapped in an optical cavity (Weber *et al.*, 2009). All these experiments have been performed with Cs or Rb atoms emitting at 852 and 780 nm, respectively. The emitted photons are therefore naturally suited for mapping in a corresponding atomic ensemble, but frequency conversion is required for long-distance transmission in optical fiber. Single photons have also been generated by trapped single ions (Keller *et al.*, 2004; Dubin *et al.*, 2007; Maunz *et al.*, 2007). Some

solid-state emitters at cryogenic temperature may also be interesting. A first example is single quantum dots embedded in microcavities. Quantum dots offer more flexibility for the wavelength of the emitted photon, in particular, single-photon sources at telecommunication wavelength based on quantum dots have been demonstrated (Ward *et al.*, 2005; Zinoni *et al.*, 2006; Hostein *et al.*, 2009). The demonstrated photon bandwidths are, however, still far too large to match the memory bandwidths. A promising solid-state alternative is based on single dye molecules embedded in a solid-state matrix. Fourier transformed single photons at 590 nm with a bandwidth of 17 MHz have recently been generated (Lettow *et al.*, 2007). The use of a different dye molecule may offer some wavelength flexibility. Finally, a last possible candidate is based on the N-V in diamond, where close to Fourier limited single photons have recently been observed, with lifetimes of about 10 ns (Batalov *et al.*, 2008).

D. Storage of single photons in atomic ensembles

We now review the protocols that have been proposed and demonstrated experimentally for the storage of single photons in ensembles of atoms. Section V.D.1 is devoted to quantum memories based on EIT (Lukin, 2003; Fleischhauer *et al.*, 2005), and Sec. V.D.2 describes another more recent class of quantum memories based on photon echoes (Tittel *et al.*, 2008). A more general review about light-matter quantum interfaces can be found in Hammerer *et al.* (2010).

1. Quantum memories based on electromagnetically induced transparency

A well-known technique for mapping quantum state of light into atomic states is based on EIT (Fleischhauer and Lukin, 2000; Fleischhauer *et al.*, 2000; Fleischhauer and Lukin, 2002). It has been the subject of several reviews (Lukin, 2003; Fleischhauer *et al.*, 2005) so we give here only the basic feature of the technique and review the relevant experiments. EIT is a quantum interference effect that renders an opaque atomic medium transparent thanks to a control laser field. This effect is associated with a strong dispersion in the atomic medium that leads to strong slowing and compression of the light. It has been shown that by turning off the control laser when the optical pulse is completely compressed in the atomic memory, it is possible stop the light, i.e., to map the state of the light onto collective spin excitations of the atoms (Fleischhauer and Lukin, 2000, 2002). The atomic state can then be converted into light again by turning on the control laser. This scheme has been demonstrated with bright coherent light both in ultracold atoms (Liu *et al.*, 2001) with storage time of about 1 ms and in hot atomic vapor (Phillips *et al.*, 2001) with storage time up to 0.5 ms. More recent experiments in hot atomic gases have led to storage and retrieval efficiencies close to 50% (Novikova *et al.*, 2007; Phillips *et al.*, 2008) for storage times of order of 100 μs. These experiments implemented the optimal control strategy introduced in Gorshkov *et al.* (2007a), (2007b), (2007c), and (2007d). More recently, a stopped light experiment has been reported with ultracold atoms loaded in a three-dimensional optical lattice. A storage time of 240 ms was reported (Schnorrberger *et al.*, 2009), albeit with a low storage and retrieval efficiency (0.3%). Stopped light has also been observed in rare-earth-doped solids (a $Pr:Y_2SiO_5$ crystal) (Turukhin *et al.*, 2001). The coherence time of the hyperfine ground state of $Pr:Y_2SiO_5$ without external magnetic fields is 500 μs. It can, however, be dramatically increased by using an appropriate small magnetic field (Fraval *et al.*, 2004) and by using dynamical control of decoherence (Fraval *et al.*, 2005). Using these techniques, Longdell *et al.* (2005) demonstrated a stopped light experiment (with efficiency of about 1%) in a $Pr:Y_2SiO_5$ crystal with storage times exceeding 1 s, which is the longest light storage time reported to date.

All the above mentioned experiments were realized with bright coherent pulses. The first experiments of storage and retrieval of single-photon fields, which represent an important milestone, were published in 2005 simultaneously by two groups. Eisaman *et al.* (2005) used a hot atomic vapor to generate conditional single-photon fields with the required wavelength and bandwidth properties. The single anti-Stokes photon pulses were then sent to another distant hot atomic ensemble where both slow and stopped light was observed. A storage and retrieval efficiency of 10% for short delays and a storage time of 1 μs were demonstrated, with the nonclassical character of the stored field persisting for 500 ns. Chanelière *et al.* (2005) used two cold Rb atomic ensembles as single-photon source and quantum memory, respectively. In this experiment, the single-photon field is implemented with the Stokes field, conditioned on a subsequent anti-Stokes detection. The single photons were then directed to another ensemble through 100 m of optical fiber to be stored. In order to minimize the noise from the excitation and control beams, the two beams are applied with a small angle. After a programmable time, the atomic excitation is converted back into a single photon. The storage and retrieval efficiency for a storage a time of 500 ns is 6%. The single-photon character of the stored and retrieved field is verified explicitly by a Hanbury-Brown–Twiss experiment after a storage of 500 ns (with a minimum anticorrelation parameter $\alpha = 0.36 \pm 0.11$), while nonclassical correlations between the retrieved Stokes photon and the anti-Stokes photon are observed for storage time exceeding 10 μs. The storage and retrieval efficiency of single photons in cold atomic ensembles has been recently increased to 17% for a storage time of 1 μs Choi *et al.* (2008); see Fig. 32.

Matsukevich *et al.* (2006b) showed that the EIT technique also allows the mapping of a polarization qubit carried by a single photon. They generated probabilistic entanglement between the polarization of the Stokes photons and the internal spin state of the stored excitation, as in Matsukevich *et al.* (2005). The polarization of the Stokes photon was then mapped onto a distant atomic ensemble, resulting in the probabilistic entanglement of two remote matter qubits. The entanglement was demonstrated in a post-selected fashion by converting the two stored qubits in photonic qubits and by measuring polarization correlations between the two photons, resulting in a violation of a Bell inequality.

EIT storage of degenerate nonclassical light generated by parametric down-conversion has also been recently demonstrated (Akiba *et al.*, 2007, 2009). Correlated photon pairs

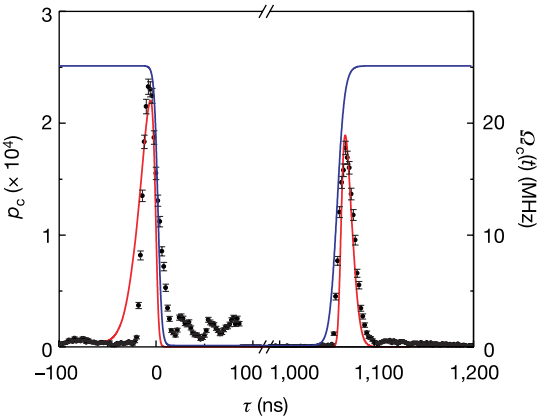

FIG. 32 (color online). Storage and retrieval of single-photon fields using EIT in a cold Cs ensemble. The points around $\tau = 0$ μs represent "leakage" of the signal field due to the finite optical depth and length of the ensemble. The points beyond $\tau = 1$ μs show the retrieved signal field. The overall storage and retrieval efficiency is $(17 \pm 1)\%$. The solid line is the estimated Rabi frequency of the control pulse. From Choi *et al.*, 2008.

and heralded single photons were generated in the PPLN waveguide source described in Sec. V.C.2 and stored in a cold Rb ensemble. In the first experiment (Akiba *et al.*, 2007), the parametric fluorescence light injected into the ensemble was spectrally much broader (600 MHz) than the EIT transparency window (8.3 MHz) and they demonstrated frequency filtered storage. The small part of the light that spectrally matched the EIT transparency window was stopped in the ensemble and thus delayed relative to the rest of the light, which propagated through the atoms. The retrieved photons (with 8% efficiency) could thus be detected using temporal filtering. They demonstrated that the coherence time of the light retrieved after a storage of 400 ns was increased to 35 ns, compared to 0.2 ns for the incident broadband light. Moreover, the conservation of the nonclassical character of the stored and retrieved light was confirmed by measuring superbunching. In the second experiment (Akiba *et al.*, 2009), the bandwidth of the incident photons was reduced to 9 MHz with a moderate-finesse optical cavity. The filtered degenerate parametric fluorescence was stored for 300 ns in a cold Rb ensemble, before being retrieved with a storage and retrieval efficiency of ~14%. The nonclassical character of the retrieved light was verified by the experimental violation of a classical inequality for photon counts. This confirms that the nonclassical properties of the degenerate parametric fluorescence are conserved during the storage in the ensemble. The storage and retrieval of conditional single-photon states were also demonstrated. The retrieved field was shown to exhibit antibunching (with an autocorrelation parameter $\alpha = 0.52 \pm 0.30$). More recently, Jin *et al.* (2010) stored and retrieved one part of an entangled pair created by down-conversion into a rubidium cold atomic ensemble. The photon pair has a bandwidth of 5 MHz and is frequency uncorrelated. They showed that the nonclassical character of the correlation between the two photons was preserved after the storage. They also stored the two polarization modes of one of the photons in two different modes of the ensemble and showed a Bell inequality violation for storage time up to 1 μs, thus demonstrating that the entanglement is stored and survives the storage.

Note also that off-resonant Raman techniques have been proposed (Nunn *et al.*, 2007) and experimentally demonstrated (Reim *et al.*, 2010) with coherent states containing about 1000 photons on average. This technique enables the storage of very short pulses. In particular, Reim *et al.* (2010) reported the storage and retrieval of subnanosecond pulses with 1 GHz bandwidth with an efficiency of 15%.

Furthermore, we mention that a detailed study of the theory of photon storage in optically thick ensembles of three-level atoms in a Λ configuration has been published in a series of papers: Gorshkov *et al.* (2007b), (2007c), (2007d), and (2008).

To end this section, we discuss the multimode properties of EIT-based storage. It has been shown that the number of modes N_m that can be efficiently stored using EIT scales as $N_m \sim \sqrt{d}$, where d is the optical depth of the sample (Nunn *et al.*, 2008). This means that extremely high values of d are needed in order to store multiple temporal modes. The reason for this poor scaling is that high-efficiency storage of many temporal modes requires at the same time a very slow group velocity in order to compress all the pulses in the sample before turning off the control fields and large transparency windows in order to store short photons.

2. Photon-echo-based quantum memories

We now review other quantum storage protocols based on photon-echo techniques. In contrast to EIT-based protocols, which rely on transparency, these protocols rely on the reversible absorption of a single-photon pulse in an inhomogeneously broadened medium. After absorption, the single-photon state is mapped onto a single collective atomic excitation at the optical transition,

$$|1\rangle_A = \sum_i c_i e^{i\delta_i t} e^{-ikz_i} |g_1 \cdots e_i \cdots g_N\rangle, \tag{39}$$

where z_i is the position of atom i and δ_i is the detuning of atom i with respect to the central frequency of the photon. This collective state rapidly dephases, since each term acquires a phase $e^{i\delta_i t}$. The goal of the quantum memory protocols described here is to engineer the atomic system such that this inhomogeneous dephasing can be reversed. If this rephasing can be implemented, the light is reemitted in a well-defined spatiotemporal mode when the atoms are all in phase again, as a result of a collective interference among all the emitters.

The rephasing of the dipoles can be triggered by optical pulses, as it is the case in traditional photon-echo techniques. These techniques, while very successful to store classical light (Lin *et al.*, 1995) and as a tool for high-resolution spectroscopy (Macfarlane, 2002), suffer from strong limitations for the storage of single photons. In particular, it has been shown that the unavoidable fluorescence due to the atoms excited by the strong optical rephasing pulse blurs the single-photon state and reduces the fidelity of the storage to an unacceptable level (Ruggiero *et al.*, 2009).

We describe here two modified photon-echo approaches that allow in principle the storage and retrieval of

single-photon fields with unit efficiency and fidelity. The first one is based on controlled reversible inhomogeneous broadening (CRIB), and the second one on atomic frequency combs.

a. Controlled reversible inhomogeneous broadening

The theory of CRIB based quantum memories has already been reviewed elsewhere (Tittel *et al.*, 2008), and we give here only a short explanation of the principle, before discussing experimental progress.

The idea of CRIB is to trigger the collective reemission of light absorbed by an ensemble of atoms by reversing the detuning of each emitter at a given time τ after the absorption, such that $\delta_i \rightarrow -\delta_i$. In this way, the state of the atoms evolves as

$$|1\rangle_A = \sum_i c_i e^{i\delta_i \tau} e^{-i\delta_i t} e^{-ikz_i} |g_1 \cdots e_i \cdots g_N\rangle, \tag{40}$$

and all the atomic dipoles are in phase again when $t = \tau$, leading to a collective emission at the time 2τ after absorption.

The initial proposal exploited the fact that the natural Doppler broadening in a hot gas of atoms can be automatically reversed by using control pulses with opposite direction (Moiseev and Kröll, 2001). Achievable storage times are, however, limited in hot gases, due to the dephasing induced by atomic motion. Three groups then described how this protocol could be extended to store single photons in the optical regime in solid-state materials (Nilsson and Kröll, 2005; Alexander *et al.*, 2006; Kraus *et al.*, 2006), typically in rare-earth-doped solids. The implementation of CRIB in solids first requires one to isolate a narrow (ideally homogeneously broadened) absorption peak within a large transparency window. This can be achieved by spectral hole burning techniques (Sellars *et al.*, 2000; de Sèze *et al.*, 2003; Alexander *et al.*, 2006; Rippe *et al.*, 2008). This line must then be artificially broadened in a controlled way, in order to spectrally match the photon to be stored. To this end, one can exploit the fact that some solid-state materials have a permanent dipole moment, which gives rise to a linear Stark effect. The resonance frequency of the atoms can then be controlled with moderate external electric fields, and a controlled broadening can be induced by applying an electric field gradient. The photon can then be absorbed by the broadened peak and stored in the excited state. After absorption, inhomogeneous dephasing takes place. The reemission can then be triggered by changing the polarity of the electric field, which reverses the detunings and leads to the rephasing of the dipoles. In that case, the photon is emitted in the forward direction. It has been shown that in this configuration and for a broadening applied transversally with respect to the propagation direction, the storage and retrieval efficiency is given by Sangouard *et al.* (2007a):

$$\eta_F(t) = d^2 e^{-d} f(t), \tag{41}$$

where d is the optical depth of the atoms after broadening and $f(t)$ is the coherence profile in the excited state, given by the Fourier transform of the initial absorption peak. The maximal storage and retrieval efficiency in that configuration is 54%, limited by the reabsorption of the echo by the optically thick transition. In addition, the storage time in the excited state is limited by the finite achievable width of the initial absorption peak.

In order to overcome these limitations, it has been proposed to transfer the excitation to an empty long-lived ground state level, using optical control pulses. The storage time is now given by the coherence time of the ground state level, which may be much longer than the excited state coherence time. Moreover, if the excitation is brought back to the excited state after storage using a counterpropagating control pulse, phase matching will enable the CRIB echo to be emitted backward. Kraus *et al.* (2006) showed that this backward readout is equivalent to a time reversal of the Maxwell-Bloch equations, which effectively suppresses reabsorption. In that case, the storage and retrieval efficiency is given by Sangouard *et al.* (2007a):

$$\eta_B(t) = (1 - e^{-d})^2 g(t) \tag{42}$$

with $g(t) = f(t - T_S)$, where T_S is the time spent in the long-lived ground state. We see that η_B can reach 100% for sufficiently high d. If the decoherence is negligible (i.e., if the initial peak is sufficiently narrow), the efficiency can reach 0.9 for $d = 3$.

Recently it has been shown theoretically that the efficiency of the storage and retrieval can reach 100% even without the transfer to the ground state, using only a two-level system (Hétet, Longdell *et al.*, 2008). This requires the application of a longitudinal broadening, i.e., a broadening where the frequency of the atoms varies along the propagation direction. Such a broadening can be obtained by the use of a longitudinal electric field gradient. This configuration is sometimes referred as "longitudinal CRIB" or "gradient echo memory."

The multimode properties of CRIB have been studied by C. Simon *et al.* (2007b) and Nunn *et al.* (2008). It has been shown that, in contrast to EIT, the number of modes N_m that can be stored with high efficiency is proportional to the initial optical depth, $N_m \sim d$.

The first proof of principle demonstration of the CRIB scheme with bright coherent states was realized in a europium-doped solid (Alexander *et al.*, 2006). The europium ions doped in the solid-state matrix have an optical transition at 580 nm and a level structure with three hyperfine states in the ground and excited states. They used optical pumping techniques to create a narrow absorption peak with a width of 25 kHz, within a 3 MHz wide transparency window. The absorption of the peak was approximately 40%. This peak was then broadened with a gradient of electric field implemented with four electrodes in a quadrupole configuration, thanks to the linear Stark effect. The broadened spectral feature was excited using 1 μs optical pulses, and the polarity of the electric field was reversed after a programmable time τ. After a further delay τ, two-level Stark echoes were observed, with a decay time of about 20 μs. In an another experiment, they also stored and recalled a train of four pulses (Alexander *et al.*, 2007). They also showed that the phase information of the input pulses was preserved during the storage. In these experiments, only a very small part of the incident pulses were reemitted in the Stark echo (between 10^{-5} and 10^{-6}). This low efficiency can be partly explained by the small absorption of the broadened peak (about 1%).

In a more recent experiment, the same group demonstrated an improved storage and retrieval efficiency of 15% using a praseodymium-doped crystal, which features an optical transition with larger oscillator strength and consequently larger absorption (Hétet, Longdell *et al.*, 2008). Using a longer crystal they recently demonstrated a quantum memory with an efficiency as high as 69% (Hedges *et al.*, 2010), which is, up to date, the most efficient quantum memory demonstrated in any system. Recently, a CRIB experiment has also been demonstrated at the single-photon level, using an erbium-doped crystal absorbing at the telecommunication wavelength of 1536 nm (Lauritzen *et al.*, 2010).

Finally, an interesting variation has been proposed, where the reversible inhomogeneous broadening is not on the optical transition, but on the Raman transition between two ground state levels (Hétet, Hosseini *et al.*, 2008; Moiseev and Tittel, 2008). The light is mapped on the atoms by detuned Raman coupling to long-lived ground states. A proof of principle demonstration with bright pulses has been reported in a rubidium vapor (Hétet, Hosseini *et al.*, 2008), where the Raman resonance line was broadened by a magnetic field gradient. This technique has been further used to demonstrate a coherent pulse sequencer (Hosseini *et al.*, 2009).

b. Atomic frequency combs

In order to fully exploit temporal multiplexing in quantum repeater architectures, the memory should be able to store many temporal modes with high efficiency. For EIT-based quantum memories, this requires extremely high and currently unrealistic values of optical depth. The scaling is better for CRIB-based quantum memories, but the required optical depths are still very high (e.g., 3000 for 100 modes with 90% efficiency) (C. Simon *et al.*, 2007b). Recently, Afzelius *et al.* (2009) proposed a new scheme, where the number of stored modes does not depend on the initial optical depth. The scheme is based on "atomic frequency combs" (AFCs).

The idea of the AFC is to tailor the absorption profile of an inhomogeneously broadened solid-state atomic medium with a series of periodic and narrow absorbing peaks of width γ separated by Δ (see Fig. 33). The single photon to be stored is then collectively absorbed by all the atoms in the comb, and the state of the light is transferred to collective atomic excitations at the optical transition. After absorption, the atoms at different frequencies will dephase, but thanks to the periodic structure of the absorption profile, a rephasing occurs after a time $2\pi/\Delta$, which depends on the comb spacing. When the atoms are all in phase again, the light is reemitted in the forward direction as a result of a collective interference between all the emitters. In order to achieve longer storage times and on-demand retrieval of the stored photons, the optical collective excitation can be transferred to a long-lived ground state before the reemission of the light. This transfer freezes the evolution of the atomic dipoles, and the excitation is stored as a collective spin wave for a programmable time. The readout is achieved by transferring back the excitation to the excited state where the rephasing of the atomic dipoles takes place. If the two control fields are applied in a counterpropagating way, the photon is reemitted backward. In that case, it has been shown that the

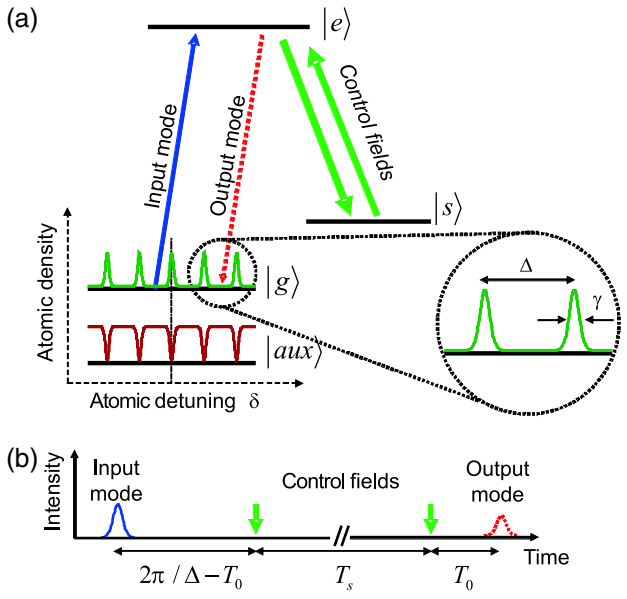

FIG. 33 (color online). The principles of the atomic frequency comb (AFC) quantum memory. (a) An inhomogeneously broadened optical transition $|g\rangle$-$|e\rangle$ is shaped into an AFC by frequency-selective optical pumping to the $|aux\rangle$ level. The peaks in the AFC have width γ (FWHM) and are separated by Δ, where we define the comb finesse as $F = \Delta/\gamma$. (b) The input mode is completely absorbed and coherently excites the AFC modes, which will dephase and then rephase after a time $2\pi/\Delta$, resulting in a photon-echo–type coherent emission. A pair of control fields on $|e\rangle$-$|s\rangle$ allow for long-time storage as a collective spin wave in $|s\rangle$, and on-demand readout after a storage time T_s. From Afzelius *et al.*, 2009.

reabsorption of the light can be suppressed thanks to a collective quantum interference. In that configuration, the theoretical storage and retrieval efficiency, assuming that the decoherence in the long-lived ground state is negligible and a perfect transfer, is given by

$$\eta_{\mathrm{AFC}} \approx (1 - e^{-d/F})^2 e^{-7/F^2}, \tag{43}$$

where d is the peak optical depth and $F = \Delta/\gamma$ is the finesse of the AFC. The trade-off with the finesse comes from the fact that the photon needs to be absorbed in the memory and reemitted. A high finesse is desirable to decrease the effect of decoherence during the reemission of the photon, while a lower finesse provides a higher effective optical depth, and hence favors the absorption of the light. We see that η_{AFC} tends toward unity for sufficiently large d and F. As shown by Afzelius *et al.* (2009), an efficiency of 0.9 can be achieved with $d = 40$ and $F = 10$, assuming that the reversible transfer to the ground state is perfectly efficient.

The number of temporal modes N_m that can be stored in an AFC quantum memory is proportional to the ratio between the storage time in the excited state $2\pi/\Delta$ and the duration of the stored photons, which is inversely proportional to the total AFC bandwidth $\Gamma = N_p\Delta$, where N_p is the total number of peaks in the AFC. Hence, we see that N_m is proportional to N_p and is independent of the optical depth. The total bandwidth of the AFC is, however, limited by the ground and excited state level spacings.

The AFC protocol has been used to realize the first demonstration of a solid light-matter interface at the single-photon level (de Riedmatten *et al.*, 2008). They demonstrated the coherent and reversible mapping of weak light fields with less than one photon per pulse on average onto an ensemble of 10^7 neodymium atoms naturally trapped in a solid (a Nd:YVO4 crystal cooled to 3 K). They also showed that the quantum coherence of the incident weak light field was almost perfectly conserved during the storage, as demonstrated by performing an interference experiment with a stored time-bin qubit (see Fig. 34). Finally, they also demonstrated experimentally that the interface makes it possible to store light in multiple temporal modes (four modes). The storage and retrieval efficiency was low (about 0.5%) in this experiment, mainly limited by the unperfect preparation of the atomic frequency comb and by unperfect optical pumping. In a more recent experiment with bright and weak pulses, Chanelière *et al.* (2009) demonstrated improved performance in terms of efficiency (9%) using a thulium-doped yttrium aluminum garnet (YAG) crystal. By optimizing the preparation procedure, Bonarota *et al.* (2010) showed that the efficiency can be increased to 18% with the same system. Finally, an efficiency of 35% has been demonstrated in a Pr^{3+}:Y_2SiO_5 crystal with bright pulses (Amari *et al.*, 2010), while an efficiency of 25% was demonstrated with weak pulses at the single-photon level (Sabooni *et al.*, 2010). The multimode capacity has also recently been increased by almost 1 order of magnitude compared to the results of de Riedmatten *et al.* (2008) in a Nd-doped Y_2SiO_5 crystal. A train of 64 pulses has been stored in the crystal for 1.5 μs (Usmani *et al.*, 2010).

In the previous experiments, only the first part of the protocol was demonstrated (i.e., the coherent mapping onto collective excitation at the optical transition and collective reemission at a predetermined time). Hence these experiments did not allow for on-demand readout. More recently, a proof of principle demonstration of the full AFC protocol including the transfer to a long-lived ground state has been demonstrated for bright pulses in a praseodymium-doped Y_2SiO_5 crystal (Afzelius *et al.*, 2010).

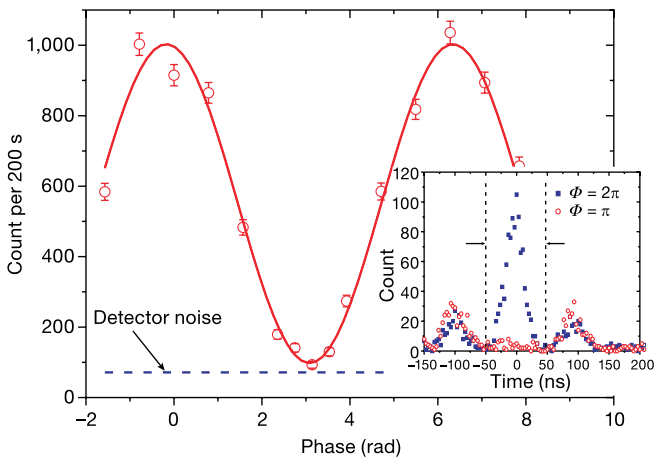

FIG. 34 (color online). Phase preservation during the storage of a time-bin qubit by an atomic frequency comb. Time-bin qubits with different phases Φ are stored and analyzed using the light-matter interface. The analysis is performed by projecting the time-bin qubit on a fixed superposition basis, which here is achieved by two partial readouts (see text for details). The inset shows the histogram of arrival times, where there is constructive interference for $\Phi = 2\pi$ and destructive interference for $\Phi = \pi$ in the middle time bin. For this particular interference fringe, a raw visibility of 82% and a visibility of 95% when subtracting detector dark counts are obtained. From de Riedmatten *et al.*, 2008.

E. Detectors

Highly efficient single-photon detectors with photon-number resolution are important for all the quantum repeater protocols presented in this review. The most common and most practical single-photon detectors are based on semiconductor avalanche photodiodes (APDs). They offer the advantage of being operated without cryogenic cooling (using Peltier elements), but their present performance is insufficient for use in a practical quantum repeater architecture. Silicon APDs feature detection efficiencies above 60% in the wavelength range from 600 to 800 nm and low dark count rates (< 50 Hz). InGaAs APDs, which can detect photons at 1550 nm, feature a much worse efficiency-to-noise ratio. Moreover, standard APD operation usually does not allow photon-number resolution. It was recently demonstrated, however, that using a technique to measure very weak avalanches at the early stage of their development, it is possible to obtain photon-number resolution (Kardynal *et al.*, 2008).

Takeuchi *et al.* (1999) demonstrated a visible light photon counter with an efficiency of 88% with an associated dark count rate of 20 kHz using avalanches across a shallow impurity conduction band in silicon at cryogenic temperature. This type of detectors has also been shown to allow for photon-number resolution (Kim *et al.*, 1999).

A new type of detector based on superconducting devices has recently shown promising performances. Detectors based on superconducting NbN nanowires (Gol'tsman *et al.*, 2001), usually called superconducting single-photon detectors (SSPD), feature a very low dark count rate and an excellent temporal resolution for high-speed counting at cryogenic temperature (< 4 K). An efficiency of 57% at 1550 nm and of 67% at 1064 nm has recently been demonstrated (Rosfjord *et al.*, 2006), by inserting the SSPD into an optical cavity and by using an antireflection coating. Photon-number-resolving capability has also been demonstrated recently (Divochiy *et al.*, 2008) in these devices.

The most advanced single-photon detector in terms of efficiency and photon-number resolution is based on superconducting transition edge sensors. For example, Lita *et al.* (2008) recently reported photon-number resolving detectors with 95% efficiency at the optimal wavelength for telecom fibers (1556 nm), with a temporal response time of about 1 μs. The drawbacks of these detectors are the slow response time and the fact that they have to be operated at very low temperature (100 mK), which necessitates sophisticated and expensive cooling techniques. Note that the slow response time is not necessarily a problem in single-mode quantum repeater architectures, since the repetition rate is given by the communication time. For architectures based on temporal multiplexing, however, it is important that the detector response time is fast enough to discriminate between the successive temporal modes.

Finally, we mention that high-efficiency photon-number-resolving single-photon detection based on atomic ensembles has also been proposed. These schemes, however, have not been demonstrated experimentally (Imamoglu, 2002; James and Kwiat, 2002).

F. Quantum channels

In this section, we describe the quantum channels that can be used to transmit single photons to remote locations for the initial entanglement generation. The main focus in this review is on optical fibers. A detailed review about the use of optical fibers as quantum channels in quantum cryptography experiments can be found in Gisin *et al.* (2002). In particular, the effect of birefringence leading to polarization mode dispersion and of chromatic dispersion are discussed. The importance of these effects decreases with the transmitted photon bandwidth and is thus likely very small for the narrow-bandwidth photons required in quantum repeater architectures. If they are not completely negligible, they would lead to errors that will be amplified in every entanglement swapping requiring entanglement purification operations; see Sec. IV.B.2. We now concentrate on two other aspects that are certainly more crucial for quantum repeaters: loss and phase stability.

In a single-mode optical fiber, light is guided thanks to the refractive index profile across the section of the fiber. To ensure single-mode operation, the core of the fiber is small (diameter of order of a few wavelengths). Over the past 30 years, a considerable effort has been made in order to reduce the transmission losses (initially several decibels per kilometer). Today, installed commercial fibers feature an attenuation of 0.35 dB/km at 1310 nm, and of 0.2 dB/km at 1550 nm. The loss around 800 nm is 2 dB/km. Recent developments have led to the fabrication of ultralow-loss optical fibers, with attenuation as low as 0.16 dB/km (Stucki *et al.*, 2009). Note that the loss remains exponential and that quantum repeater architectures will be useful to increase the transmission rates even if optical fibers with lower losses are developed (unless the attenuation can be reduced dramatically, which seems unlikely in the foreseeable future).

In quantum repeater architectures where the entanglement generation is based on single-photon detection, such as the DLCZ scheme, the phase acquired in long fiber links must remain constant for times that are typically of order of seconds. Minar *et al.* (2008) studied the phase stability of installed fiber links for quantum repeater applications. They found that the phase of a 36 km long Mach-Zehnder interferometer in an urban environment remains stable at an acceptable level (0.1 rad) for a duration of about 100 μs, which provides information about the time scale available for active phase stabilization. Note that a phase noise of 0.1 rad at 1550 nm corresponds to a fiber length fluctuation of 25 nm, and thus to a timing jitter of 0.12 fs.

The stabilization of phase noise in optical fibers is also relevant for other applications. There is currently an active area of research aiming at the transmission of frequency references over large distances in optical fibers, in order to synchronize or compare remote optical-frequency atomic clocks (Coddington *et al.*, 2007; Foreman, Ludlow *et al.*, 2007; Newbury *et al.*, 2007; Musha *et al.*, 2008). In this case, the phase noise in the fiber link directly translates into a spectral broadening of the frequency reference. To preserve the precision of optical clocks, the light should be transmitted with subfemtosecond jitter over long distances through the fiber. Noise cancellation schemes have been developed, which work well as long as the phase noise is negligible during the round trip time of the fiber [see Foreman, Holman *et al.* (2007) for a recent review].

Another interesting possibility to achieve a phase stable operation is to excite the two remote memories in a Sagnac interferometer configuration (Childress *et al.*, 2005; Minar *et al.*, 2008). In this way, the excitation lasers for the two memories and the emitted photons travel the same path in a counterpropagating fashion. Hence as long as the phase fluctuations are slower than the travel time, the phase difference is canceled automatically. Minar *et al.* (2008) showed that high-visibility first-order interference ($V > 98\%$) could be achieved without any active stabilization for fiber loops as long as 70 km in an urban environment.

Optical fibers are not the only way of implementing a quantum channel. The long-distance distribution of photons through free space is also an active field of investigation. Single photons and entangled photon pairs have been transmitted over distances as great as 144 km (Ursin *et al.*, 2007; Fedrizzi *et al.*, 2009). Free-space channels are also subject to significant loss for long distances. For example, the total channel loss in Fedrizzi *et al.* (2009) was 64 dB, where the attenuation was dominated by turbulent atmospheric effects. An interesting extension of this approach to long-distance quantum communication is the use of satellites, in which case only a small part of the photon path is in the atmosphere and the dominant losses are due to beam divergence. Realistic links would involve fast-moving low-orbit satellites. There are several feasibility studies, both theoretical (Villoresi *et al.*, 2004; Bonato *et al.*, 2009) and experimental (Peng *et al.* 2005; Villoresi *et al.*, 2008). We emphasize that the quantum repeater principle can be applied to any kind of lossy channel, including satellite-based transmission.

G. Coupling losses

In Sec. IV.B, we studied the performances of various quantum repeater architectures with respect to the quantum memory and detector efficiencies. In practice, other kinds of loss need to be taken into account: the passive losses in the optical elements and the fiber coupling losses. These losses are of crucial importance for the performance of quantum repeaters. Passive loss between the memory and the detector (together with the loss between the photon source and the memory for experiments with absorptive memories) affects the repeater performances in the same way as the memory efficiency. One may thus introduce an effective memory efficiency that takes the passive loss into account.

To illustrate the importance of passive losses, consider the experiment of J. Simon *et al.* (2007b), which demonstrated a DLCZ-like memory with a cold Cs ensemble in an optical cavity. This experiment has demonstrated the highest intrinsic retrieval efficiency to date ($\eta_R = 84\%$). However, if

one takes into account the probability to escape the cavity ($T = 0.17$), the transmission efficiency of the interference filter used in the experiment ($q_1 = 0.61$), and the fiber coupling efficiency ($q_2 = 0.65$), the effective retrieval efficiency given by the conditional probability to have an anti-Stokes photon in front of the detector is $\eta_R^{\text{eff}} = \eta_R T q_1 q_2 \simeq 0.06$. In free-space experiments the highest η_R^{eff} measured in a DLCZ source so far is of order of 25% (Laurat *et al.*, 2006).

We emphasize that in order to build a practical quantum repeater that beats direct transmission, all these passive losses must be considerably reduced.

VI. OTHER APPROACHES TOWARD QUANTUM REPEATERS

There is a significant number of proposals for realizing quantum repeaters using ingredients other than atomic ensembles and linear optics. An exhaustive treatment of these proposals would be a task for another review paper comparable to this one. Here we will restrict ourselves to a very brief overview. One class of proposals keeps atomic ensembles and linear optical processing as important ingredients, but supplements them with either additional nonlinear elements such as the Kerr effect (He *et al.*, 2008) or light shift induced blockade (Shahriar *et al.*, 2007), or uses entangled coherent states instead of single photons (Brask, Rigas *et al.*, 2010; Sangouard *et al.*, 2010, or explores the way to improve the retrieval and detector efficiencies with the fluorescent detection of stored excitations (Brask, Jiang *et al.*, 2010).

Most alternative proposals, however, involve individual quantum systems. One natural system to consider is trapped ions, since quantum information processing in general is extremely well developed in this system. For example, the entanglement between a single ion and a single photon has been reported by Blinov *et al.* (2004) and the interference of photon pairs emitted from two remote trapped ions has been presented by Maunz *et al.* (2007).

Many experiments have been realized that demonstrate key ingredients for quantum repeaters, including the entanglement between a single ion and a single photon (Blinov *et al.*, 2004), the interference of photon pairs emitted from two remote trapped ions (Maunz *et al.*, 2007). For entangling distant ions, there is a number of proposals via both single-photon (Bose *et al.*, 1999; Cabrillo *et al.*, 1999) and two-photon detections (Duan and Kimble, 2003; Feng *et al.*, 2003; Simon and Irvine, 2003), some of which have been realized experimentally (Moehring *et al.*, 2007; Matsukevich *et al.*, 2008). More recently, quantum teleportation (Olmschenk *et al.*, 2009) and quantum gate between remote ions (Maunz *et al.*, 2009) have also been reported. Motivated by this impressive body of work, the performance of quantum repeaters with trapped ions has been analyzed more quantitatively, including a discussion of possible multiplexing (Sangouard *et al.*, 2009). This analysis showed that ion-based repeaters have the potential to significantly outperform atomic-ensemble-based approaches, notably because all entanglement swapping operations can be performed with unit probability. Note, however, that the ion has to be embedded within a high-finesse cavity to achieve a high-efficiency photon collection. Furthermore, the calculation reported by Sangouard *et al.* (2009) assumed that the wavelength of the photons emitted by the ions are converted to a telecom wavelength about 1.5 μm, as shown experimentally by Curtz *et al.* (2010) and Takesue (2010), to profit from the optimal transmission of optical fibers in that range.

Another active field of research on quantum repeaters investigates the potential of single quantum systems in the solid state. In particular, Childress *et al.* (2005), (2006) developed a detailed proposal for a quantum repeater architecture adapted to the use of N-V centers in diamond or of quantum dots as quantum memories. Note that the entanglement between a single photon and a N-V center has recently been demonstrated experimentally (Togan *et al.*, 2010). The basic entanglement generation step in this proposal is based on single-photon detections. A protocol based on two-photon detections that uses spins in quantum dots as quantum memories was proposed by C. Simon *et al.* (2007a). The "hybrid quantum repeater" approach of van Loock *et al.* (2006), (2008) that combines the transmission of coherent states with the use of individual quantum systems is also primarily motivated by solid-state systems.

Note that the present review is focused on the most immediate goal of outperforming direct transmission, thus emphasizing simple protocols that are close to current experimental capabilities. There are also numerous contributions to the field of quantum repeaters that take a longer-term and/or more abstract view. Examples include work on the use of dynamic programming (Jiang *et al.*, 2007a), error correcting codes (Jiang *et al.*, 2008), decoherence-free subspaces (Dorner *et al.*, 2008), and an analysis of the role of memory errors (Hartmann *et al.*, 2007).

VII. CONCLUSIONS AND OUTLOOK

Since the seminal DLCZ paper, there has been significant progress toward the realization of quantum repeaters with atomic ensembles and linear optics both on the theoretical and on the experimental fronts. On the theoretical side, various improved protocols have been proposed, improving both the achievable entanglement distribution rate and the robustness. Quantifying the expected performance of the various protocols, one finds that the prospect of efficient multiplexing, in particular, seems to make it realistic to implement a simple quantum repeater that outperforms the direct transmission of quantum states in the not too distant future.

Spurred in part by the original DLCZ proposal, in part by more recent ideas, experiments are progressing rapidly. On the one hand, elementary links for certain quantum repeater protocols have already been demonstrated, though far from the performance required to be practically useful. On the other hand, impressive values have been achieved for key parameters such as storage time, memory efficiency, or multimode capacity, though not yet simultaneously in a single system. Besides requiring the capacity to generate, store, and swap entanglement, constructing a viable quantum repeater will also require technological elements such as stabilized long-distance fiber links, and the virtual elimination of coupling losses between the various components.

We suspect that the first quantum repeater that beats direct transmission will probably be realized using atomic ensembles, linear optics, and photon counting. In the longer run, this approach may well be overtaken by other systems with increased capabilities. New capabilities may come from modifying ensemble-based approaches, for example, by including techniques based on continuous variables, where good quantum memories have already been demonstrated (Julsgaard *et al.*, 2004). In a recent experiment, coherent-state–type entanglement was created using photon counting (Ourjoumtsev *et al.*, 2009), suggesting that hybrid approaches combining photon counting and homodyne detection may be promising. Another promising modification may be the use of ensembles in optical lattices, where long light storage times have recently been demonstrated for the first time (Schnorrberger *et al.*, 2009), and where more advanced information processing may be possible compared to conventional ensembles. However, it is also quite conceivable that single quantum systems, as mentioned briefly in Sec. VI, will eventually be more powerful than ensembles. Whichever approach may turn out to be the most adapted, based on recent progress we believe that in the long run intercontinental entanglement will not be out of reach.

ACKNOWLEDGMENTS

We thank M. Afzelius, T. Chanelière, Y.-A. Chen, K. S. Choi, C. W. Chou, T. Coudreau, H. Deng, R. Dubessy, D. Felinto, M. Halder, S. Hastings-Simon, H. J. Kimble, S. Kröll, J. Laurat, B. Lauritzen, J.-L. Le Gouët, I. Marcikic, J. Minář, C. Ottaviani, J.-W. Pan, S. Polyakov, V. Scarani, W. Sohler, M. Staudt, S. Tanzilli, W. Tittel, S. Van Enk, I. Usmani, H. Zbinden, and B. Zhao for fruitful collaborations, as well as H. Briegel, M. Eisaman, Q. Glorieux, P. Goldner, P. Grangier, S. Guibal, L. Guidoni, O. Guillot-Noël, B. He, G. Hétet, D. Jaksch, A. Kuzmich, A. Lvovsky, D. Matsukevich, C. Monroe, J. Nunn, A. Ourjoumtsev, M. Plenio, E. Polzik, M. Razavi, S. Removille, M. Sellars, A. Sørensen, K. Surmacz, R. Tualle-Brouri, P. Van Loock, and I. Walmsley for helpful comments and interesting discussions. We gratefully acknowledge support by the EU Integrated Project *Qubit Applications* and *Qessence*, the Swiss NCCR *Quantum Photonics*, and the ERC Advanced Grant *QORE*. C. S. was supported by an NSERC Discovery Grant and an AI-TF New Faculty Award.

APPENDIX A: CALCULATING THE ENTANGLEMENT DISTRIBUTION TIME

1. Creation of entanglement for an elementary link

For a success probability P_0 one has an exponential distribution of waiting times n (in units of L_0/c)

$$p(n) = (1 - P_0)^{n-1} P_0,$$

which gives an expectation value

$$\langle n \rangle = \sum_{n=0}^{\infty} n p(n) = \frac{1}{P_0}.$$

2. Waiting for a success in two neighboring elementary links

In order to be able to attempt the first swapping, entanglement creation has to succeed in two neighboring elementary links. The corresponding waiting time is the maximum of two waiting times, each of which follows the distribution given for the elementary link. We will denote the distribution for this combined waiting time by $\tilde{p}(n)$ and its expectation value by $\langle \tilde{n} \rangle$. One has

$$\tilde{p}(n) = p(n)^2 + 2p(n) \sum_{k=1}^{n-1} p(k),$$

taking into account all cases where for at least one of the two links we have to wait until n for a success. The new waiting time is

$$\langle \tilde{n} \rangle = \sum_{n=1}^{\infty} n \tilde{p}(n) = 2 \sum_{n=0}^{\infty} n p(n) \left(\sum_{k=1}^{n-1} p(k) + \frac{1}{2} p(n) \right).$$

It is easy to see that the expression inside the parentheses is bounded by 1. As a consequence, one must have

$$\langle \tilde{n} \rangle \leq 2 \langle n \rangle.$$

Obviously one also has

$$\langle n \rangle \leq \langle \tilde{n} \rangle,$$

since waiting for two independent successes has to take at least as long as waiting for a single success, so defining

$$f \equiv \frac{\langle \tilde{n} \rangle}{\langle n \rangle}$$

one certainly has

$$1 \leq f \leq 2.$$

However, we can also calculate f explicitly. This requires explicitly calculating $\tilde{p}(n)$ and $\langle \tilde{n} \rangle$. One finds

$$\tilde{p}(n) = P_0^2 (1 - P_0)^{2n-2} + 2P_0 (1 - P_0)^{n-1} \times [1 - (1 - P_0)^{n-1}],$$

which gives

$$\langle \tilde{n} \rangle = \frac{3 - 2P_0}{(2 - P_0) P_0} \approx \frac{3}{2P_0},$$

where the last relation holds in the limit of small P_0.

3. First entanglement swapping

The next step is the first entanglement swapping, which succeeds with a probability P_1. Neglecting the time step required for the swapping itself, the mean waiting time for a success will be equal to $\langle \tilde{n} \rangle$ with probability P_1. This is for the case where the swapping works right away. It will be $2\langle \tilde{n} \rangle$ with probability $(1 - P_1)P_1$ (the second swapping attempt is successful), etc. Taking into account all possibilities, the waiting time for a successful swapping, and thus for the establishment of entanglement over the length of 2 elementary links is

$$\langle n_1\rangle = \langle \tilde{n}\rangle \sum_{k=0}^{\infty}(k+1)(1-P_1)^k P_1 = \frac{\langle \tilde{n}\rangle}{P_1} \approx \frac{3}{2P_0P_1}. \tag{A1}$$

4. Higher levels in the repeater protocol

We have seen that at the lowest level of the repeater the average waiting time for having a success in two neighboring links is essentially exactly $3/2$ times longer than the average waiting time for one link. The situation is more complicated for higher levels of the repeater, because the corresponding distribution of waiting times $p(n)$ for each individual link is no longer a simple exponential distribution. In fact, its form at each level of iteration depends not only on P_0 but also on the success probabilities for entanglement swapping at all lower levels (P_i). To our knowledge, nobody has so far succeeded in obtaining useful analytical results for the general case. However, numerical evidence (Jiang *et al.*, 2007b; Brask and Sorensen, 2008) suggests that $3/2$ is still a good approximation for the factor f. One certainly always has $1 \le f \le 2$. We also note that the exact value of f for each level has a relatively small impact on log-scale comparison plots such as those in this paper.

5. Second entanglement swapping and general formula

Whatever the exact value of $\langle \tilde{n}_1\rangle$, the same argument as for the first swapping shows that the expectation value for the waiting time for a successful second-level swapping, and thus for the establishment of entanglement spanning four elementary links is

$$\langle n_2\rangle = \frac{\langle \tilde{n}_1\rangle}{P_2}, \tag{A2}$$

where P_2 is the success probability for the second-level swapping. The general formula for the waiting time after l levels (corresponding to 2^l elementary links) is thus (in the limit of small P_0)

$$\langle n_l\rangle = \frac{f_0 f_1 \cdots f_{l-1}}{P_0P_1P_2\cdots P_l}, \tag{A3}$$

with $f_0 = 3/2$, and $1 \le f_i \le 2$ for all f_i.

The final postselection step in protocols based on single-photon detections can be treated in full analogy to entanglement swapping. Again one needs two lower-level copies to create one higher-level one, so there is an f factor and a success probability P_{ps}.

APPENDIX B: MULTIPHOTON ERRORS IN THE DLCZ PROTOCOL

Here we explain in more detail how to calculate the multiphoton errors in the DLCZ protocol (Jiang *et al.*, 2007b; Minar *et al.*, 2007). The starting point is Eq. (6), where we now explicitly write the $O(p)$ terms, but set the phases $\phi_a = \phi_b = 0$,

$$\left(1+\sqrt{\frac{p}{2}}s_a^\dagger a^\dagger + \frac{p}{4}(s_a^\dagger)^2(a^\dagger)^2 + O(p^{3/2})\right) \times \left(1+\sqrt{\frac{p}{2}}s_b^\dagger b^\dagger + \frac{p}{4}(s_b^\dagger)^2(b^\dagger)^2 + O(p^{3/2})\right)|0\rangle. \tag{B1}$$

The $O(\sqrt{p})$ terms give the results that are desired in the protocol. The higher orders in p give rise to errors.

The probability for a detector that is photon-number resolving, but that has nonunit efficiency η, to detect a single photon in mode $\tilde{b}$, given that there are n photons present in that mode, is

$$p_n = n\eta(1-\eta)^{n-1}. \tag{B2}$$

In the entanglement generation step $\eta = \eta_d\eta_t$, with $\eta_t \ll 1$, such that one can approximate $p_1 = \eta$ and $p_2 = 2\eta$.

As a consequence, the state of the two modes s_a and s_b conditional on one click in either $d = (1/\sqrt{2})(a+b)$ or $\tilde{d} = (1/\sqrt{2})(a-b)$ (for simplicity we also set the phases $\xi_a = \xi_b = 0$) is

$$\rho_{AB} = |\psi_+\rangle\langle\psi_+| + \frac{p}{2}(|20\rangle\langle 20| + |11\rangle\langle 11| + |02\rangle\langle 02|) + \frac{p}{2\sqrt{2}}(|20\rangle\langle 11| + |11\rangle\langle 02| + \text{H.c.}) + O(p^2), \tag{B3}$$

where

$$|\psi_+\rangle = \frac{1}{\sqrt{2}}(|01\rangle + |10\rangle) \tag{B4}$$

with $|01\rangle = |0\rangle_A|1\rangle_B$, etc. Here we assume that a corrective phase shift of π between s_a and s_b has been applied in the case of a detection in $\tilde{d}$.

When these states are used to create entanglement between non-neighboring stations using entanglement swapping, the errors are amplified. Suppose we have established states

$$\rho_{AB} = \sum_{k,l,k',l'} \rho^{AB}_{kl,k'l'}|kl\rangle\langle k'l'| \tag{B5}$$

and ρ_{CD}. Entanglement swapping proceeds by reconverting the atomic modes s_b and s_c into photonic modes b' and c', and then combining the modes b' and c' on a beam splitter such that $b' = (1/\sqrt{2})(\tilde{b}+\tilde{c})$, $c' = (1/\sqrt{2})(\tilde{b}-\tilde{c})$. Entanglement swapping also works with a single click.

The new state created in the entanglement swapping step is

$$\rho^{AD}_{kn,k'n'} = \sum_{l,l',m,m'} \rho^{AB}_{kl,k'l'}\rho^{CD}_{mn,m'n'}\delta_{l+m,l'+m'} \times \eta(1-\eta)^{l+m-1}2^{-l-m}\sqrt{l!m!l'!m'!} \times \sum_{r=0}^{l+m} r!(l+m-r)!f(l,m,r)f(l',m',r), \tag{B6}$$

where now $\eta = \eta_m\eta_d$, with

$$f(l,m,r) = \sum_{p=0}^{l}\frac{(-1)^p}{p!(l-p)!(p+m-r)!(r-p)!}. \tag{B7}$$

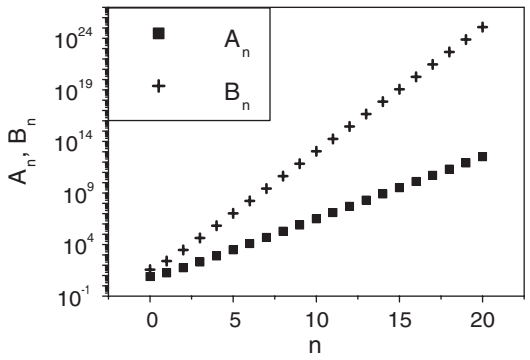

FIG. 35. The coefficients A_n and B_n as a function of n. One sees the scaling with $N^2 = 2^{2n}$ and $N^4 = 2^{4n}$, respectively.

The number of iterations depends on the nesting level of the repeater (which depends on the distance to be covered). We denote the state after the highest-level swapping operations by ρ_{AZ}. The final step of the protocol is the projection onto one photon on each side (see above), which in the ideal case could be written as

$$\sigma_{AZ} = P_{1_A 1_Z} \rho_{A_1 Z_1} \rho_{A_2 Z_2} P_{1_A 1_Z}, \tag{B8}$$

where $P_{1_A 1_Z}$ is the projector onto the states that have exactly one photon in location A (taking A_1 and A_2 together) and one photon in location Z. In practice, the detectors are again not perfect (see above). We therefore have to consider the probabilities for single detections following Eq. (B2). The correct formula for the final density matrix is then

$$\sigma^{AZ}_{klmn,k'l'm'n'} = \rho^{A_1 Z_1}_{km,k'm'} \rho^{A_2 Z_2}_{ln,l'n'} p_{k+l} p_{m+n} p_{k'+l'} p_{m'+n'}. \tag{B9}$$

Here k, l, m, n refer to the modes a_1', a_2', z_1', z_2', etc. The fidelity is given by the overlap of this state, properly renormalized, with the ideal final state.

To second order in p, the results are the following. Given as a function of the nesting level n, the fidelity $F(n)$ has the form

$$F(n) = 1 - A_n p(1-\eta) + B_n p^2 (1-\eta)^2, \tag{B10}$$

where the coefficients for the lowest values of n are $A_0 = 8, A_1 = 18, A_2 = 56, A_3 = 204, A_4 = 788$, $B_0 = 37, B_1 = 250, B_2 = 2966, B_3 = 43\,206, B_4 = 669\,702$.

The dependence on $(1-\eta)$ indicates that ideal photon-number resolving detectors in combination with perfect memories would allow one to identify all undesirable multiphoton events, and thus to eliminate the considered errors. From $n = 3$ onward, A_n scales approximately as 2^{2n} or equivalently as N^2, where $N = 2^n$ is the number of links. This scaling becomes virtually exact for large values of n; see Fig. 35. Similarly, B_n scales approximately as N^4.

The scaling with N^2 of the multiphoton errors is related to the fact that the size of the vacuum component in the state scales linearly with N. In fact, the errors in the final post-selected two-photon state that lead to the given fidelity reduction arise from the combination of the multiphoton (i.e., two-photon) component for one pair of ensembles with the vacuum component for the other pair of ensembles, with both permutations contributing.

REFERENCES

Afzelius, M., C. Simon, H. de Riedmatten, and N. Gisin, 2009, Phys. Rev. A **79**, 052329.

Afzelius, M., I. Usmani, A. Amari, B. Lauritzen, A. Walther, C. Simon, N. Sangouard, J. Minar, H. de Riedmatten, N. Gisin, and S. Kröll, 2010, Phys. Rev. Lett. **104**, 040503.

Akiba, K., K. Kashiwagi, M. Arikawa, and M. Kozuma, 2009, New J. Phys. **11**, 013049.

Akiba, K., K. Kashiwagi, T. Yonehara, and M. Kozuma, 2007, Phys. Rev. A **76**, 023812.

Alexander, A. L., J. J. Longdell, and M. J. Sellars, 2007, J. Opt. Soc. Am. B **24**, 2479.

Alexander, A. L., J. J. Longdell, M. J. Sellars, and N. B. Manson, 2006, Phys. Rev. Lett. **96**, 043602.

Amari, A., A. Walther, M. Sabooni, M. Huang, S. Kröll, M. Afzelius, I. Usmani, B. Lauritzen, N. Sangouard, H. de Riedmatten, and N. Gisin, 2010, J. Lumin. **130**, 1579.

Appel, J., E. Figueroa, D. Korystov, M. Lobino, and A. I. Lvovsky, 2008, Phys. Rev. Lett. **100**, 093602.

Balic, V., D. A. Braje, P. Kolchin, G. Y. Yin, and S. E. Harris, 2005, Phys. Rev. Lett. **94**, 183601.

Bao, X.-H., Y. Qian, J. Yang, H. Zhang, Z.-B. Chen, T. Yang, and J.-W. Pan, 2008, Phys. Rev. Lett. **101**, 190501.

Batalov, A., C. Zierl, T. Gaebel, P. Neumann, I.-Y. Chan, G. Balasubramanian, P. R. Hemmer, F. Jelezko, and J. Wrachtrup, 2008, Phys. Rev. Lett. **100**, 077401.

Bell, J. S., 1964, Physics (Long Island City, N.Y.) **1**, 195.

Bennett, C. H., and G. Brassard, 1984, *Proceedings of the IEEE International Conference on Computers, Systems, and Signal Processing*, 175.

Bennett, C. H., G. Brassard, S. Popescu, B. Schumacher, J. A. Smolin, and W. K. Wootters, 1996, Phys. Rev. Lett. **76**, 722.

Black, A. T., J. K. Thompson, and V. Vuletic, 2005, Phys. Rev. Lett. **95**, 133601.

Blinov, B. B., D. Moehring, L.-M. Duan, and C. Monroe, 2004, Nature (London) **428**, 153.

Bonarota, M., J. Ruggiero, J. L. Le Gouet, and T. Chaneliere, 2010, Phys. Rev. A **81**, 033803.

Bonato, C., A. Tomaello, V. Da Deppo, G. Naletto, and P. Villoresi, 2009, New J. Phys. **11**, 045017.

Bose, S., P. L. Knight, M. B. Plenio, and V. Vedral, 1999, Phys. Rev. Lett. **83**, 5158.

Braje, D. A., V. Balic, S. Goda, G. Y. Yin, and S. E. Harris, 2004, Phys. Rev. Lett. **93**, 183601.

Brask, J. B., L. Jiang, A. V. Gorshkov, V. Vuletic, A. S. Sorensen, and M. D. Lukin, 2010, Phys. Rev. A **81**, 020303.

Brask, J. B., I. Rigas, E. S. Polzik, U. L. Andersen, and A. S. Sorensen, 2010, Phys. Rev. Lett. **105**, 160501.

Brask, J. B., and A. S. Sorensen, 2008, Phys. Rev. A **78**, 012350.

Briegel, H.-J., W. Dür, J. I. Cirac, and P. Zoller, 1998, Phys. Rev. Lett. **81**, 5932.

Burnham, D. C., and D. L. Weinberg, 1970, Phys. Rev. Lett. **25**, 84.

Cabrillo, C., J. I. Cirac, P. García-Fernández, and P. Zoller, 1999, Phys. Rev. A **59**, 1025.

Chanelière, T., M. Afzelius, and J.-L. Le Gouët, 2009, arXiv:0902.2048.

Chanelière, T., D. N. Matsukevich, S. D. Jenkins, T. A. B. Kennedy, M. S. Chapman, and A. Kuzmich, 2006, Phys. Rev. Lett. **96**, 093604.

Chanelière, T., D. N. Matsukevich, S. D. Jenkins, S.-Y. Lan, T. A. B. Kennedy, and A. Kuzmich, 2005, Nature (London) **438**, 833.
Chanelière, T., D. N. Matsukevich, S. D. Jenkins, S.-Y. Lan, R. Zhao, T. A. B. Kennedy, and A. Kuzmich, 2007, Phys. Rev. Lett. **98**, 113602.
Chen, S., Y.-A. Chen, T. Strassel, Z.-S. Yuan, B. Zhao, J. Schmiedmayer, and J.-W. Pan, 2006, Phys. Rev. Lett. **97**, 173004.
Chen, S., Y.-A. Chen, B. Zhao, Z.-S. Yuan, J. Schmiedmayer, and J.-W. Pan, 2007, Phys. Rev. Lett. **99**, 180505.
Chen, Y.-A., S. Chen, Z.-S. Yuan, B. Zhao, C.-S. Chuu, J. Schmiedmayer, and J.-W. Pan, 2008, Nature Phys. **4**, 103.
Chen, Z.-B., B. Zhao, Y.-A. Chen, J. Schmiedmayer, and J.-W. Pan, 2007, Phys. Rev. A **76**, 022329.
Childress, L., J. M. Taylor, A. S. Sorensen, and M. D. Lukin, 2005, Phys. Rev. A **72**, 052330.
Childress, L., J. M. Taylor, A. S. Sorensen, and M. D. Lukin, 2006, Phys. Rev. Lett. **96**, 070504.
Choi, K. S., H. Deng, J. Laurat, and H. J. Kimble, 2008, Nature (London) **452**, 67.
Chou, C. W., H. de Riedmatten, D. Felinto, S. V. Polyakov, S. J. van Enk, and H. J. Kimble, 2005, Nature (London) **438**, 828.
Chou, C. W., J. Laurat, H. Deng, K. S. Choi, H. de Riedmatten, D. Felinto, and H. J. Kimble, 2007, Science **316**, 1316.
Chou, C. W., S. V. Polyakov, A. Kuzmich, and H. J. Kimble, 2004, Phys. Rev. Lett. **92**, 213601.
Chuu, C.-S., T. Strassel, B. Zhao, M. Koch, Y.-A. Chen, S. Chen, Z.-S. Yuan, J. Schmiedmayer, and J.-W. Pan, 2008, Phys. Rev. Lett. **101**, 120501.
Clauser, J. F., 1974, Phys. Rev. D **9**, 853.
Coddington, I., W. C. Swann, L. Lorini, J. C. Bergquist, Y. Le Coq, C. W. Oates, Q. Quraishi, K. S. Feder, J. W. Nicholson, P. S. Westbrook, S. A. Diddams, and N. R. Newbury, 2007, Nat. Photon. **1**, 283.
Collett, M. J., 1988, Phys. Rev. A **38**, 2233.
Collins, D., N. Gisin, and H. de Riedmatten, 2005, J. Mod. Opt. **52**, 735.
Collins, O. A., S. D. Jenkins, A. Kuzmich, and T. A. B. Kennedy, 2007, Phys. Rev. Lett. **98**, 060502.
Curtz, N., R. Thew, C. Simon, N. Gisin, and H. Zbinden, 2010, arXiv:1006.4585.
Cviklinski, J., J. Ortalo, J. Laurat, A. Bramati, M. Pinard, and E. Giacobino, 2008, Phys. Rev. Lett. **101**, 133601.
Darquie, B., M. P. A. Jones, J. Dingjan, J. Beugnon, S. Bergamini, Y. Sortais, G. Messin, A. Browaeys, and P. Grangier, 2005, Science **309**, 454.
de Riedmatten, H., M. Afzelius, M. U. Staudt, C. Simon, and N. Gisin, 2008, Nature (London) **456**, 773.
de Riedmatten, H., J. Laurat, C. W. Chou, E. W. Schomburg, D. Felinto, and H. J. Kimble, 2006, Phys. Rev. Lett. **97**, 113603.
de Riedmatten, H., I. Marcikic, W. Tittel, H. Zbinden, and N. Gisin, 2003, Phys. Rev. A **67**, 022301.
de Riedmatten, H., I. Marcikic, J. A. W. van Houwelingen, W. Tittel, H. Zbinden, and N. Gisin, 2005, Phys. Rev. A **71**, 050302.
de Sèze, F., V. Lavielle, I. Lorgeré, and J. L. Le Gouët, 2003, Opt. Commun. **223**, 321.
Dieks, D., 1982, Phys. Lett. A **92**, 271.
Divochiy, A. *et al.*, 2008, Nat. Photon. **2**, 377.
Dorner, U., A. Klein, and D. Jaksch, 2008, Quantum Inf. Comput. **8**, 0468.
Du, S., P. Kolchin, C. Belthangady, G. Y. Yin, and S. E. Harris, 2008, Phys. Rev. Lett. **100**, 183603.
Duan, L.-M., and H. J. Kimble, 2003, Phys. Rev. Lett. **90**, 253601.
Duan, L.-M., M. D. Lukin, J. I. Cirac, and P. Zoller, 2001, Nature (London) **414**, 413.
Dubin, F., D. Rotter, M. Mukherjee, C. Russo, J. Eschner, and R. Blatt, 2007, Phys. Rev. Lett. **98**, 183003.
Eisaman, M. D., A. André, F. Massou, M. Fleischhauer, A. S. Zibrov, and M. D. Lukin, 2005, Nature (London) **438**, 837.
Eisaman, M. D., L. Childress, A. Andre, F. Massou, A. S. Zibrov, and M. D. Lukin, 2004, Phys. Rev. Lett. **93**, 233602.
Ekert, A. K., 1991, Phys. Rev. Lett. **67**, 661.
Fedrizzi, A., R. Ursin, T. Herbst, M. Nespoli, R. Prevedel, T. Scheidl, F. Tiefenbacher, T. Jennewein, and A. Zeilinger, 2009, Nature Phys. advanced online publication.
Felinto, D., C. W. Chou, H. de Riedmatten, S. V. Polyakov, and H. J. Kimble, 2005, Phys. Rev. A **72**, 053809.
Felinto, D., C. W. Chou, J. Laurat, E. W. Schomburg, H. de Riedmatten, and H. J. Kimble, 2006, Nature Phys. **2**, 844.
Feng, X.-L., Z.-M. Zhang, X.-D. Li, S.-Q. Gong, and Z.-Z. Xu, 2003, Phys. Rev. Lett. **90**, 217902.
Fleischhauer, M., A. Imamoglu, and J. P. Marangos, 2005, Rev. Mod. Phys. **77**, 633.
Fleischhauer, M., and M. D. Lukin, 2000, Phys. Rev. Lett. **84**, 5094.
Fleischhauer, M., and M. D. Lukin, 2002, Phys. Rev. A **65**, 022314.
Fleischhauer, M., S. F. Yelin, and M. D. Lukin, 2000, Opt. Commun. **179**, 395.
Foreman, S. M., K. W. Holman, D. D. Hudson, D. J. Jones, and J. Ye, 2007, Rev. Sci. Instrum. **78**, 021101.
Foreman, S. M., A. D. Ludlow, M. H. G. de Miranda, J. E. Stalnaker, S. A. Diddams, and J. Ye, 2007, Phys. Rev. Lett. **99**, 153601.
Fraval, E., M. J. Sellars, and J. J. Longdell, 2004, Phys. Rev. Lett. **92**, 077601.
Fraval, E., M. J. Sellars, and J. J. Longdell, 2005, Phys. Rev. Lett. **95**, 030506.
Gisin, N., G. Ribordy, W. Tittel, and H. Zbinden, 2002, Rev. Mod. Phys. **74**, 145.
Gol'tsman, G. N., O. Okunev, G. Chulkova, A. Lipatov, A. Semenov, K. Smirnov, B. Voronov, A. Dzardanov, C. Williams, and R. Sobolewski, 2001, Appl. Phys. Lett. **79**, 705.
Gorshkov, A. V., A. Andre, M. D. Lukin, and A. S. Sorensen, 2007a, Phys. Rev. A **76**, 033804.
Gorshkov, A. V., A. Andre, M. D. Lukin, and A. S. Sorensen, 2007b, Phys. Rev. A **76**, 033805.
Gorshkov, A. V., A. André, M. Fleischhauer, A. S. Sørensen, and M. D. Lukin, 2007c, Phys. Rev. Lett. **98**, 123601.
Gorshkov, A. V., A. André, M. D. Lukin, and A. S. Sørensen, 2007d, Phys. Rev. A **76**, 033806.
Gorshkov, A. V., T. Calarco, M. D. Lukin, and A. S. Sørensen, 2008, Phys. Rev. A **77**, 043806.
Grangier, P., G. Roger, and A. Aspect, 1986, Europhys. Lett. **1**, 173.
Halder, M., A. Beveratos, N. Gisin, V. Scarani, C. Simon, and H. Zbinden, 2007, Nature Phys. **3**, 692.
Halder, M., A. Beveratos, R. T. Thew, C. Jorel, H. Zbinden, and N. Gisin, 2008, New J. Phys. **10**, 023027.
Hammerer, K., A. Sorensen, and E. Polzik, 2010, Rev. Mod. Phys. **82**, 1041.
Hartmann, L., B. Kraus, H.-J. Briegel, and W. Dur, 2007, Phys. Rev. A **75**, 032310.
He, B., Y.-H. Ren, and J. Bergou, 2008, arXiv:0808.2320.
Hedges, M. P., J. J. Longdell, Y. Li, and M. J. Sellars, 2010, Nature (London) **465**, 1052.
Heinze, G., A. Rudolf, F. Beil, and T. Halfmann, 2010, Phys. Rev. A **81**, 011401(R).
Hétet, G., M. Hosseini, B. M. Sparkes, D. Oblak, P. K. Lam, and B. C. Buchler, 2008, Opt. Lett. **33**, 2323.
Hétet, G., J. J. Longdell, A. L. Alexander, P. K. Lam, and M. J. Sellars, 2008, Phys. Rev. Lett. **100**, 023601.

Hijlkema, M., B. Weber, H. P. Specht, S. C. Webster, A. Kuhn, and G. Rempe, 2007, Nature Phys. **3**, 253.
Honda, K., D. Akamatsu, M. Arikawa, Y. Yokoi, K. Akiba, S. Nagatsuka, T. Tanimura, A. Furusawa, and M. Kozuma, 2008, Phys. Rev. Lett. **100**, 093601.
Hong, C. K., and L. Mandel, 1985, Phys. Rev. A **31**, 2409.
Hong, C. K., Z. Y. Ou, and L. Mandel, 1987, Phys. Rev. Lett. **59**, 2044.
Hosseini, M., B. M. Sparkes, G. Hetet, J. J. Longdell, P. K. Lam, and B. C. Buchler, 2009, Nature (London) **461**, 241.
Hostein, R., R. Braive, M. Larque, K.-H. Lee, A. Talneau, L. L. Gratiet, I. Robert-Philip, I. Sagnes, and A. Beveratos, 2009, Appl. Phys. Lett. **94**, 123101.
Imamoglu, A., 2002, Phys. Rev. Lett. **89**, 163602.
Inoue, R., N. Kanai, T. Yonehara, Y. Miyamoto, M. Koashi, and M. Kozuma, 2006, Phys. Rev. A **74**, 053809.
Jacobs, B. C., T. B. Pittman, and J. D. Franson, 2002, Phys. Rev. A **66**, 052307.
James, D. F. V., and P. G. Kwiat, 2002, Phys. Rev. Lett. **89**, 183601.
Jiang, L., J. Taylor, K. Nemot, W. Munro, R. Van Meter, and M. Lukin, 2008, arXiv:0809.3629.
Jiang, L., J. M. Taylor, N. Khaneja, and M. D. Lukin, 2007a, Proc. Natl. Acad. Sci. U.S.A. **104**, 17291.
Jiang, L., J. M. Taylor, and M. D. Lukin, 2007b, Phys. Rev. A **76**, 012301.
Jin, X.-M. *et al.*, 2010, arXiv:1004.4691.
Julsgaard, B., A. Kozhekin, and E. S. Polzik, 2001, Nature (London) **413**, 400.
Julsgaard, B., J. Sherson, J. I. Cirac, J. Fiurášek, and E. S. Polzik, 2004, Nature (London) **432**, 482.
Kaltenbaek, R., R. Prevedel, M. Aspelmeyer, and A. Zeilinger, 2009, Phys. Rev. A **79**, 040302.
Kardynal, B., Z. Yuan, and A. Shields, 2008, Nat. Photon. **2**, 425.
Keller, M., B. Lange, K. Hayasaka, W. Lange, and H. Walther, 2004, Nature (London) **431**, 1075.
Kim, J., S. Takeuchi, Y. Yamamoto, and H. H. Hogue, 1999, Appl. Phys. Lett. **74**, 902.
Kimble, H. J., 2008, Nature (London) **453**, 1023.
Kolchin, P., 2007, Phys. Rev. A **75**, 033814.
Kolchin, P., S. Du, C. Belthangady, G. Y. Yin, and S. E. Harris, 2006, Phys. Rev. Lett. **97**, 113602.
Kraus, B., W. Tittel, N. Gisin, M. Nilsson, S. Kroll, and J. I. Cirac, 2006, Phys. Rev. A **73**, 020302.
Kuklewicz, C. E., F. N. C. Wong, and J. H. Shapiro, 2006, Phys. Rev. Lett. **97**, 223601.
Kuzmich, A., W. P. Bowen, A. D. Boozer, A. Boca, C. W. Chou, L.-M. Duan, and H. J. Kimble, 2003, Nature (London) **423**, 731.
Lan, S.-Y., S. D. Jenkins, T. Chaneliere, D. N. Matsukevich, C. J. Campbell, R. Zhao, T. A. B. Kennedy, and A. Kuzmich, 2007, Phys. Rev. Lett. **98**, 123602.
Lan, S.-Y., A. G. Radnaev, O. A. Collins, D. N. Matsukevich, T. A. Kennedy, and A. Kuzmich, 2009, Opt. Express **17**, 13639.
Laurat, J., K. S. Choi, H. Deng, C. W. Chou, and H. J. Kimble, 2007, Phys. Rev. Lett. **99**, 180504.
Laurat, J., C.-W. Chou, H. Deng, K. Choi, F. D, H. de Riedmatten, and H. Kimble, 2007, New J. Phys. **9**, 207.
Laurat, J., H. de Riedmatten, D. Felinto, C.-W. Chou, E. W. Schomburg, and H. J. Kimble, 2006, Opt. Express **14**, 6912.
Lauritzen, B., J. Minar, H. de Riedmatten, M. Afzelius, N. Sangouard, C. Simon, and N. Gisin, 2010, Phys. Rev. Lett. **104**, 080502.
Lettow, R., V. Ahtee, R. Pfab, A. Renn, E. Ikonen, S. Götzinger, and V. Sandoghdar, 2007, Opt. Express **15**, 15842.
Lin, H., T. Wang, and T. W. Mossberg, 1995, Opt. Lett. **20**, 1658.
Lita, A. E., A. J. Miller, and S. W. Nam, 2008, Opt. Express **16**, 3032.
Liu, C., Z. Dutton, C. H. Behroozi, and L. V. Hau, 2001, Nature (London) **409**, 490.
Longdell, J. J., E. Fraval, M. J. Sellars, and N. B. Manson, 2005, Phys. Rev. Lett. **95**, 063601.
Lukin, M. D., 2003, Rev. Mod. Phys. **75**, 457.
Macfarlane, R. M., 2002, J. Lumin. **100**, 1.
Matsukevich, D. N., T. Chaneliere, S. D. Jenkins, S.-Y. Lan, T. A. B. Kennedy, and A. Kuzmich, 2006a, Phys. Rev. Lett. **97**, 013601.
Matsukevich, D. N., T. Chaneliere, S. D. Jenkins, S.-Y. Lan, T. A. B. Kennedy, and A. Kuzmich, 2006b, Phys. Rev. Lett. **96**, 030405.
Matsukevich, D. N., T. Chanelière, M. Bhattacharya, S.-Y. Lan, S. D. Jenkins, T. A. B. Kennedy, and A. Kuzmich, 2005, Phys. Rev. Lett. **95**, 040405.
Matsukevich, D. N., and A. Kuzmich, 2004, Science **306**, 663.
Matsukevich, D. N., P. Maunz, D. Moehring, S. Olmschenk, and C. Monroe, 2008, Phys. Rev. Lett. **100**, 150404.
Maunz, P., D. L. Moehring, S. Olmschenk, K. C. Younge, D. N. Matsukevich, and C. Monroe, 2007, Nature Phys. **3**, 538.
Maunz, P., S. Olmschenk, D. Hayes, D. N. Matsukevich, L.-M. Duan, and C. Monroe, 2009, Phys. Rev. Lett. **102**, 250502.
McKeever, J., A. Boca, A. D. Boozer, R. Miller, J. R. Buck, A. Kuzmich, and H. J. Kimble, 2004, Science **303**, 1992.
Mermin, N. D., 1993, Rev. Mod. Phys. **65**, 803.
Minar, J., H. de Riedmatten, C. Simon, H. Zbinden, and N. Gisin, 2008, Phys. Rev. A **77**, 052325.
Minar, J., C. Simon, and N. Sangouard, 2007 (unpublished).
Moehring, D. L., P. Maunz, S. Olmschenk, K. C. Younge, D. N. Matsukevich, L.-M. Duan, and C. Monroe, 2007, Nature (London) **449**, 68.
Moiseev, S., and W. Tittel, 2008, arXiv:0812.1730.
Moiseev, S. A., and S. Kröll, 2001, Phys. Rev. Lett. **87**, 173601.
Moreau, E., I. Robert, J. M. Gerard, I. Abram, L. Manin, and V. Thierry-Mieg, 2001, Appl. Phys. Lett. **79**, 2865.
Musha, M., F.-L. Hong, K. Nakagawa, and K.-i. Ueda, 2008, Opt. Express **16**, 16459.
Neergaard-Nielsen, J. S., B. M. Nielsen, H. Takahashi, A. I. Vistnes, and E. S. Polzik, 2007, Opt. Express **15**, 7940.
Newbury, N. R., P. A. Williams, and W. C. Swann, 2007, Opt. Lett. **32**, 3056.
Nielsen, M. A., and I. L. Chuang, 2000, *Quantum Computation and Quantum Information* (Cambridge University Press, Cambridge, England).
Nilsson, M., and S. Kröll, 2005, Opt. Commun. **247**, 393.
Novikova, I., A. V. Gorshkov, D. F. Phillips, A. S. Sorensen, M. D. Lukin, and R. L. Walsworth, 2007, Phys. Rev. Lett. **98**, 243602.
Nunn, J., K. Reim, K. C. Lee, V. O. Lorenz, B. J. Sussman, I. A. Walmsley, and D. Jaksch, 2008, Phys. Rev. Lett. **101**, 260502.
Nunn, J., I. A. Walmsley, M. G. Raymer, K. Surmacz, F. C. Waldermann, Z. Wang, and D. Jaksch, 2007, Phys. Rev. A **75**, 011401.
Olmschenk, S., D. N. Matsukevich, P. Maunz, D. Hayes, L. Duan, and C. Monroe, 2009, Science **323**, 486.
Ottaviani, C., C. Simon, H. de Riedmatten, M. Afzelius, B. Lauritzen, N. Sangouard, and N. Gisin, 2009, arXiv:0903.3153.
Ou, Z. Y., and Y. J. Lu, 1999, Phys. Rev. Lett. **83**, 2556.
Ourjoumtsev, A., F. Ferreyrol, R. Tualle-Brouri, and P. Grangier, 2009, Nature Phys. **5**, 189.
Pan, J.-W., D. Bouwmeester, H. Weinfurter, and A. Zeilinger, 1998, Phys. Rev. Lett. **80**, 3891.
Pan, J.-W., S. Gasparoni, R. Ursin, G. Weihs, and A. Zeilinger, 2003, Nature (London) **423**, 417.

Pan, J.-W., C. Simon, C. Brukner, and A. Zeilinger, 2001, Nature (London) **410**, 1067.
Pan, J.-W., Z.-B. Chen, M. Zukowski, H. Weinfurter, and A. Zeilinger, 2008, arXiv:0805.2853.
Peng, C.-Z. *et al.*, 2005, Phys. Rev. Lett. **94**, 150501.
Phillips, D. F., A. Fleischhauer, A. Mair, R. L. Walsworth, and M. D. Lukin, 2001, Phys. Rev. Lett. **86**, 783.
Phillips, N. B., A. V. Gorshkov, and I. Novikova, 2008, Phys. Rev. A **78**, 023801.
Pittman, T. B., and J. D. Franson, 2003, Phys. Rev. Lett. **90**, 240401.
Polyakov, S. V., C. W. Chou, D. Felinto, and H. J. Kimble, 2004, Phys. Rev. Lett. **93**, 263601.
Razavi, M., M. Piani, and N. Lutkenhaus, 2008, arXiv:0810.5334.
Reim, K. F., J. Nunn, V. O. Lorenz, B. J. Sussman, K. C. Lee, N. K. Langford, D. Jaksch, and I. A. Walmsley, 2010, Nat. Photon. **4**, 218.
Rippe, L., B. Julsgaard, A. Walther, Y. Ying, and S. Kroll, 2008, Phys. Rev. A **77**, 022307.
Rosfjord, K. M., J. K. W. Yang, E. A. Dauler, A. J. Kerman, V. Anant, B. M. Voronov, G. N. Gol'tsman, and K. K. Berggren, 2006, Opt. Express **14**, 527.
Ruggiero, J., J.-L. Le Gouet, C. Simon, and T. Chaneliere, 2009, Phys. Rev. A **79**, 053851.
Sabooni, M., F. Beaudoin, A. Walther, N. Lin, A. Amari, M. Huang, and S. Kröll, 2010, Phys. Rev. Lett. **105**, 060501.
Sangouard, N., R. Dubessy, and C. Simon, 2009, Phys. Rev. A **79**, 042340.
Sangouard, N., C. Simon, M. Afzelius, and N. Gisin, 2007a, Phys. Rev. A **75**, 032327.
Sangouard, N., C. Simon, T. Coudreau, and N. Gisin, 2008a, Phys. Rev. A **78**, 050301.
Sangouard, N., C. Simon, N. Gisin, J. Laurat, R. Tualle-Brouri, and P. Grangier, 2010, J. Opt. Soc. Am. B **27**, A137.
Sangouard, N., C. Simon, J. Minar, H. Zbinden, H. de Riedmatten, and N. Gisin, 2007b, Phys. Rev. A **76**, 050301.
Sangouard, N., C. Simon, B. Zhao, Y.-A. Chen, H. de Riedmatten, J.-W. Pan, and N. Gisin, 2008b, Phys. Rev. A **77**, 062301.
Santori, C., D. Fattal, J. Vuckovic, G. S. Solomon, and Y. Yamamoto, 2002, Nature (London) **419**, 594.
Schnorrberger, U., J. Thompson, S. Trotzky, R. Pugatch, N. Davidson, S. Kuhr, and I. Bloch, 2009, arXiv:0903.0135.
Scholz, M., L. Koch, and O. Benson, 2009a, Phys. Rev. Lett. **102**, 063603.
Scholz, M., L. Koch, R. Ullmann, and O. Benson, 2009b, Appl. Phys. Lett. **94**, 201105.
Scully, M. O., and M. S. Zubairy, 2003, Science **301**, 181.
Sellars, M., G. Pryde, N. Manson, and E. Krausz, 2000, J. Lumin. **87–89**, 833.
Shahriar, M. S., G. S. Pati, and K. Salit, 2007, Phys. Rev. A **75**, 022323.
Sherson, J. F., H. Krauter, R. K. Olsson, B. Julsgaard, K. Hammerer, I. Cirac, and E. S. Polzik, 2006, Nature (London) **443**, 557.
Shuker, M., O. Firstenberg, R. Pugatch, A. Ron, and N. Davidson, 2008, Phys. Rev. Lett. **100**, 223601.
Simon, C., H. de Riedmatten, M. Afzelius, N. Sangouard, H. Zbinden, and N. Gisin, 2007b, Phys. Rev. Lett. **98**, 190503.
Simon, C., and W. T. M. Irvine, 2003, Phys. Rev. Lett. **91**, 110405.
Simon, C., and J.-W. Pan, 2002, Phys. Rev. Lett. **89**, 257901.
Simon, C., Y.-M. Niquet, X. Caillet, J. Eymery, J.-P. Poizat, and J.-M. Gerard, 2007a, Phys. Rev. B **75**, 081302.
Simon, J., H. Tanji, S. Gosh, and V. Vuletic, 2007a, Nature Phys. **3**, 765.
Simon, J., H. Tanji, J. K. Thompson, and V. Vuletic, 2007b, Phys. Rev. Lett. **98**, 183601.
Staudt, M. U., M. Afzelius, H. de Riedmatten, S. R. Hastings-Simon, C. Simon, R. Ricken, H. Suche, W. Sohler, and N. Gisin, 2007, Phys. Rev. Lett. **99**, 173602.
Staudt, M. U., S. R. Hastings-Simon, M. Afzelius, D. Jaccard, W. Tittel, and N. Gisin, 2006, Opt. Commun. **266**, 720.
Staudt, M. U., S. R. Hastings-Simon, M. Nilsson, M. Afzelius, V. Scarani, R. Ricken, H. Suche, W. Sohler, W. Tittel, and N. Gisin, 2007, Phys. Rev. Lett. **98**, 113601.
Stucki, D., N. Walenta, F. Vannel, R. Thew, N. Gisin, H. Zbinden, S. Gray, C. Towery, and S. Ten, 2009, New J. Phys. **11**, 075003.
Surmacz, K., J. Nunn, F. C. Waldermann, K. C. Lee, Z. Wang, I. A. Walmsley, and D. Jaksch, 2007, arXiv:0710.5033v1.
Takesue, H., 2010, arXiv:1006.0364.
Takeuchi, S., J. Kim, Y. Yamamoto, and H. H. Hogue, 1999, Appl. Phys. Lett. **74**, 1063.
Tanzilli, S., H. de Riedmatten, W. Tittel, H. Zbinden, P. Baldi, M. De Micheli, D. Ostrowsky, and N. Gisin, 2001, Electron. Lett. **37**, 26.
Tanzilli, S., W. Tittel, M. Halder, O. Alibart, P. Baldi, N. Gisin, and H. Zbinden, 2005, Nature (London) **437**, 116.
Thompson, J. K., J. Simon, H. Loh, and V. Vuletic, 2006, Science **313**, 74.
Tittel, W., M. Afzelius, T. Chanelière, R. Cone, S. Kröll, S. Moiseev, and M. Sellars, 2009, Laser Photon. Rev. **4**, 244.
Togan, E., Y. Chu, A. S. Trifonov, L. Jiang, J. Maze, L. Childress, M. V. G. Dutt, A. S. Sorensen, P. R. Hemmer, A. S. Zibrov, and M. D. Lukin, 2010, Nature (London) **466**, 730.
Turukhin, A. V., V. S. Sudarshanam, M. S. Shahriar, J. A. Musser, B. S. Ham, and P. R. Hemmer, 2001, Phys. Rev. Lett. **88**, 023602.
Ursin, R. *et al.*, 2007, Nature Phys. **3**, 481.
Usmani, I., M. Afzelius, H. de Riedmatten, and N. Gisin, 2010, Nature Commun. **1**, 1.
van der Wal, C. H., M. D. Eisaman, A. Andre, R. L. Walsworth, D. F. Phillips, A. S. Zibrov, and M. D. Lukin, 2003, Science **301**, 196.
van Enk, S. J., N. Lutkenhaus, and H. J. Kimble, 2007, Phys. Rev. A **75**, 052318.
van Loock, P., T. D. Ladd, K. Sanaka, F. Yamaguchi, K. Nemoto, W. J. Munro, and Y. Yamamoto, 2006, Phys. Rev. Lett. **96**, 240501.
van Loock, P., N. Lutkenhaus, W. J. Munro, and K. Nemoto, 2008, Phys. Rev. A **78**, 062319.
Vasilyev, D. V., I. V. Sokolov, and E. S. Polzik, 2008, Phys. Rev. A **77**, 020302.
Villoresi, P., T. Jennewein, F. Tamburini, M. Aspelmeyer, C. Bonato, R. Ursin, C. Pernechele, V. Luceri, G. Bianco, A. Zeilinger, and C. Barbieri, 2008, New J. Phys. **10**, 033038.
Villoresi, P., F. Tamburini, M. Aspelmeyer, T. Jennewein, R. Ursin, C. Pernechele, G. Bianco, A. Zeilinger, and C. Barbieri, 2004, arXiv:quant-ph/0408067.
Vudyasetu, P. K., R. M. Camacho, and J. C. Howell, 2008, Phys. Rev. Lett. **100**, 123903.
Walther, P., M. D. Eisaman, A. Andre, F. Massou, M. Fleischhauer, A. S. Zibrov, and M. D. Lukin, 2007, Int. J. Quantum. Inform. **5**, 51.
Wang, H., T. Horikiri, and T. Kobayashi, 2004, Phys. Rev. A **70**, 043804.
Ward, M. B., O. Z. Karimov, D. C. Unitt, Z. L. Yuan, P. See, D. G. Gevaux, A. J. Shields, P. Atkinson, and D. A. Ritchie, 2005, Appl. Phys. Lett. **86**, 201111.

Weber, B., H. P. Specht, T. Muller, J. Bochmann, M. Mucke, D. L. Moehring, and G. Rempe, 2009, Phys. Rev. Lett. **102**, 030501.
Wolfgramm, F., X. Xing, A. Cerè, A. Predojević, A. M. Steinberg, and M. W. Mitchell, 2008, Opt. Express **16**, 18145.
Wootters, W. K., 1998, Phys. Rev. Lett. **80**, 2245.
Wootters, W. K., and W. H. Zurek, 1982, Nature (London) **299**, 802.
Wu, L.-A., H. J. Kimble, J. L. Hall, and H. Wu, 1986, Phys. Rev. Lett. **57**, 2520.
Yoshikawa, Y., K. Nakayama, Y. Torii, and T. Kuga, 2007, Phys. Rev. Lett. **99**, 220407.
Yoshikawa, Y., K. Nakayama, Y. Torii, and T. Kuga, 2009, Phys. Rev. A **79**, 025601.
Yuan, Z.-S., Y.-A. Chen, S. Chen, B. Zhao, M. Koch, T. Strassel, Y. Zhao, G.-J. Zhu, J. Schmiedmayer, and J.-W. Pan, 2007, Phys. Rev. Lett. **98**, 180503.
Yuan, Z.-S., Y.-A. Chen, B. Zhao, S. Chen, J. Schmiedmayer, and J.-W. Pan, 2008, arXiv:0803.1810v1.
Zhao, B., Y.-A. Chen, X.-H. Bao, T. Strassel, C.-S. Chuu, X.-M. Jin, J. Schmiedmayer, Z.-S. Yuan, S. Chen, and J.-W. Pan, 2008, Nature Phys. **5**, 95.
Zhao, B., Z.-B. Chen, Y.-A. Chen, J. Schmiedmayer, and J.-W. Pan, 2007, Phys. Rev. Lett. **98**, 240502.
Zhao, R., Y. O. Dudin, S. D. Jenkins, C. J. Campbell, D. N. Matsukevich, T. A. B. Kennedy, and A. Kuzmich, 2008, Nature Phys. **5**, 100.
Zinoni, C., B. Alloing, C. Monat, V. Zwiller, L. H. Li, A. Fiore, L. Lunghi, A. Gerardino, H. de Riedmatten, H. Zbinden, and N. Gisin, 2006, Appl. Phys. Lett. **88**, 131102.
Zukowski, M., A. Zeilinger, M. A. Horne, and A. K. Ekert, 1993, Phys. Rev. Lett. **71**, 4287.